| REPORT DOCUMENTATION PAGE | AFRL-SR-BL-TR-00- | 88 |
|---|---|---|



0140



| 1. AGENCY USE ONLY *(Leave blank)* | 2. REPORT DATE | Final Technical Report | 11 Jun 96 to 31 May 00 |
|---|---|---|---|
| | 28 September 1999 | | |

**4. TITLE AND SUBTITLE**
Rockburst Research Applied to Nuclear Event Discrimination

**5. FUNDING NUMBERS**
F49620-96-1-0288

**6. AUTHOR(S)**
Holly Hoffman, Misty Cook, Hana Baker, Marvin Speece, Bill Sill, Chuck Wideman, Tom Moon, Curtis Link

**7. PERFORMING ORGANIZATION NAME(S) AND ADDRESS(ES)**
Montana Tech of the University of Montana
Geophysics Engineering Department
1300 West Park Street
Butte, MT 59701-8997

**8. PERFORMING ORGANIZATION REPORT NUMBER**

**9. SPONSORING/MONITORING AGENCY NAME(S) AND ADDRESS(ES)**
AFOSR/NM
801 N. Randolph St, Rm 732
Arlington, VA 22203-1977

**10. SPONSORING/MONITORING AGENCY REPORT NUMBER**
F49620-96-1-0288

**11. SUPPLEMENTARY NOTES**

**12a. DISTRIBUTION AVAILABILITY STATEMENT**
Approved for public release; distribution unlimited.

**12b. DISTRIBUTION CODE**

**13. ABSTRACT** *(Maximum 200 words)*

Rockbursts produce seismic signals that are similar to those associated with near surface earthquakes and explosions. Some of the methods developed for source mechanism studies also encompass imaging techniques appropriate for nuclear event verification, and, as a result, have implications for the Comprehensive Test Ban Treaty (CTBT). Past experiments have demonstrated a clear relationship between Barkhausen Noise (BN) and stress in pipeline steel samples. Stress can affect the nature of the pinning sites at domain boundaries which in turn plays a role in the way that domain walls move and cause BN pulses. We have conducted experiments to detect a relationship between BN and stress in magnetite-rich rocks. These experiments were performed by applying uniaxial loading from 4500N to 55000N to cylindrical core samples of magnetite-rich rocks obtained from the Stillwater Complex in Montana. A pick-up coil was used to detect the BN pulses and an electromagnet was used to magnetize the samples. BN pulses were recorded during a specified time interval for each increment of loading. The pick-up coil was positioned to be near magnetite-rich regions of the sample. We have observed a linear increase in the number of BN pulses with increased loading. Ongoing research is focused on refining the experimental procedure to increase the bandwidth of recording and eliminate possible sources of noise in the experiments. The results of this study might help us to understand the nature of the remagnetization that often accompanies large-scale tectonic events. Moreover, this study could lead to a method of nondestructive testing to determine state of stress at mine walls.

**14. SUBJECT TERMS**
Workshop, conference, Defense related signal processing

**15. NUMBER OF PAGES**
91

**16. PRICE CODE**

| 17. SECURITY CLASSIFICATION OF REPORT | 18. SECURITY CLASSIFICATION OF THIS PAGE | 19. SECURITY CLASSIFICATION OF ABSTRACT | 20. LIMITATION OF ABSTRACT |
|---|---|---|---|
| UNCLASSIFIED | UNCLASSIFIED | UNCLASSIFIED | UL |

**Final Report**

***Rockburst Research Applied to Nuclear Event Discrimination***

**Department of Defense EPSCoR Grant No. F49620-96-1-0288**

September 30, 1999

Holly Hoffman, Misty Cook, Hana Baker,
Marvin Speece, Bill Sill, Chuck Wideman, Tom Moon, Curtis Link

## SUMMARY

The basis for this research is that rockbursts produce seismic signals that are similar to those associated with near surface earthquakes and explosions. A complete understanding of source mechanisms is necessary for the correct identification of these events. Some of the methods developed for source mechanism studies also encompass imaging techniques appropriate for nuclear event verification, and, as a result, have implications for the Comprehensive Test Ban Treaty (CTBT).

PCI/Atlantic Scientific INSAR software was purchased last fall for elevation change detection at a rockburst site using radar interferometry. We have been familiarizing ourselves with this software and radar remote sensing. Images have recently been acquired that cover the site of a large rockburst.

The air wave can interfere with the rock wave in Ground Penetrating Radar (GPR) transillumination experiments making it difficult to pick the rock wave first arrivals in mines. This was particularly a problem at small transmitter to receiver distances. The distinction between these arrivals could be overcome by the use of higher frequency antennas at small transmitter to receiver distances. Lower frequency antennas might still be necessary for longer transmitter to receiver distances to obtain the necessary depth of penetration. A comparison of the tomograms from the 1997 and 1998 GPR experiments at the Stillwater Mine, Montana, will help us to decide if we can use this method to detect change in a pillar. A comparison with electrical measurements on the same pillar will help with this interpretation.

Past experiments have demonstrated a clear relationship between Barkhausen Noise (BN) and stress in pipeline steel samples. Stress can affect the nature of the pinning sites at domain boundaries which in turn plays a role in the way that domain walls move and cause BN pulses. We have conducted experiments to detect a relationship between BN and stress in magnetite-rich rocks. These experiments were performed by applying uniaxial loading from 4500N to 55000N to cylindrical core samples of magnetite-rich rocks obtained from the Stillwater Complex in Montana. A pick-up coil was used to detect the BN pulses and an electromagnet was used to magnetize the samples. BN pulses were recorded during a specified time interval for each increment of loading. The pick-up coil was positioned to be near magnetite-rich regions of the sample. We have observed a linear increase in the number of BN pulses with increased loading. Ongoing research is focused on refining the experimental procedure to increase the bandwidth of recording and eliminate possible sources of noise in the experiments. The results of this study might help us to understand the nature of the remagnetization that often accompanies large-scale tectonic events. Moreover, this study could lead to a method of nondestructive testing to determine state of stress at mine walls.

A series of electrical measurements have been made on a new pillar of rock in the Stillwater Mine over a period of two years. The measurements have been used to generate models of the resistivity in the pillar and the surrounding rock.

The models show a cyclic or seasonal change in resistivity of some of the rock surrounding the pillar. This was unexpected , given the depth of the rock below the surface. The resistivity in the interior of the pillar showed a general decrease over time. The decrease is attributed to the opening of cracks and the redistribution of pore water.

Source mechanisms for an addition 15 rockbursts in the Lucky Friday Mine of Northern Idaho have been determined. The rockburst events had equivalent Richter magnitudes ranging from approximately 2.5 to 3.5, and in some cases caused extensive damage to mine workings. All of the events were within 5700 ft of the surface, and would therefore be classified as extremely near surface seismic events. Naturally occurring earthquakes in this geographic region have focal mechanisms much deeper than the rockburst events. All of the rockburst source mechanisms have equivalent double couple sources similar to those caused by earthquakes. None of the rockburst events can be explained by implosive or explosive types of source mechanisms.

Identification of the state of rock bolts inside boreholes is a difficult problem. Rock bolts that are not seated properly inside a borehole can fail under a variety of conditions resulting in catastrophic cave-ins and rockbursts. For this study, modeled frequency response curves were compared to closed-form solutions for axial vibrations, lateral vibrations, and strings clamped at both ends. In addition, the computer results were compared to results from a laboratory experiment utilizing two different rock bolts. Finally, rock bolts from the Stillwater Mine were modeled and results were obtained for two seating situations.

Using a Tinius-Ohlsen testing machine, a Simmons eye rock bolt and DYWIDAG rock bolt were placed under varying amounts of tension to investigate frequency mode response. Impulse forces were applied as hammer taps to the ends and sides of the bolts and the resulting sounds were recorded with an audiocassette recorder. These recordings were analyzed in the frequency domain and compared with computer modeling results.

Investigation focused on axial responses rather than bending or transverse responses due to higher signal-to-noise ratio for axial impulses. Frequency peaks occurred at 4200 Hz and 3450 Hz for the Simmons eye bolt axial modes. The effect of clamp placement on the bolt and non-direct hits on the bolt end most likely contribute to the combination of axial and bending peaks.

Impulse response measurements for the DYWIDAG rock bolt showed frequency peaks at 750 Hz, 1250 Hz, and 2100 Hz. Modeling indicated that the combination of rock-bolt ridges and clamp placement contributed to the multiple peaks and lowered the frequencies.

In addition to laboratory measurements, hammer impulse tests were performed on in situ rock bolts in the Stillwater mine. Underground miners maintain that they can predict mine wall loading by the sound of a rock hammer hitting a rock bolt. The fundamental frequency contained in the mine recordings was 1260 Hz. This frequency peak occurred within a 400 Hz range. Different rock-bolt lengths, ridges on the sides of the rock bolts, non-direct hammer strikes on the ends of the rock bolts, and variable coupling of the bolts to the rock all contribute to the variation in frequencies. Due to the variable nature of rock-bolt coupling, the range in frequencies observed from the mine rock bolts is probably not attributable to changes in loading.

## TABLE OF CONTENTS

## REMOTE SENSING METHODS APPLIED TO ROCKBURST MONITORING

### Background

Remote sensing methods were to be employed in order to observe any changes that might occur at the surface above a mining area as a result of a rockburst. Originally, hyperspectral or multispectral images were to be purchased for temporal change detection over a rockburst site; however, due to an early budget reduction in the proposal, there was not enough money allocated to carry out this part of the project. In addition, it became evident early on that rather than focusing on spectral change detection, it might be more advantageous to look at surface displacements using the relatively new technique of radar interferometry. Consequently, the time allocated to this project was spent familiarizing us with radar interferometry and trying to secure funds from another source in order to carry out the remote sensing part of the project.

### Update

At the beginning of this report period, NASA funds were obtained through a JOVE Augmentation Grant to help support this part of this project. As a consequence, PCI/Atlantic Scientific INSAR software was purchased for elevation change detection at a rockburst site using radar interferometry. We have been familiarizing ourselves with this software and radar remote sensing. Images have recently been acquired that cover the site of a large rockburst.

## GROUND PENETRATING RADAR MONITORING

### Introduction

We conducted Ground Penetrating Radar (GPR) tomography experiments at the Stillwater Mine in Montana to see if we could detect pillar changes using this method. Experiments were completed on July 8 and 9, 1997, January 13, 1998, and August 26, 1998.

The Stillwater mine is a platinum-palladium underground mine located at the edge of the Beartooth Mountains, near Nye, Montana. This mine is the only platinum-palladium mine in operation in the United States. Here, platinum and palladium are mined from the Stillwater Complex. The rocks of this large, layered, mafic intrusive complex are predominantly gabbro and related rock types. This igneous intrusion runs along the northwest margin of the Beartooth Mountains in Stillwater and Sweetgrass counties. The middle Cambrian intrusion exhibits a west to northwest strike with a 50 to 90 degree dip. The complex is host to pyroxenes, gabbros, norites, diorites and anorthosites intruded into Precambrian rocks and overlain by Paleozoic sediments (Yates, 1984). Historically, this mine has not been prone to rockbursts; but, as mining has progressed deeper, rock failure has become more of a threat.

### Procedure

In these tests, the transillumination mode of data gathering was employed in which the transmitting and receiving antennas were placed on opposite sides of a pillar (Figure 1). The receiving antenna remained fixed while the transmitter was moved to create a total of fifteen receiver gathers. This method of data gathering proved to be efficient. Table 1 shows the field recording parameters used for this study.

Arrival times of the rock wave were picked by hand from the receiver gathers. These times, together with the source and receiver locations, will be used to invert for velocity by the Simultaneous Iterative Reconstruction Technique (SIRT) (Peterson et al., 1985). Software developed at the former United States Bureau of Mines was used to invert for velocity structure of the pillar for the 1997 experiment. The software is called 3DTOM and runs under DOS on personnel computers (Jackson and Tweeton, 1996). A graduate student is processing and interpreting these data as part of a thesis project.

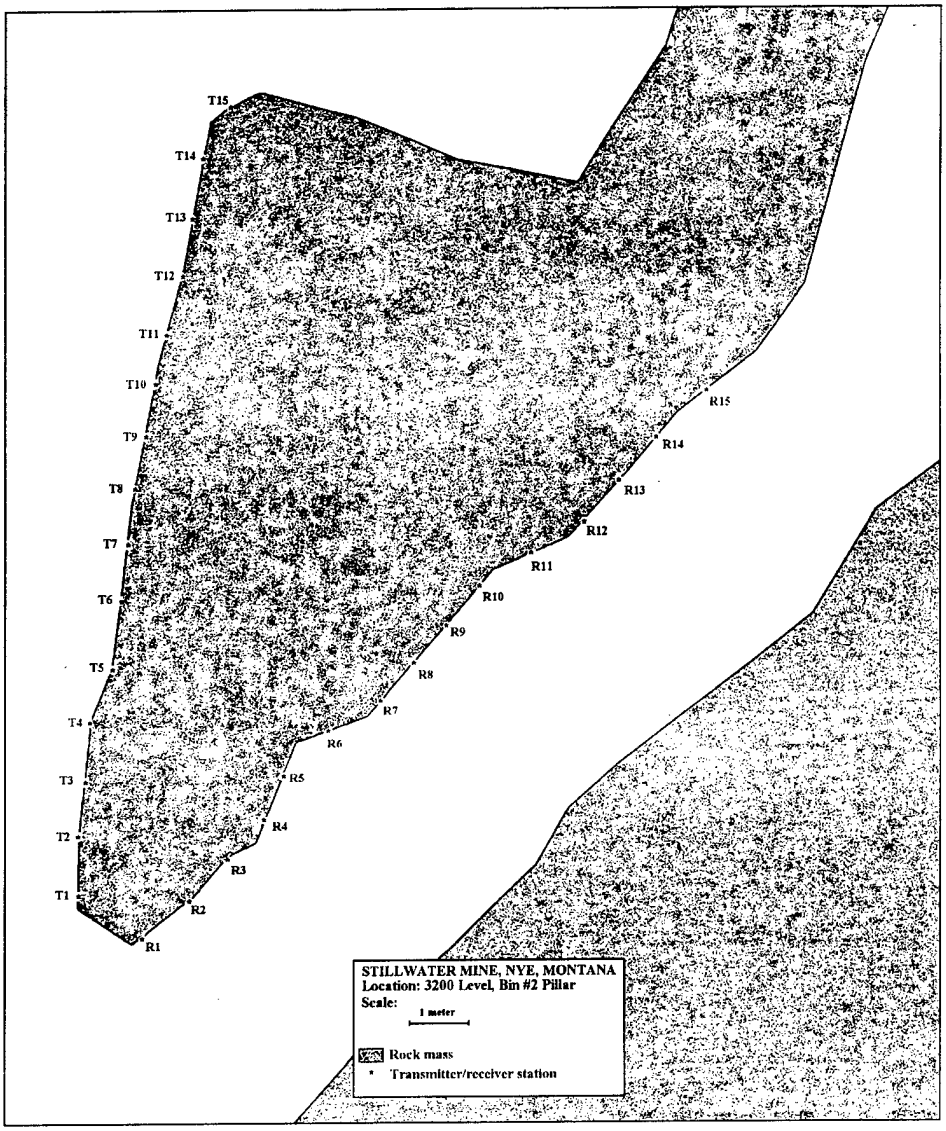


Fig. 1. Plan view for GPR and electrical resistance tomography studies at the Stillwater Mine. T1 and R1 are transmitter and receiver station locations respectively.

Table 1. Data Collection Parameters

| | |
|---|---|
| Samples | 1024 |
| Sample Frequency | 1008.94 MHz |
| Stacks | 128 |
| Antennas | 100 MHz |
| Antenna orientation | Vertical |

The velocity tomogram for the 1997 experiment is shown in Figure 2 and the corresponding raypath density plot is shown in Figure 3. These data were processed using SIRT with a straight raypath forward model. The termination criteria was 15 iterations or a residual tolerance of 0.01, whichever occurs first. A nodal constraint of 300 m/μs was used for nodes occurring in the tunnel region adjacent to the pillar face. This is the electromagnetic wave speed of free space.

The tomogram (Figure 2) shows the outline of the pillar with higher velocities occurring near the pillar face. Ordinarily, we would observe high relative velocities at the nose of the pillar due to increased pore volume caused by fracturing. Low velocities, however, are observed at the nose of the pillar in the lower left of Figure 2. This is a correspondingly area of low raypath coverage (Figure 3) and this might be an artifact of the inversion.

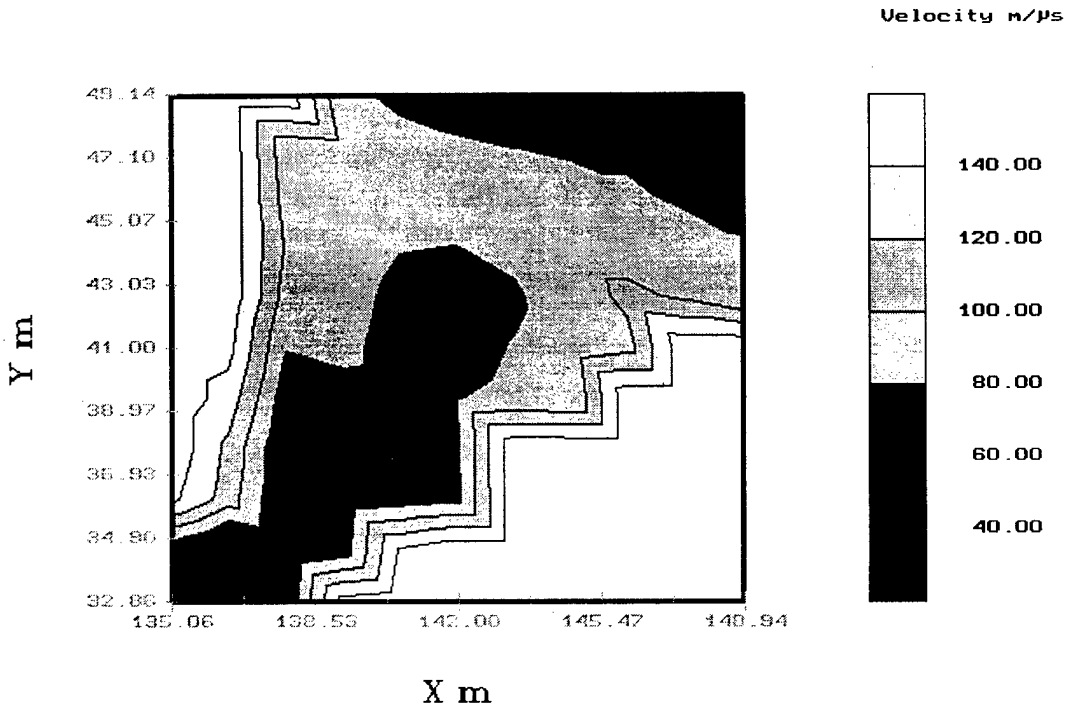


Fig. 2. GPR wave-speed tomogram for pillar study at Stillwater Mine.

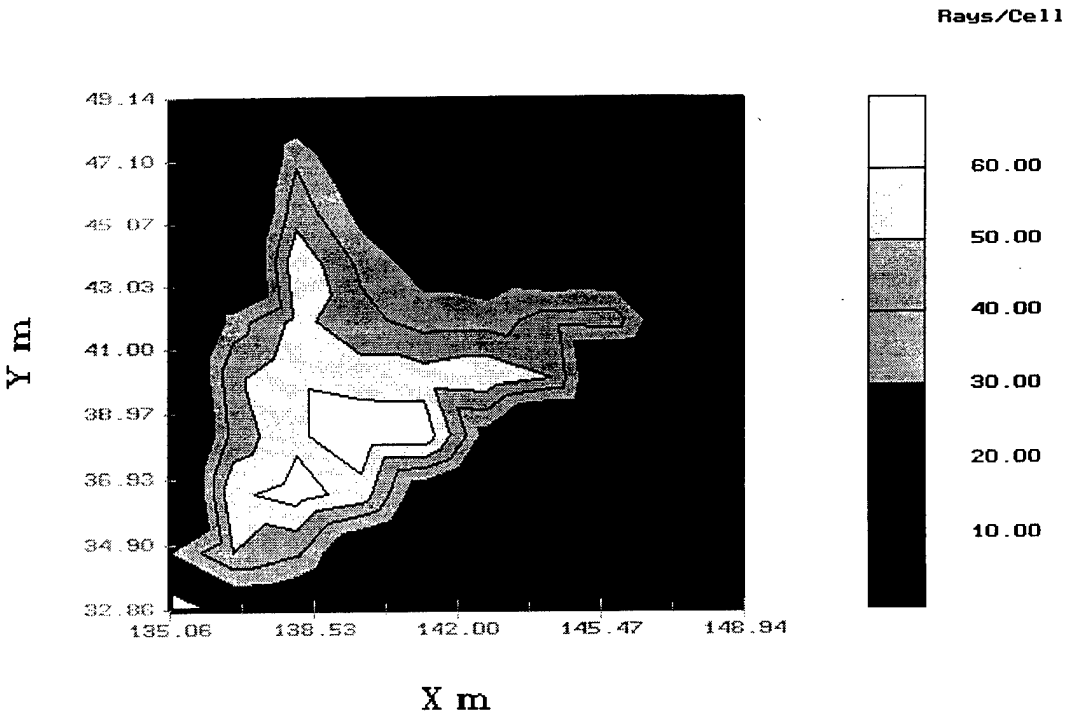


Fig. 3. Raypath sample density plot. Contours show the outline of the pillar in the middle of a rectangular model grid.

## Discussion and Conclusions

Reflections from the tunnel walls as well as scattering from metal in the tunnel can often interfere with reflections received from discontinuities in the rock. Preliminary tests of a wire mesh ("chicken wire") to help shield our antennas proved inconclusive.

The air wave can interfere with the rock wave in transillumination experiments making it difficult to pick the rock wave first arrivals. This was particularly a problem at small transmitter to receiver distances. The distinction between these arrivals could be partly overcome by the use of higher frequency antennas at small transmitter to receiver distances. Lower frequency antennas might still be necessary for longer transmitter to receiver distances to obtain the necessary depth of penetration. Due to the limited depth of penetration observed in the Stillwater Mine we must use 100 MHz antennas for this pillar.

A comparison of the tomograms from the 1997 and 1998 GPR experiments will help us to decide if we can use this method to detect changes in the pillar. A comparison with electrical measurements on the same pillar will help with this interpretation.

## BARKHAUSEN NOISE MONITORING

### Introduction

Barkhausen Noise (BN) refers to the electromagnetic pulses produced when magnetic domain walls move in a magnetic material in response to the applied magnetic field. Professor Heinrich Barkhausen (1919) demonstrated that the magnetization of a sample, which is characterized by a hysteresis curve, is not continuous but in fact is made up of a series of steps which are produced as domain walls move in response to the applied magnetic field (Figure 4). We have conducted experiments to detect BN in magnetite-rich rock subjected to loading.

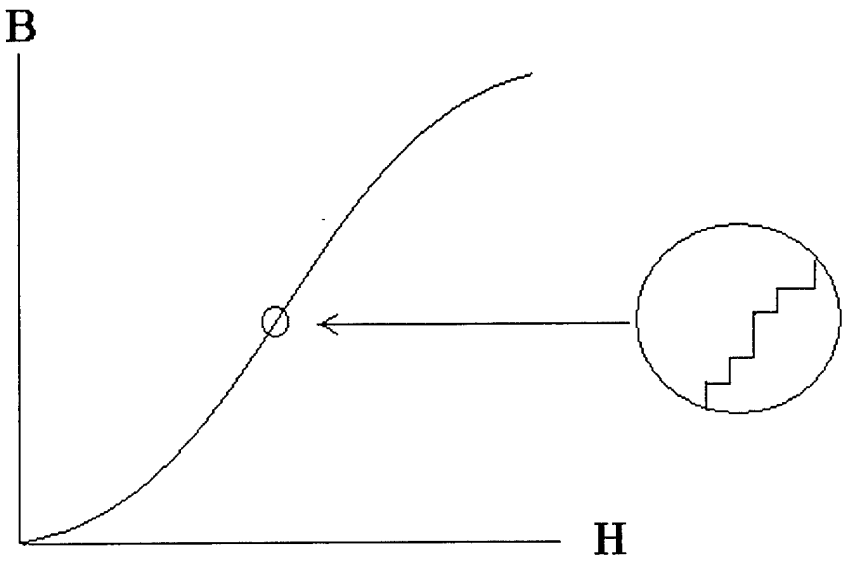


Fig. 4. Generalized hysteresis curve for a magnetic material showing Barkhausen noise (B—magnetic induction; H—magnetic field strength; after Bozorth, 1951).

### Domains

Domains have their own magnetic strength and direction. The sum of the strengths and directions of all the domains results in the total magnetization of the entire sample. Generally, the domains are different sizes and have different directions of magnetization, which is typical for ferromagnetic and ferrimagnetic material. Domain walls, shown in black, in Figure 5, separate the individual domains from each other. Domains walls become fixed or pinned at crystalline imperfections. When a ferromagnetic material is placed in a magnetic field, the domain walls move. The movement of the domain walls increases the size of the domains that have the same magnetization direction as the magnetic field, and decreases the size of the domains with opposing directions (Figure 5b).

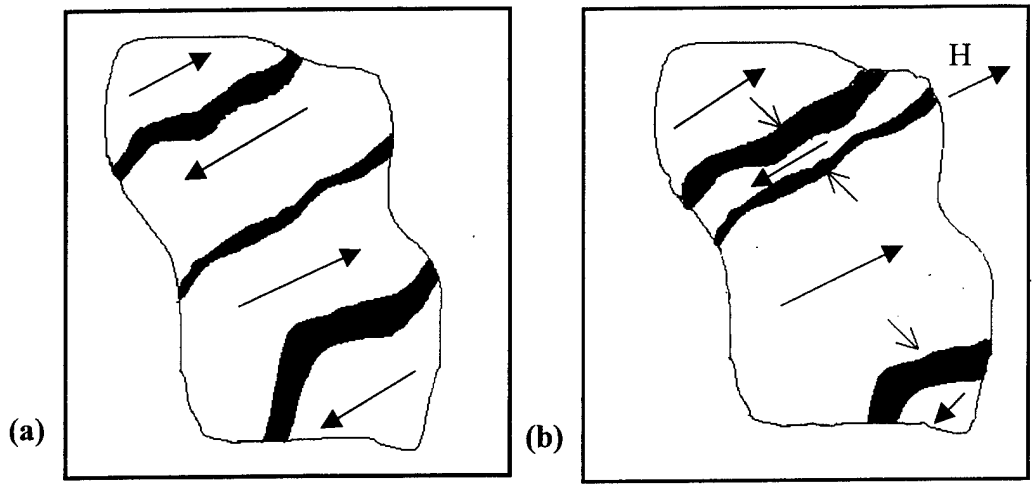


Fig 5. (a) Example of unmagnetized domains. The direction of the arrows indicates the direction of the magnetization of the sample. The black areas are the domain walls, which move when the material is magnetized. (b) Domains magnetized by the field H. The fine arrows indicate the direction of the motion of the domain walls.

This movement increases the overall magnetization of the field in the direction of H, giving rise to a hysteresis curve. The domain wall movement, however, is not smooth. A wall moves until it reaches a pinning site, at which point it is held up until the magnetic field is large enough to move the wall past the site. Once the site is overcome the wall moves smoothly until it encounters another pinning site. This process continues until the sample is saturated. These quick wall movements, or jumps over the pinning sites, in ferromagnetic material can induce an electromagnetic pulse called BN.

**Barkhausen Noise and Stress**

BN has been related to grain size (Tiitto, 1977; Ranjan et al., 1987), carbon content (Ranjan et al., 1987), pearlite colony and lamellar spacing (Sundstrom and Torronen, 1979; Clapham et al., 1991), and residual stress (Sandstrom and Torronen, 1979; Dhar and Atherton, 1993). Elastic stresses influence how domains choose their easy direction of magnetization. As the result of this magnetoelastic interaction, compressive stresses will decrease the intensity of BN and tensile stresses increase the intensity of BN (Jagadish et al., 1990). Consequently, a measurement of the intensity of BN in a sample can provide information about the residual stress. BN is commonly observed by using a pick-up coil and an amplifier (Figure 6).

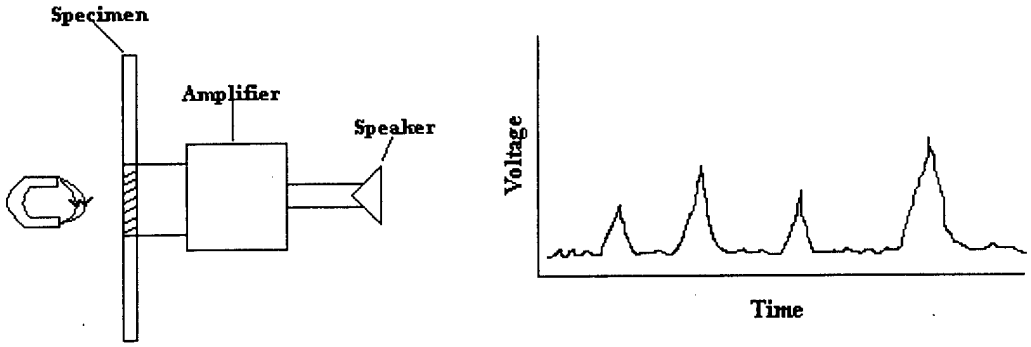


Fig. 6. Method of observing Barkhausen noise (after Bozorth, 1951).

Magnetoelastic testing using BN measurements have been used primarily in the nondestructive testing of pipeline steel (Tiitto, 1991; Jagadish et al., 1990; Krause et al., 1995; Mandel et al., 1996). This method of nondestructive testing has not been tried on earth materials, although the Barkhausen effect has been observed in rocks. Furthermore, some have suggested that domain wall adjustments bring about remagnetization during tectonic events in response to the changing stress field (Hudson et al., 1989; Borradaile, 1996).

## Experimental Procedure

A block diagram of the circuit that was built to record BN can be seen in Figure 7. An electromagnet with a 10 Hz driving signal was used to generate a magnetic field of about 86,000 gammas. A read head from a Sony Walkman was used to detect BN. The data were recorded using a computer sound card with a sample rate of 22 KHz. Sample data and the 10 Hz driving signal are shown in Figure 8. Figure 9 shows filtered data with BN.

A compressional load was applied to a cylindrical core samples that were obtained from the Stillwater Complex in Montana. The core samples were selected to be magnetite rich. Figure 10 shows the experimental setup. A Tinius-Olsen Hydraulic Tension and Compression Tester was used to load the sample. The read head was oriented to be near magnetite-rich portions of the samples. BN was recorded for a small time interval at each 1000 lb. increment of loading.

## Results and Conclusions

Figure 11 shows the total number of pulses recorded at each load level as a function of load. We have observed a linear increase in the number of BN pulses with increased loading. Ongoing research is focused on refining the experimental procedure to increase the bandwidth of recording and eliminate possible sources of noise in the experiments. The results of this study might help us to understand the nature of the remagnetization that often accompanies large-scale tectonic events. Moreover, this study could lead to a method of nondestructive testing to determine state of stress at mine walls.

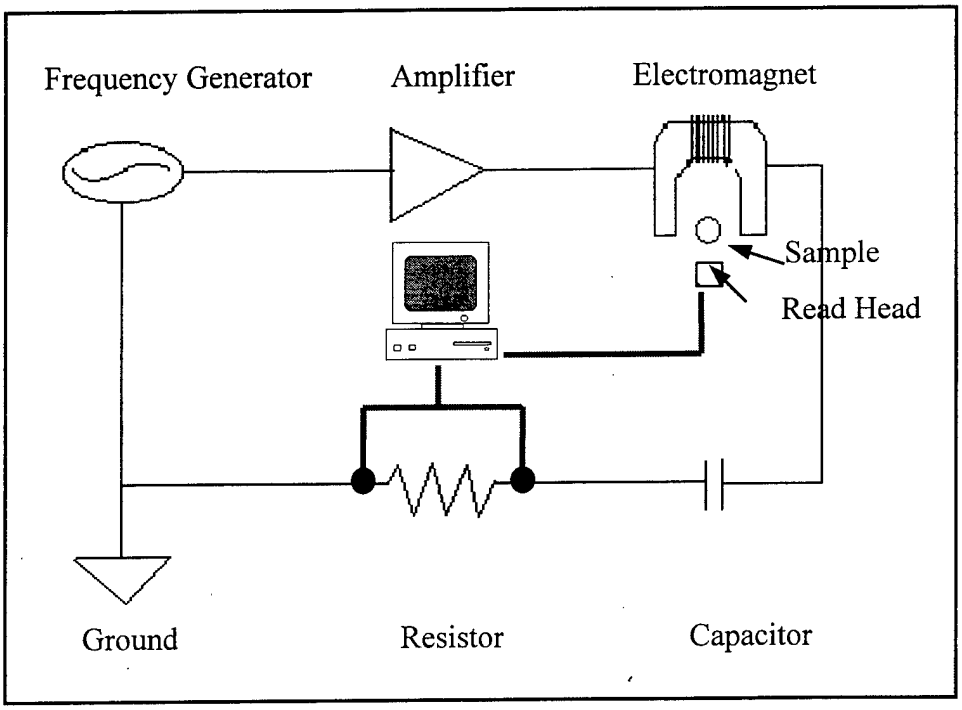


Fig. 7. Experimental setup to detect BN.

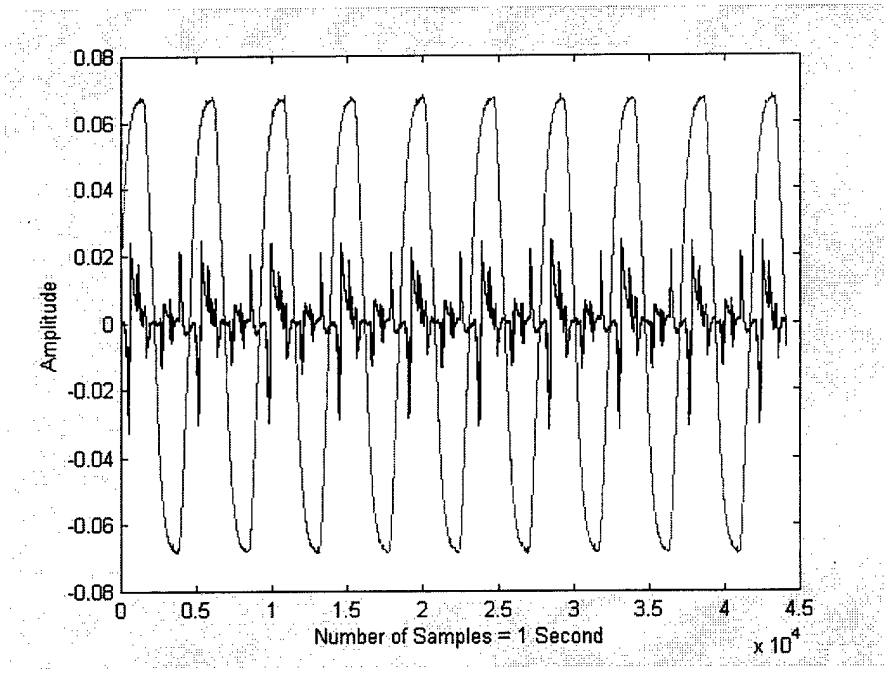


Fig. 8. Unfiltered record showing the higher amplitude driving signal and the signal recorded from the read head.

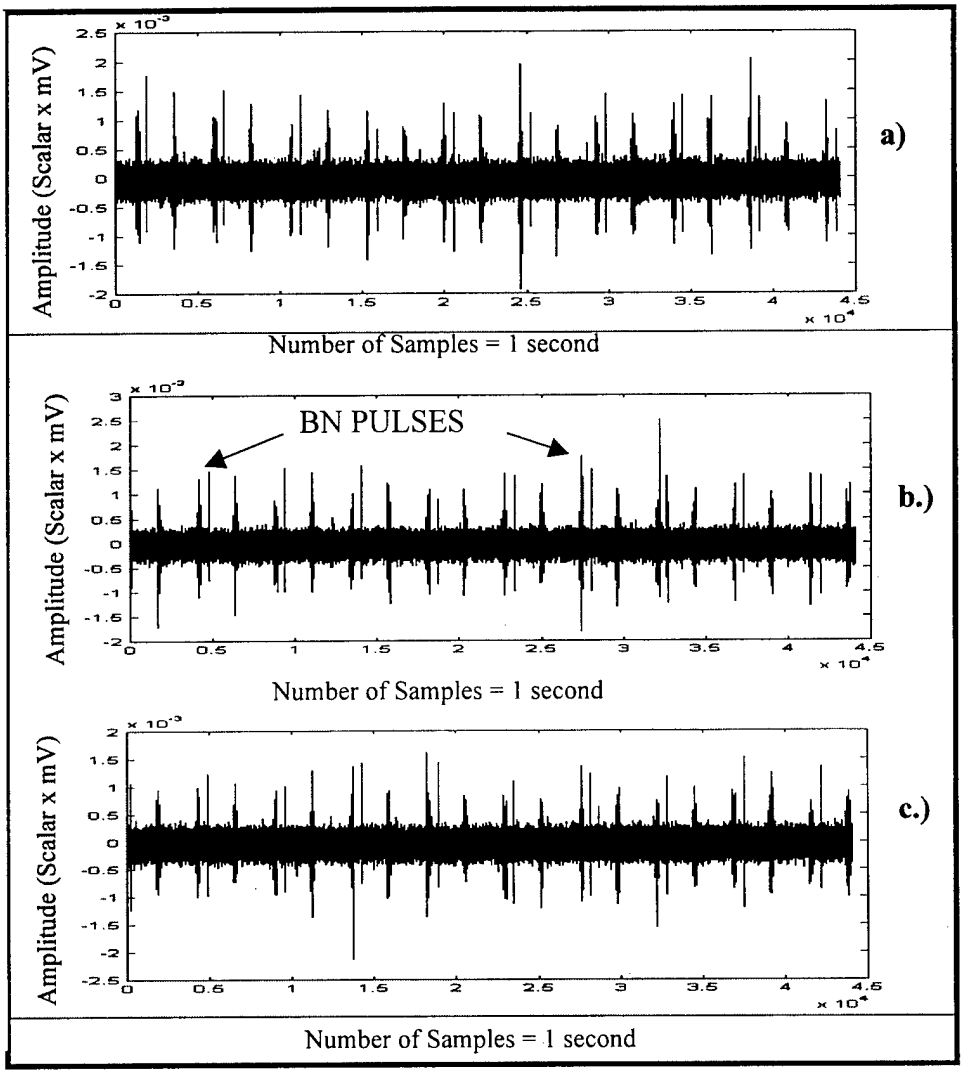


Fig. 9. Three tests with BN pulses. (a) Magnetized read head only (b) A nail placed in the magnetic field. (c) A core sample containing magnetite in the magnetic field.

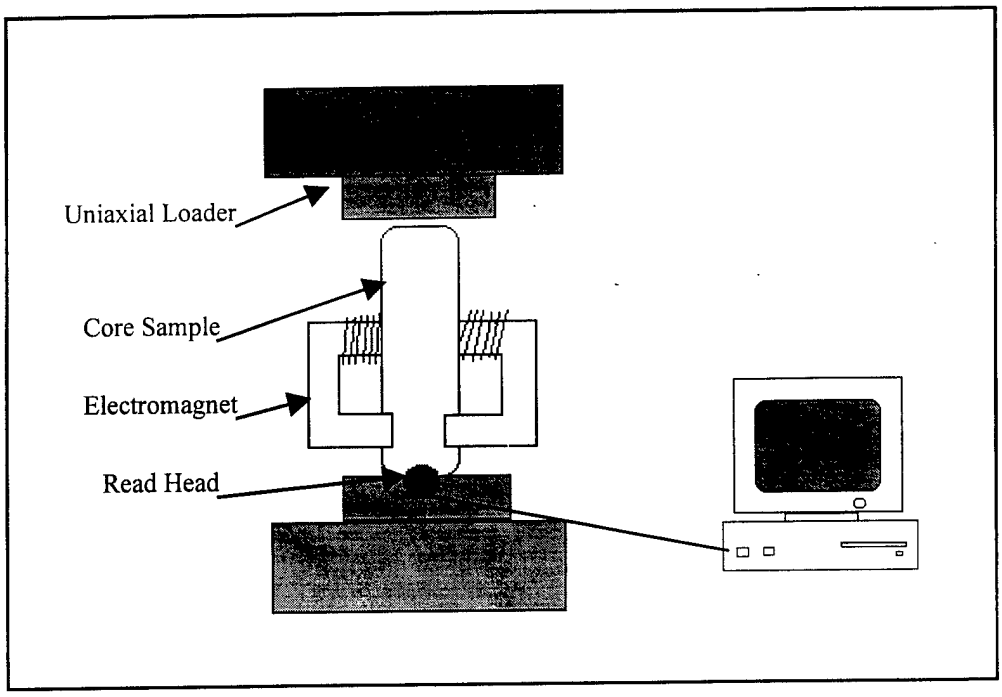


Fig. 10. Experimental loading setup.

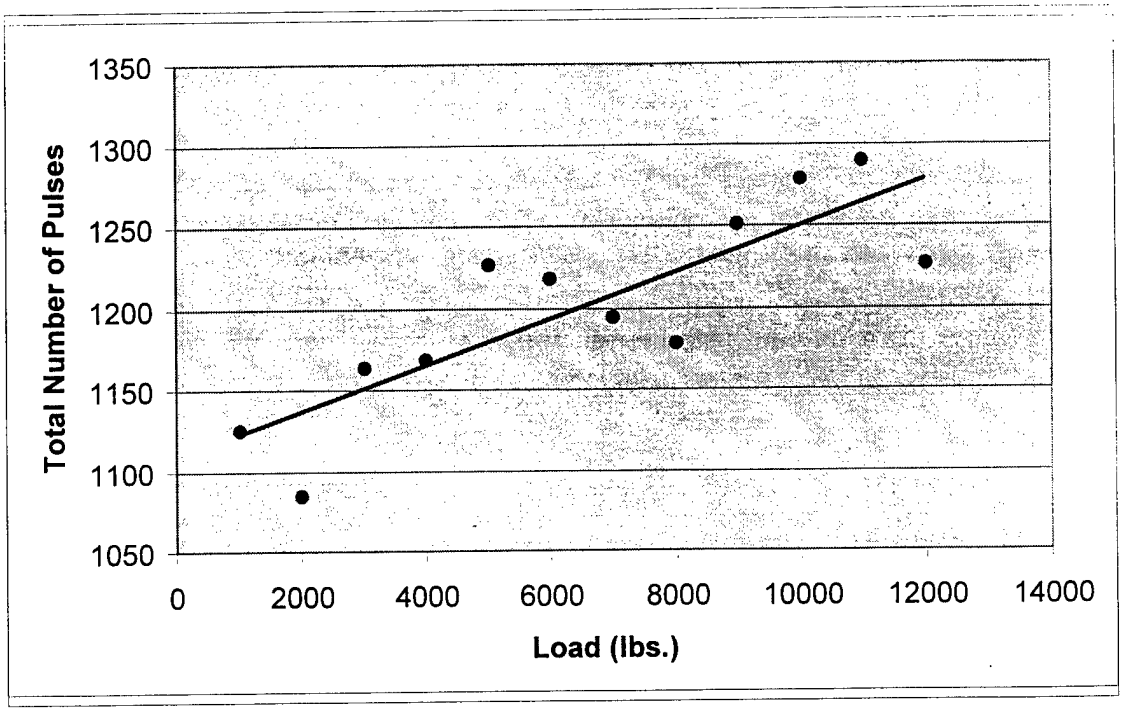


Fig. 11. Total number of BN pulses for each load level (●). A least squares best fit line has been added to show an increasing linear trend in the data.

# ELECTRICAL RESISTIVITY MONITORING

## Introduction

The electrical resistivity monitoring of a pillar of rock on the 3200 level of the Stillwater Mine, Nye, MT has been in progress for two years. During that time, seven sets of measurements have been made. The pillar is at depth of about 2000 feet below the ground surface and was excavated shortly before the observations began. The pillar is roughly triangular in cross section. (See Figure 1.) Eight electrodes were utilized to make electrical measurements of the pillar and surrounding rock. These measurements were used to develop a tomographic model of the pillar and the neighboring rock. The model is a region 15 by 18 meters, subdivided into 270 blocks, 1 meter on a side.

## Results

Figure 12 shows a surface plot of the resistivity (vertical axis) versus the horizontal position in the model. The electrode positions are shown as circles and the outline of the pillar is shown by the line connecting the circles. The model shows high resistivity (3,000 ohm-m) in the interior of the pillar, low resistivity (200 ohm-m) in the tunnels alongside the pillar and intermediate resistivity (1,000 ohm-m) in the surrounding rock.

Over the first six months (Figures 12 to 15) there is a gradual increase in the resistivity of the rock outside the pillar from 1,000 ohm-m to 3,000 ohm-m and some increases and decreases within the pillar. By the time one year has passed, (Figure 16) the region exterior to the pillar has returned to values similar to that at the start (Figure 12) and the values within the pillar are somewhat lower.

During the second year (Figures 16 to 18), the resistivity in the region outside the pillar increases in the winter (Figure 17) and decreases in the summer (Figure 18), similar to the cycle in the first year. This cyclic behavior in the exterior region suggests a source connected with the weather conditions at the surface. One possibility is that the freezing of the precipitation and the shallow groundwater removes a source of porewater at depth (2,000 feet), resulting in a increase in the resistivity. The apparent in-phase response of the rocks at depth to the available liquid water at the surface implies a well connected hydraulic system.

The resistivity changes in the pillar are more easily seen by plotting the ratio of the modeled resistivity at a particular date to the resistivity at the start of the series. These results are shown in Figures 19 to 24 as contour plots of log2(resistivity ratio). An increase (decrease) of one unit is then equal to an increase of 2x (decrease of ½x ) in the resistivity. Figures 19, 20 and 21 show a pattern of decreasing resistivity in the central part of the pillar, while at the same time the resistivity is increasing outside of the pillar. The decrease is still present in the summer of 1998 (Figure 22) and persists the following winter (Figure 23). The effect is present the next summer with some decrease in magnitude (Figure 24) and there is the suggestion that the low is moving from the pillar into the surrounding rock.

## Discussion and Conclusions

The monitoring and modeling of pillar region for two years has revealed an apparent seasonal cycle in some of the rock surrounding the pillar and a general decrease in the resistivity of the pillar. There is a possibility that this decrease is migrating from the pillar to the surrounding rock.

In the last report, a discussion of some other observed resistivity changes in response to stress did not seem to help in the interpretation of this data from the Stillwater Mine. Temperature effects this deep in a mine also seem unlikely. It was suggested that opening of cracks and redistribution of pore water might be a more plausible explanation. The apparent response of some of the surrounding rock to the availability of surface water was completely unexpected.

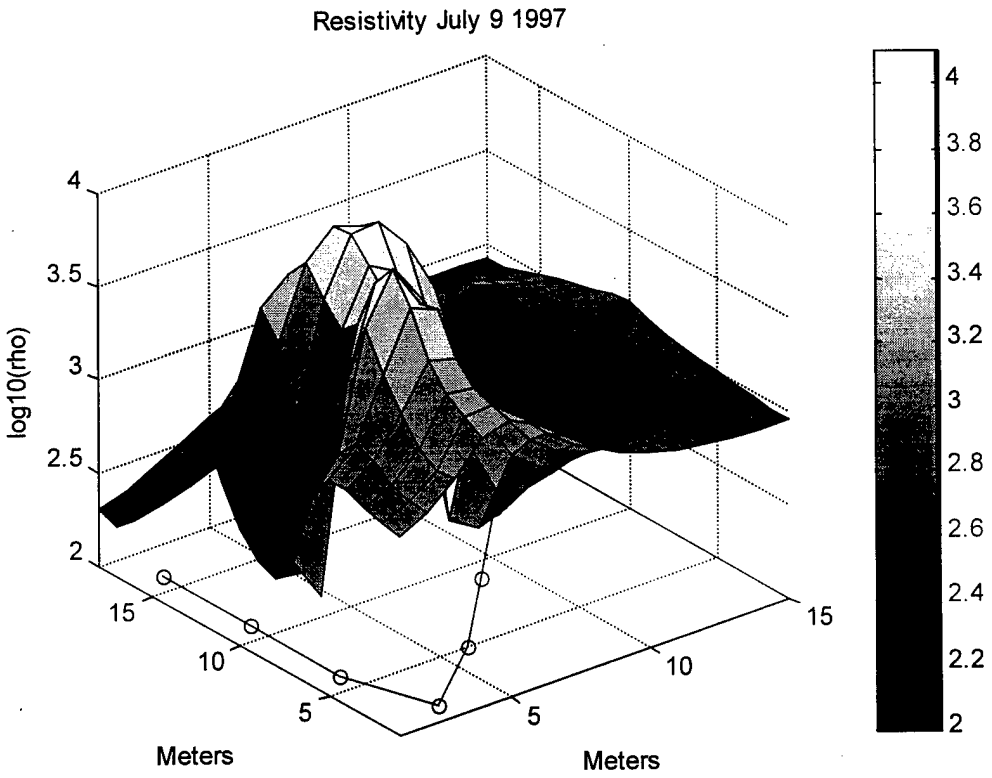


Fig. 12. Surface plot of resistivity in a pillar in the Stillwater Mine. The electrode positions are shown as circles and the outline of the pillar is shown by the line connecting the circles.

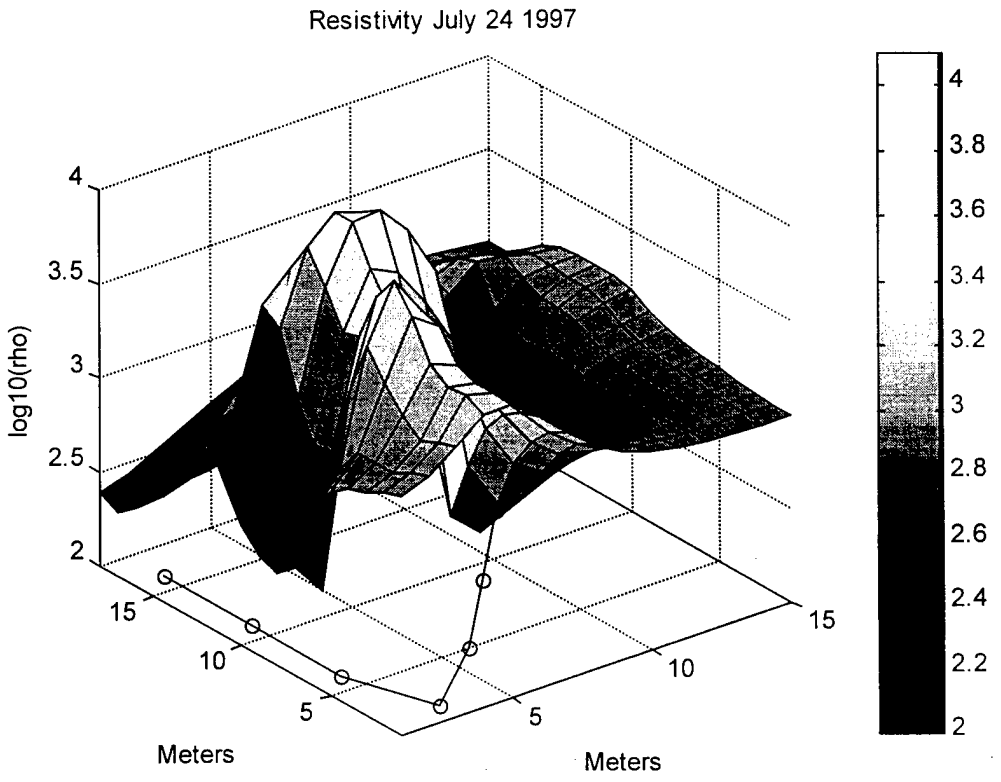


Fig. 13. Surface plot of resistivity in a pillar in the Stillwater Mine. The electrode positions are shown as circles and the outline of the pillar is shown by the line connecting the circles.

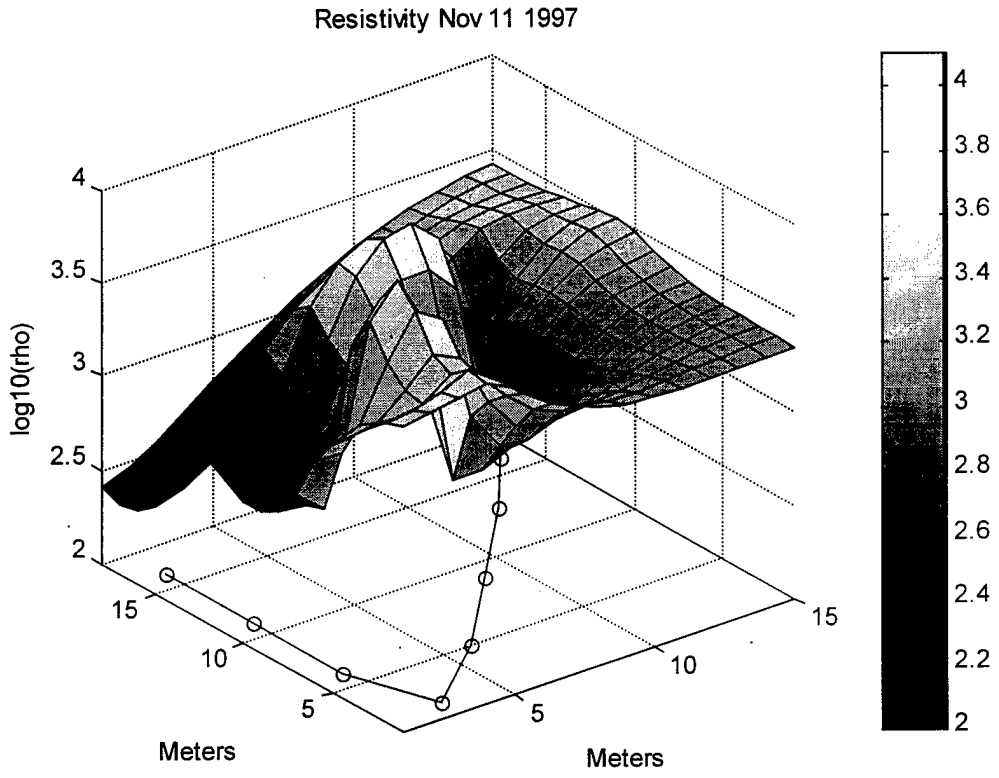


Fig. 14. Surface plot of resistivity in a pillar in the Stillwater Mine. The electrode positions are shown as circles and the outline of the pillar is shown by the line connecting the circles.

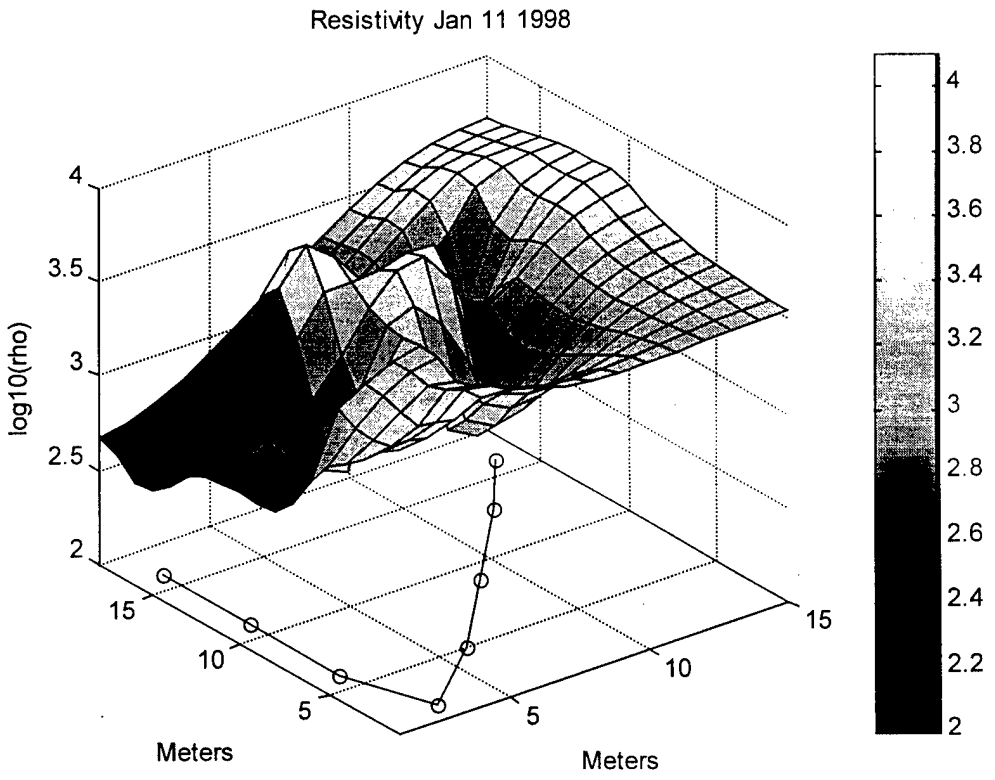


Fig. 15. Surface plot of resistivity in a pillar in the Stillwater Mine. The electrode positions are shown as circles and the outline of the pillar is shown by the line connecting the circles.

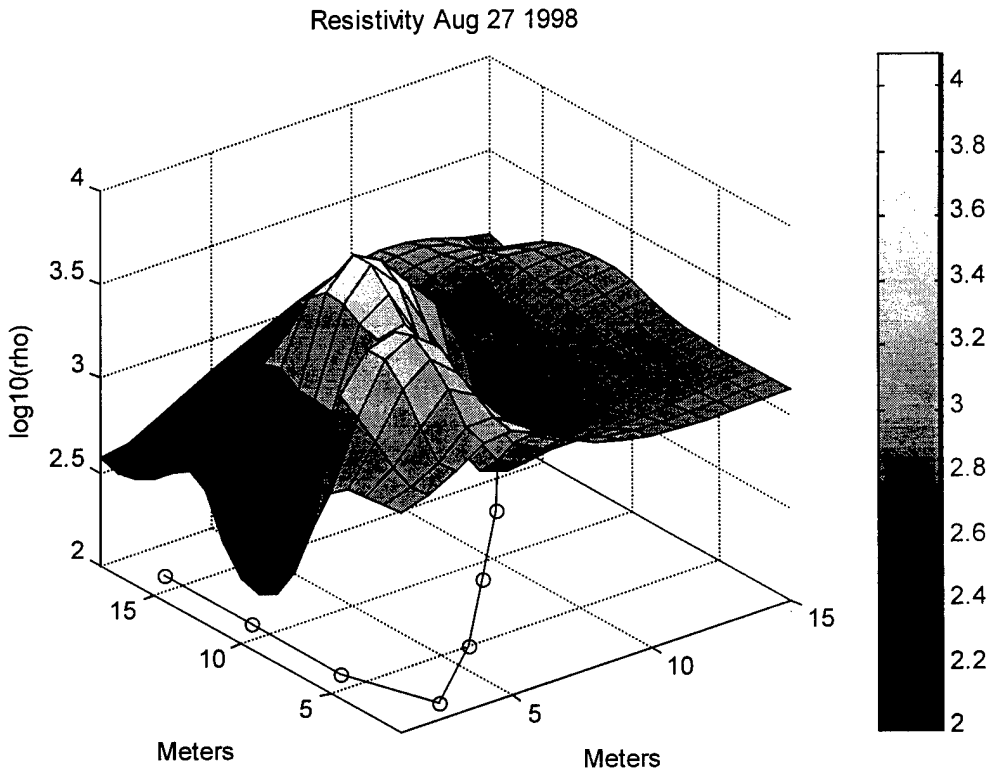


Fig. 16. Surface plot of resistivity in a pillar in the Stillwater Mine. The electrode positions are shown as circles and the outline of the pillar is shown by the line connecting the circles.

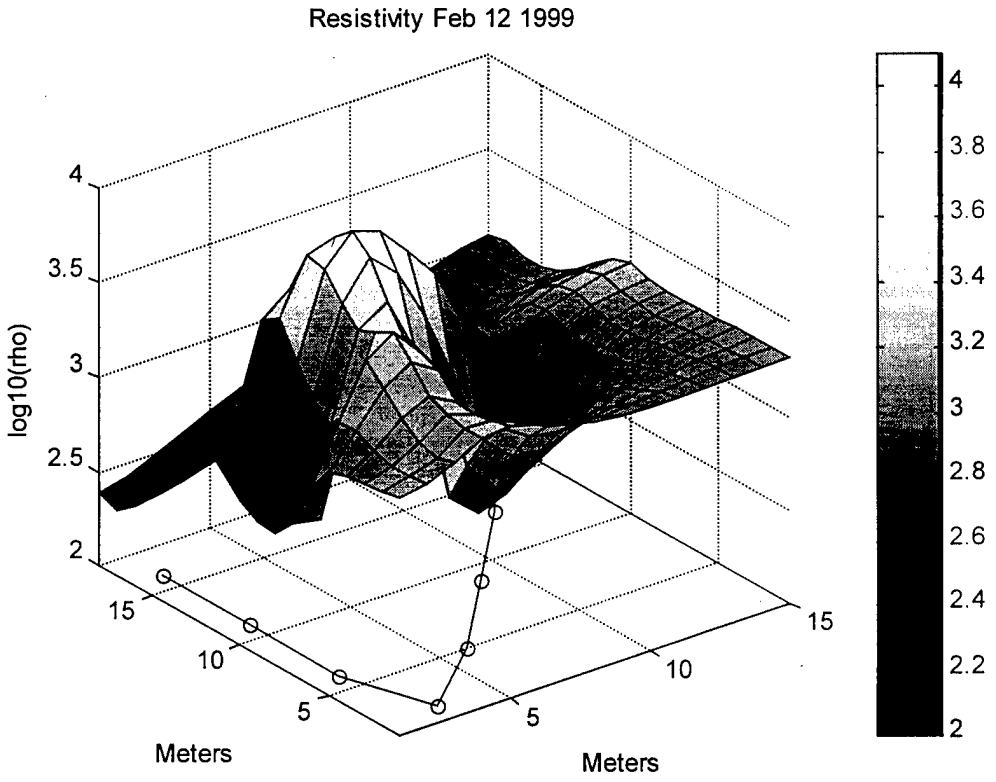


Fig. 17. Surface plot of resistivity in a pillar in the Stillwater Mine. The electrode positions are shown as circles and the outline of the pillar is shown by the line connecting the circles.

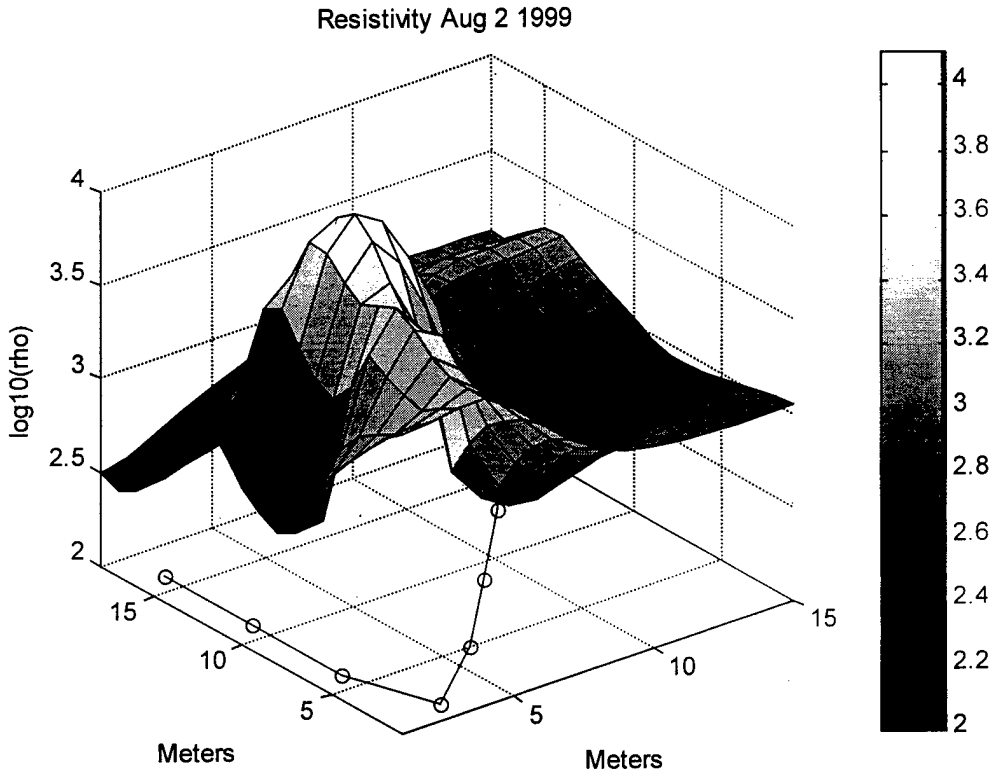


Fig. 18. Surface plot of resistivity in a pillar in the Stillwater Mine. The electrode positions are shown as circles and the outline of the pillar is shown by the line connecting the circles.

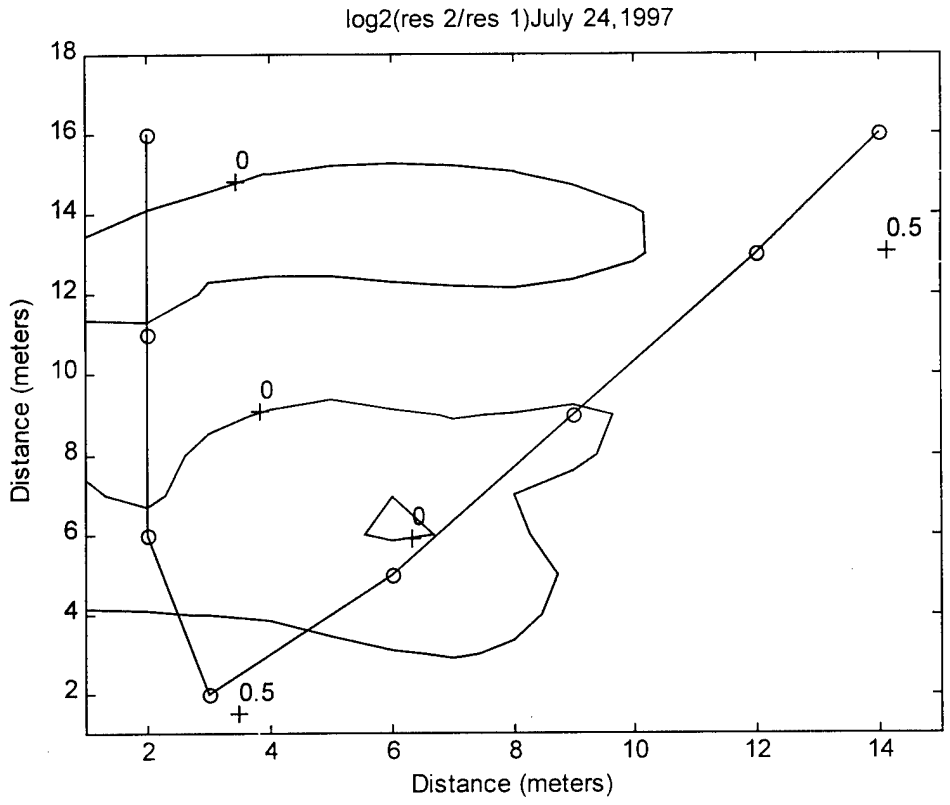


Fig. 19. Contour plot of log2(resistivity ratio) for a pillar in the Stillwater Mine. The electrode positions are shown as circles and the outline of the pillar is shown by the line connecting the circles.

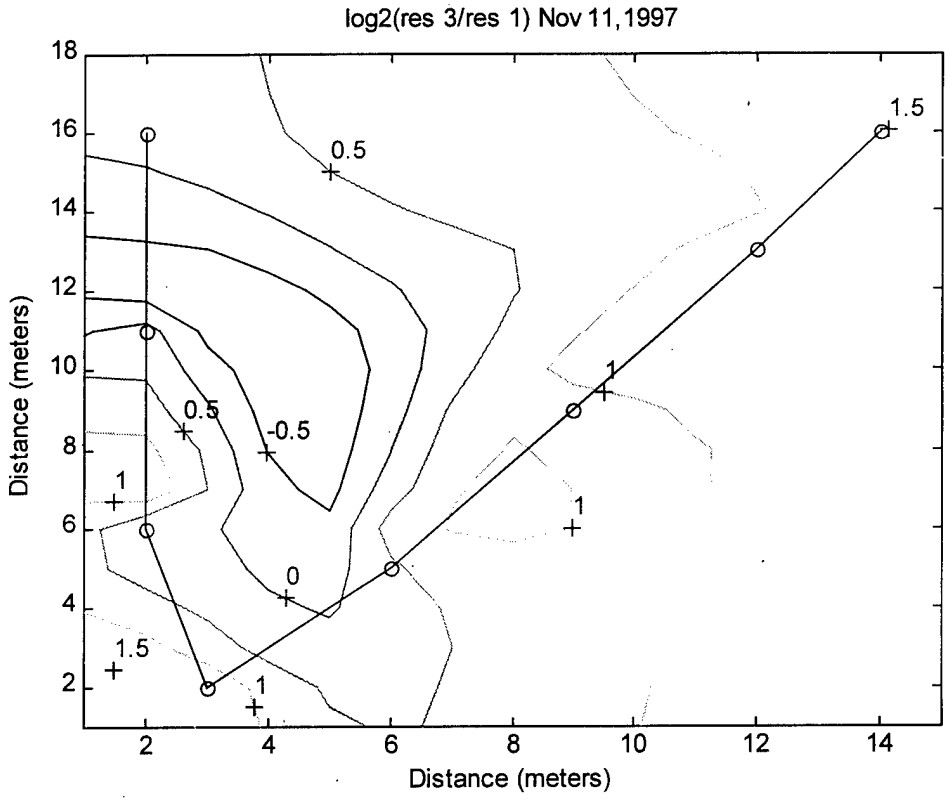


Fig. 20. Contour plot of log2(resistivity ratio) for a pillar in the Stillwater Mine. The electrode positions are shown as circles and the outline of the pillar is shown by the line connecting the circles.

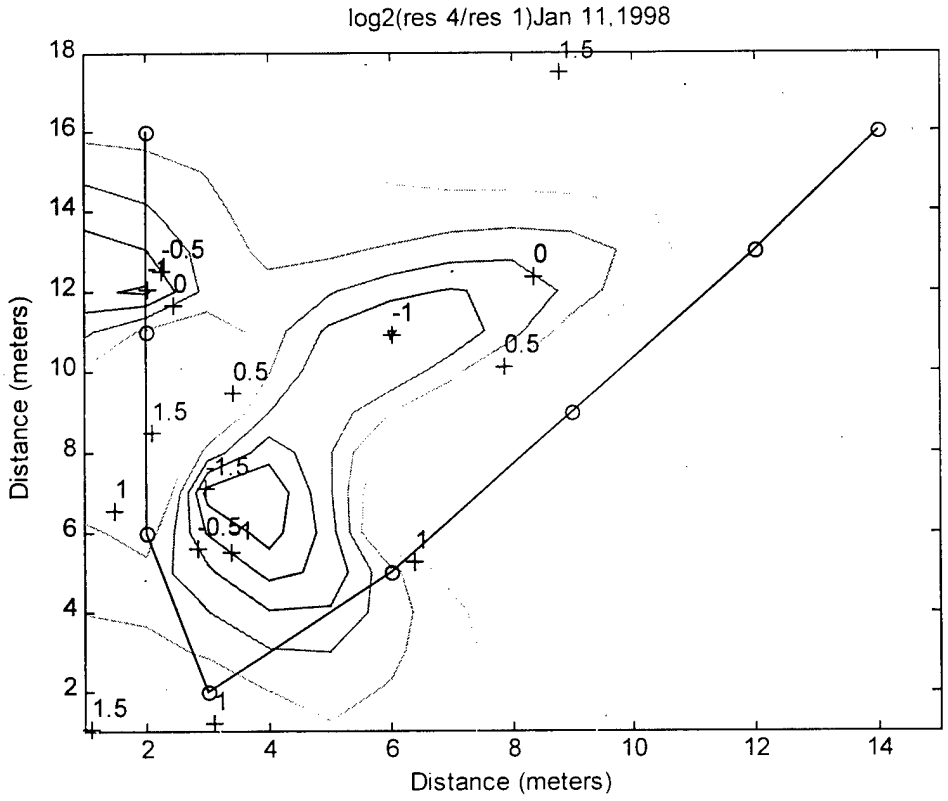


Fig. 21. Contour plot of log2(resistivity ratio) for a pillar in the Stillwater Mine. The electrode positions are shown as circles and the outline of the pillar is shown by the line connecting the circles.

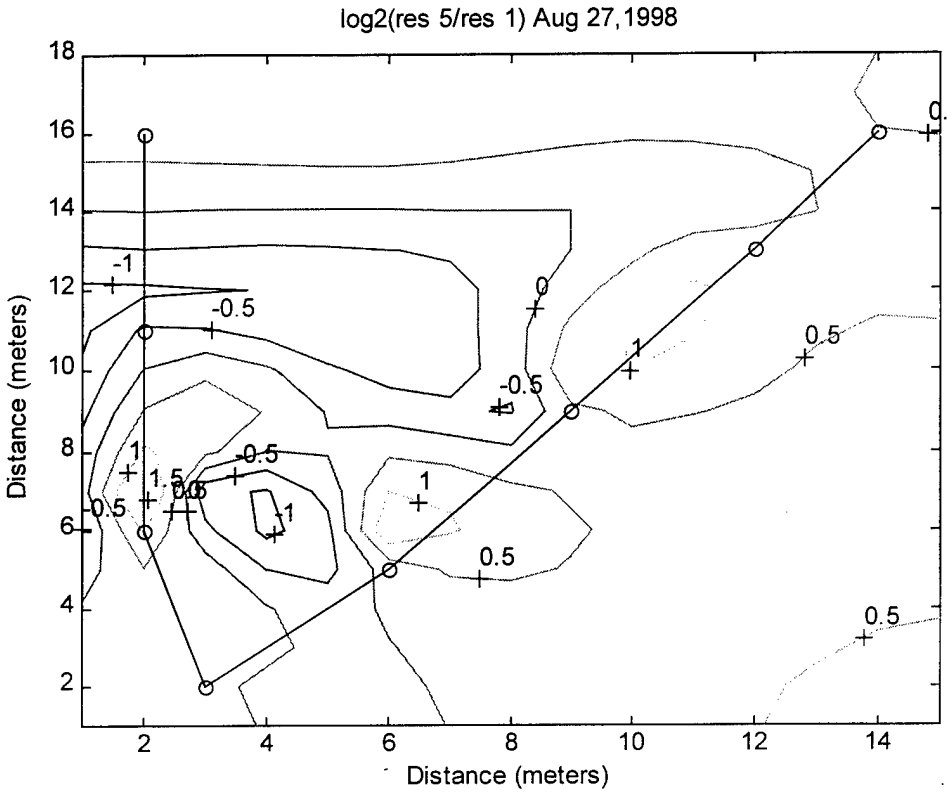


Fig. 22. Contour plot of log2(resistivity ratio) for a pillar in the Stillwater Mine. The electrode positions are shown as circles and the outline of the pillar is shown by the line connecting the circles.

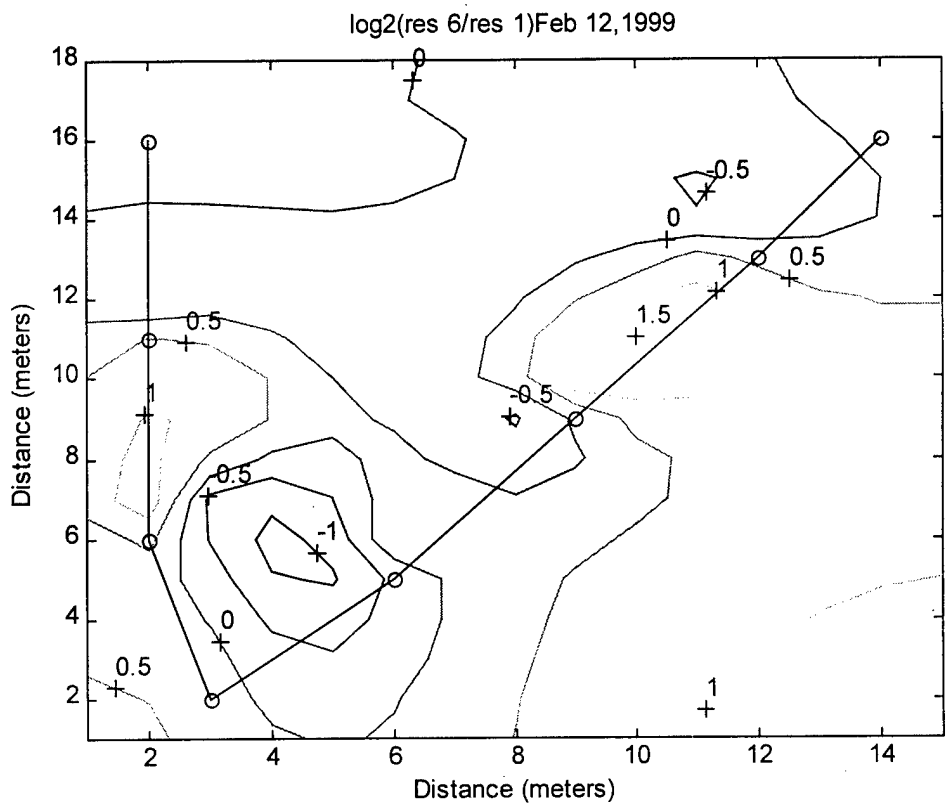


Fig. 23. Contour plot of log2(resistivity ratio) for a pillar in the Stillwater Mine. The electrode positions are shown as circles and the outline of the pillar is shown by the line connecting the circles.

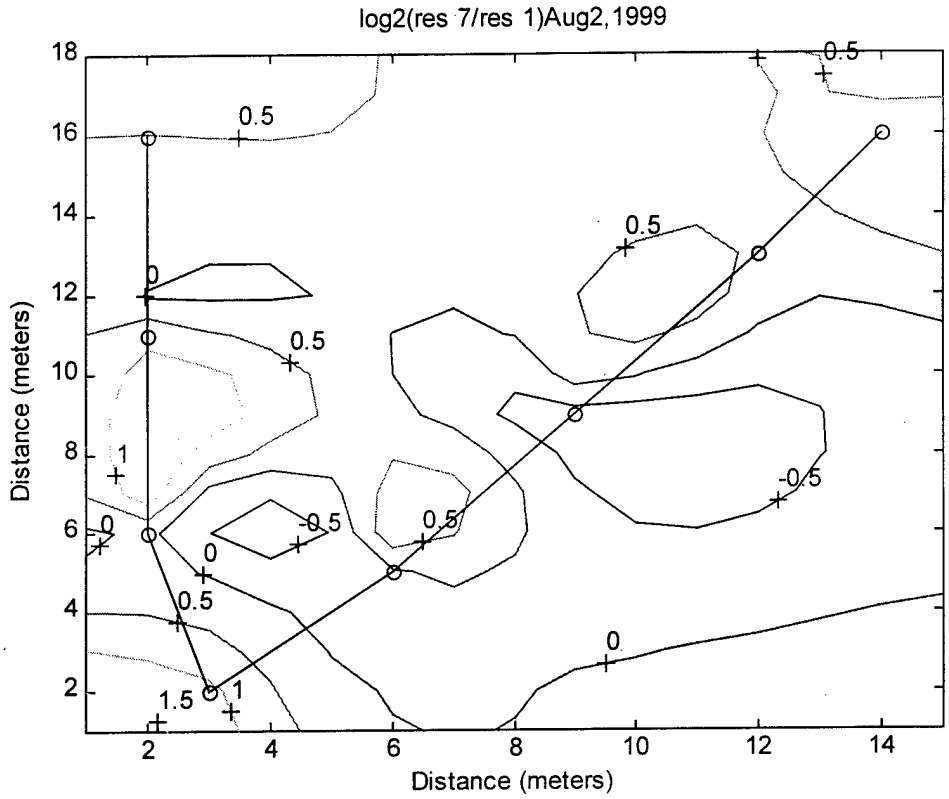


Fig. 24. Contour plot of log2(resistivity ratio) for a pillar in the Stillwater Mine. The electrode positions are shown as circles and the outline of the pillar is shown by the line connecting the circles.

# ROCKBURST SOURCE MECHANISM STUDIES


## Summary

Source mechanisms for an addition 15 rockbursts in the Lucky Friday Mine of Northern Idaho have been determined. The rockburst events had equivalent Richter magnitudes ranging from approximately 2.5 to 3.5, and in some cases caused extensive damage to mine workings. All of the events were within 5700 ft of the surface, and would therefore be classified as extremely near surface seismic events. Naturally occurring earthquakes in this geographic region have focal mechanisms much deeper than the rockburst events. All of the rockburst source mechanisms have equivalent double couple sources similar to those caused by earthquakes. None of the rockburst events can be explained by implosive or explosive types of source mechanisms.


## Background

An array of geophones is distributed throughout the Lucky Friday Mine near Mullen, Idaho. The positions of the geophones are restricted by the accessibility of mine openings, so the spatial distribution of the detectors is limited. Researchers at the U. S. Bureau of Mines have recognized the problems associated with using geophones within mines for source mechanism studies. For source mechanism determinations, not all quadrants are equally covered, and optimal distances may not be obtained. Some of the geophones are near the elevation of the rockbursts, and the result is that there are uncertainties in stereonet projections. There are often several geophones near nodal planes for various seismic wave phases, so that small location errors in the source position cause large changes in source mechanism estimation. In the case of the Lucky Friday Mine, there is an independent seismic system that has many geophones located near the working faces of the mine, and that system is utilized to locate events within a few meters. The independent seismic system is called the micro-seismic system, and the source mechanism system is called the macro-seismic system. In most cases, the effects of source location error may be minimized.

## Results

Table 2 lists studied rockburst events. All of the rockburst events occurred within 5500 ft of the surface. Therefore all of the mining induced seismic events tend to have shallower epicenters than the natural earthquakes of the region. All of the rockbursts have source mechanisms that are similar to standard double couple events produced by tectonic activity, and therefore the source mechanisms are similar to earthquake sources. None of the events appear to have either implosive or explosive source mechanisms. Standard "beach ball' type illustrations used to show earthquake events are shown in Appendix A, and are used to show the possible double couple mechanisms for each rockburst event studied. In some cases, more than one solution is possible. When multiple solutions are found, they are included. The first solution shown for each event is the preferred solution because that particular one is most compatible with the geometry of the mine workings.

Table 2. Table of Events

| DATE | TIME | MAGNITUDE | COMMENTS |
|---|---|---|---|
| 1-13-95 | 12:36:07 AM | | Dip slip N/S |
| 5-27-95 | 04:17:22 AM | | Dip slip E/W |
| 6-22-95 | 09:38:18 PM | | Dip slip E/W |
| 9-19-95 | 01:40:37 PM | | Strike slip NW/SE |
| 2-8-96 | 06:01:30 PM | 3.5 | Strike slip NE/SW |
| 3-2-96 | 12:37:35 AM | 2.6 | Dip slip NE/SW |
| 4-2-96 | 10:00:01 PM | 2.8 | Strike slip NW/SE |
| 5-30-96 | 03:00:40 AM | 3.5 | Strike slip NE/SW |
| 9-26-96 | 02:59:29 PM | 2.8 | Strike slip N/S |
| 11-1-96 | 06:24:26 PM | 2.7 | Strike slip E/W |
| 12-20-96 | 12:38:37 AM | 2.6 | Dip slip E/W |
| 2-14-97 | 12:37:55 PM | 2.5 | Dip slip NW/SE |
| 3-14-97 | 12:09:18 PM | 3.6 | Dip slip NW/SE |
| 5-25-97 | 08:34:08 AM | 2.6 | Dip slip NW/SE |
| 06-27-97 | 08:02:38 PM | 3.5 | Strike slip NW/SE |

# MODELING OF ROCK-BOLT FLEXURAL MODES

## Introduction

Rock bolts are important components in modern underground mining operations. Rock bolts provide basic support for unstable, fractured rock by coupling rock subunits or linking with stable rock beyond weak rock zones (MESA, 1989). Numerous types of rock bolts are available including grouted bolts, mechanical bolts, and friction bolts. The two types that are discussed in this report are grouted bolts and friction bolts. The Stillwater Mine in Nye, Montana uses grouted bolts that are eight feet long and split-set bolts five feet long. A modal analysis of the split-set bolt is discussed in a following section. Additionally, computer simulated frequency responses of a 'rebar' bolt are compared with closed-form solutions and experimental data.

One of the difficulties in determining the effectiveness of rock bolts is the difficulty of determining the exact condition of the bolt in the borehole (Jumikis, 1983). One goal of this project was to determine how close computer-modeling results were to closed-form solutions and experimental data in terms of frequency response.

## Rock Bolts

An overview of basic rock-bolt characteristics is contained in the following sections.

### Split-set

The split-set bolt is classified as a friction bolt because no grouting material is used to hold the bolt in place. This friction coupling permits the bolt to yield when movement occurs rather than fail (Ingersoll-Rand, 1996). The bolt is a hollow tube, typically 1 ½" in diameter, ¼" thick, with a ½" split along one side (Figure 25). A ring flange is welded to one end to hold the faceplate against the rock and the other end is tapered for easier installation.

Boreholes for split-set bolts are typically 1 3/8" in diameter. The bolt is driven into the borehole with a driver tool and instantly exerts a radial pressure against the rock along the entire length of the bolt (Ingersoll-Rand, 1996). In addition to the radial pressure, plate loading is also generated immediately.

The natural modes of the split-set bolt were calculated using finite element analysis. The finite element mesh that was used was a rectangular shell mesh with a specified thickness of 0.10 inches. The mesh was five feet long, which is the length of the bolts used in the Stillwater Mine. A close-up of the mesh is shown in Figure 26.

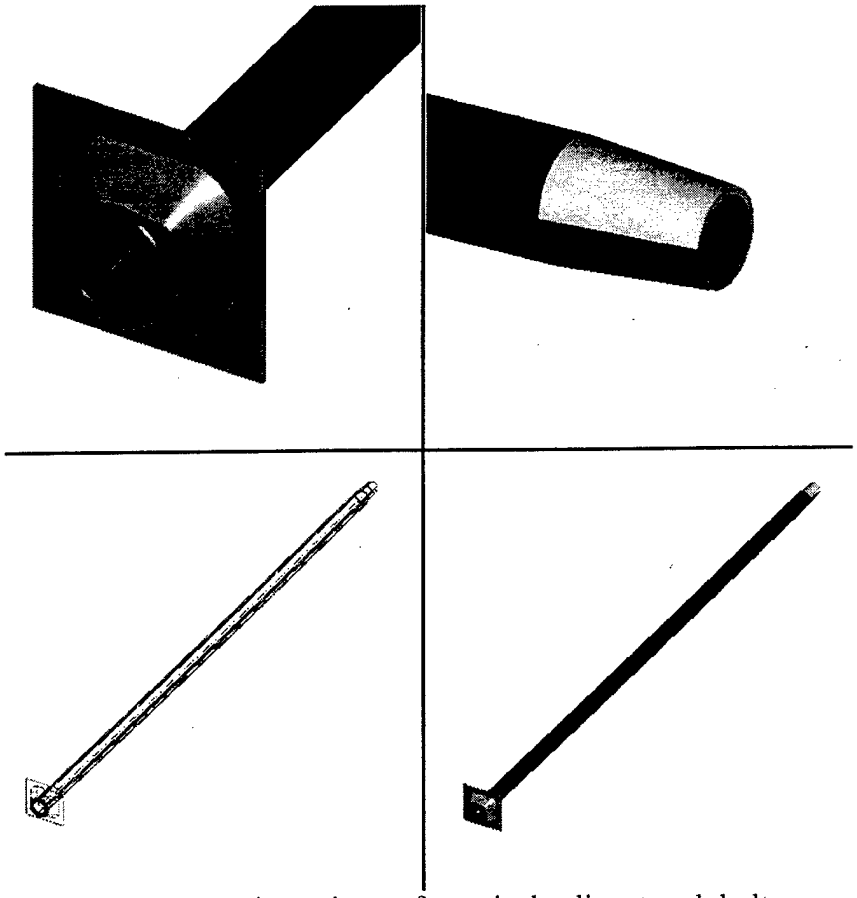

Fig. 25. Various views of a typical split-set rock bolt.

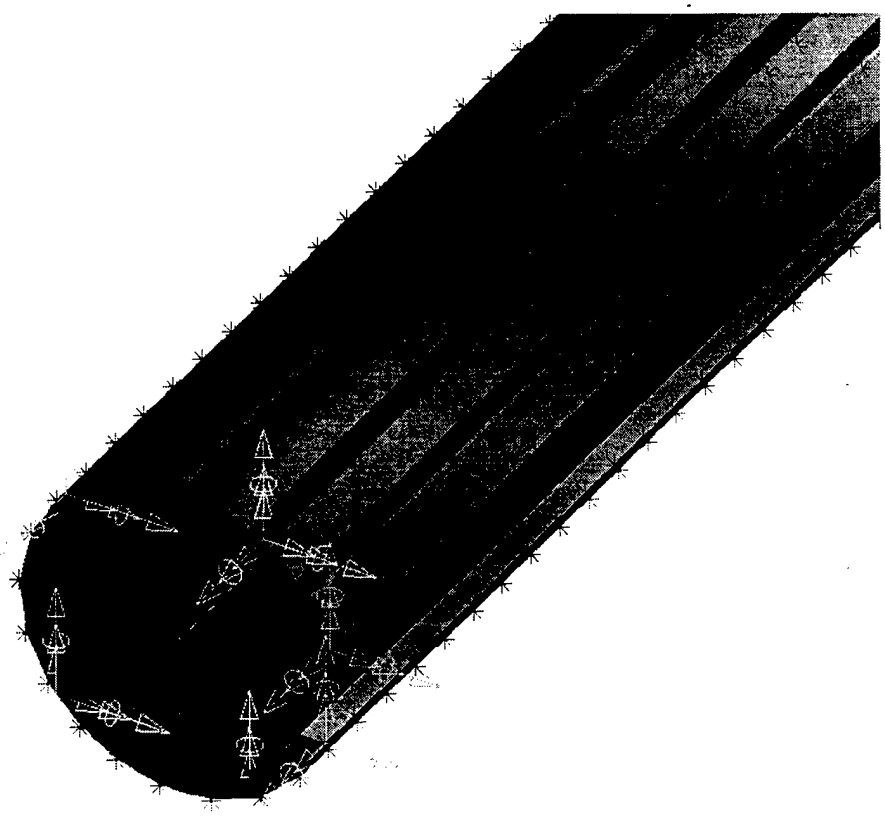

Fig. 26. Details of the split-set rock-bolt mesh.

In Figure 26, asterisks represent element nodes. The rectangular form of the elements is evident and the boundary conditions used in the modal analysis are shown as arrows on the edge of the bolt.

**Rebar**

The rebar bolt represents a fundamentally different system than the split-set rock bolt. For the case of rebar, the borehole diameter is larger than the rock-bolt diameter. Typically used rock-bolt diameters are ¾" and common borehole diameters are 1 3/8". Grouting material choices are resin or cement. Both materials have decided advantages and disadvantages. Resin is faster setting, but is more expensive than cement.

The rock bolt is installed by inserting tubes of the grouting material and catalyst, then driving the bolt into the borehole. Twisting the bolt inside the borehole breaks the tubes of grouting material and catalyst and mixes them together to form an adhesive bond (Hoek, 1995). Rebar lacks the instantaneous support typified by split-set bolts, but is nevertheless an effective bolting device.

Because a rebar bolt is solid; unlike a split-set bolt, a beam mesh was used in the finite element method. The cross-sectional area of the bolt varied between 11/16" and 13/16" because of the ridges present on rebar. A beam mesh was created by creating a

line along the length of the beam and specifying a cross-section. The element length was 1/8" which is equal to the spacing of the ridges.

## Split-set Modal Analysis

One of the primary goals of the modal analysis was to compare computer-generated results with in situ measurements from the Stillwater Mine. Because split-set bolts were not used in the mine test area, the split-set analysis was performed to become familiar with the modeling software and to compare with modeling results from the rebar. The computer-generated modes are found in Appendix B for modes one, three, five, six, and seven.

The split along the side of the hollow tube has an interesting effect on the modes of the split-set bolt. Mode three consists of a radial expansion, along with a slight bending mode (Figure B-2, Appendix B). The first mode consists of a simple bending mode with little or no radial expansion (Figure B-1). Modes five and seven display bending modes with minimal radial expansion (Figures B-3, B-5), however mode six (Figure B-4) demonstrates both bending and expansion.

## Rebar Bolt Analysis

### Closed-form solution vs. I-DEAS

To determine the validity of finite element modeling of rock bolts, the results of the computer-simulated solutions were compared to analytic results. Closed-form solutions for axial vibrations, lateral vibrations, and a clamped string were used for the comparison.

Axial bolt vibrations

The closed-form solution for axial vibrations in a rock bolt that is clamped or free at both ends is given by (1) (Tannant, 1995). Calculations from this equation were compared to the finite element modeling results for the same bolt configuration. In equation (1), $f_n$ is the axial frequency of the rock bolt, Y is Young's modulus of steel, $\rho$ is the density of steel, and L is the length of the rock bolt.

$$f_n = n\left(\frac{\sqrt{\frac{Y}{\rho}}}{2L}\right) \tag{1}$$

Young's modulus for steel is 200 GPa and the density of steel is 7800 kg/m$^3$. Using a length of two meters for the bolt yields a first harmonic frequency of 1270 Hz.

Using I-DEAS, a beam mesh two meters long was created with a diameter of 16 mm. Using fixed boundary conditions at both ends, the first axial mode of the bolt was calculated. The frequency of the first harmonic frequency of the bolt, as calculated by I-DEAS, was 1290 Hz. The percent difference between the I-DEAS solution and the closed-form solution is 1.57%. The two solutions are very close indicating that I-DEAS accurately models the axial frequency of a bolt clamped at both ends.

Lateral bolt vibrations

The second closed-form equation is for lateral bolt vibrations and is given in (2) where $f_n$ is the fundamental frequency, L is the length of the rock bolt, Y is Young's modulus for steel (200 GPa), ρ is the density of steel (7800 kg/m3), I is moment of inertia, and A is the circular cross-sectional area of the bolt.

$$f_n = \beta_n^2 \left(\frac{1}{2\pi L}\right)\sqrt{\frac{YI}{\rho A}} \tag{2}$$

As for (1), the length of the rock bolt is two meters and the diameter is 16 mm. Moment of inertia (I) is calculated using (3) (Weaver, Jr., 1980).

$$I = \frac{\pi r^4}{4} \tag{3}$$

The variable $\beta_n^2$ is a boundary condition constant the values for which were found in *Engineering Vibration* (Inman, 1996). Values for each boundary condition and the fundamental frequencies from both solutions are given in Table 3.

Table 3. Lateral Bolt Vibration Fundamental Frequencies

| Boundary Condition | $\beta_n^2$ | Closed-form solution (Hz) | I-DEAS solution (Hz) | % difference |
|---|---|---|---|---|
| Fixed-Free | 3.52 | 2.84 | 2.88 | 1.41 |
| Fixed-Hinged | 15.4 | 12.41 | 12.62 | 1.69 |
| Fixed-Fixed | 22 | 17.73 | 18.31 | 3.27 |

The percent differences show that the I-DEAS finite element modeling accurately models the lateral bolt vibrations.

Clamped string

The third closed-form equation was for the fundamental frequency of a string clamped at both ends under tension (4) (Tannant, 1995) where $f_n$ is the frequency, L is the length of the rock bolt (two m), T is the tension in the string, ρ is the density of steel (7800 kg/m3), and A is the cross-sectional area of the rock bolt.

$$f_n = n\left(\frac{1}{2L}\right)\sqrt{\frac{T}{\rho A}} \tag{4}$$

The diameter of the 'string' is 16 mm. Typical tensions in rock bolts range from 10 kN to 50 kN. In I-DEAS, the minimum and maximum of the range were used to calculate frequencies. The results are given in Table 4.

Table 4. Tensions and Frequencies for Closed-Form Solution Comparison with Finite Element Modeling

| Tension | Closed-form solution (Hz) | I-DEAS solution (Hz) | % difference |
|---|---|---|---|
| 10 kN | 20 | 29 | 45.00 |
| 50 kN | 45 | 51 | 13.33 |

The figures showing the results above are given in Appendix C as C-1 and C-2. The percent differences from this comparison are high and can be explained by the following: the equation for the clamped string was for a non-rigid string. However, a rock bolt is rigid and this most likely accounts for the large difference values.

Results

The results from the axial bolt vibration and lateral bolt vibration were encouraging. Percent differences for the first two comparisons were low and indicative of realistic modeling parameters. The percent differences for the clamped string were large but can be explained by the difference in rigidity of the rock bolt and the string closed form solution.

**Experimental data vs. I-DEAS modeling**

Another experiment was conducted to determine how accurately I-DEAS models compare with experimental results.

Laboratory testing

The experiment consisted of putting two rock bolts under tension and tapping the ends of the rock bolts with a hammer. Using a microphone, the frequencies of the induced vibrations were recorded. The experiment was semi-controlled in the sense that the tensions were measured, but not the amount of force for each tap.

The applied tensions to both the rebar and cold-rolled steel bolts were 1000 pounds and 5000 pounds. Each bolt was tapped twice on the top and the bottom. The sound recordings were transformed to the frequency domain and plotted. Signal-to-noise ratios were also calculated.

I-DEAS modeling

*Cold-rolled steel*

The initial and most important part of modeling in I-DEAS is to create the correct finite element mesh. Grip marks were imbedded into the bolt from the experiment, and the length of each grip was 3 5/8" long. The top grip started one inch from the top of the bolt, and the bottom grip was 7 ½" from the base of the bolt. Total length of the rock bolt, from the extra mass around the eye, was 19 ¾", leaving an effective length between the grips of 4". The diameter of the rock bolt was 5/8" (Figure 27).

A beam cross-section of 5/8" diameter was created for the entire beam. The elements were formed to be 1/8" long. To recreate the effects of the grips, boundary conditions were set at every node in the areas that the grips were placed. All of the rotational degrees of freedom and translation in the axial direction were free in the boundary conditions (Figure 27).

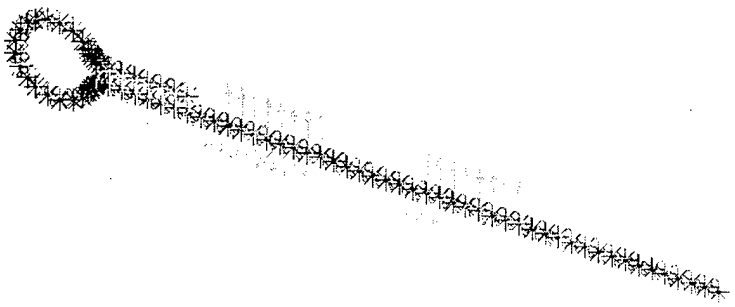

Fig. 27. Cold-rolled steel bolt mesh.

In addition to the boundary conditions, a load of 1000 pounds was applied to the boundary conditions closest to each end to represent the tension applied to the rock bolt. To compare results from the sound recordings and modeling in I-DEAS, solutions were developed for the normal modes of the bolt. These normal modes represent what occurs if the bolt is excited at a certain frequency (Figure 28).

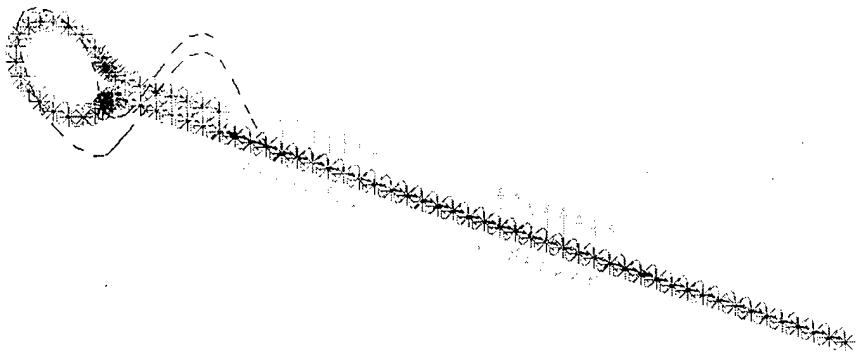

Fig. 28. Normal mode at 4240 Hz for cold-rolled steel bolt.

The normal mode frequency for the cold-rolled steel bolt under a tension of 1000 pounds was 4240 Hz (Figure 28). This agrees with the experimental results shown later.

*Rebar*

A similar analysis was completed for a rebar bolt. The dimensions of the rebar bolt were different than the cold-rolled steel bolt. The total length of the rebar was 26 5/8". The grips were 3 5/8" from one end, and 2 7/8" from the other end. As with the cold-rolled steel, the grip lengths are 3 5/8" but they react in different ways. Because the rebar has ridges, the grip contact points occur only along the ridges. Originally, the bolt model was meshed by making the element widths the same width as the ridge spacing (1/8") with a cross-section 11/16" in diameter. However, this was changed so that the diameter of every third element was 13/16", which is the diameter of the ridges (Figure 29).

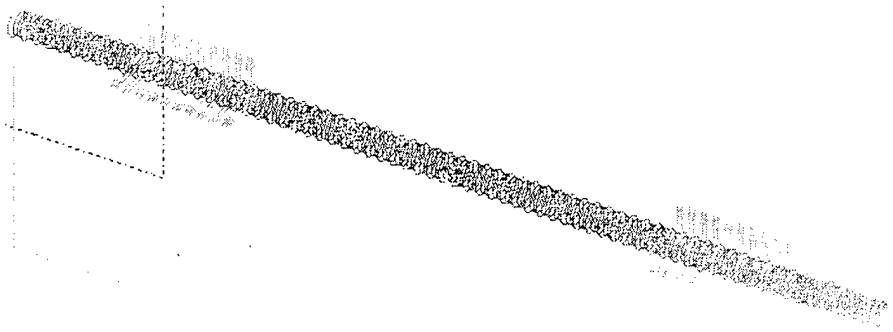

Fig. 29. Rebar rock bold mesh for finite element modeling.

The boundary conditions were applied to the bolt along the nodes of the ridge elements. Again, all but the end boundary condition allowed free rotational displacement and free translational displacement in the axial direction. The end boundary condition allowed free rotational displacement, but all of the translational displacements were fixed (Figure 30).

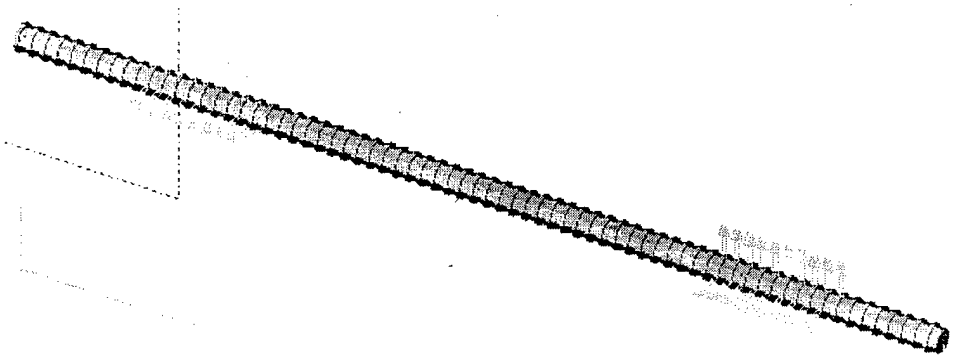

Fig. 30. Solid rebar and boundary conditions.

Next, an excitation function was created in I-DEAS to provide an impulse to the bolt to simulate a hammer tap on the experimental bolt. The applied excitation was a unit force of one pound. Because the actual force of the hammer tap could not be easily

determined, a unit force of one pound was used for the excitation. The force was applied axially and the reactions that are plotted are frequency responses in the axial direction. Without completely controlled experimental conditions, the hits may have been partially lateral, resulting in bending modes that do not appear on the computer simulated response plot. Results of the excitation are shown in Figure 31.

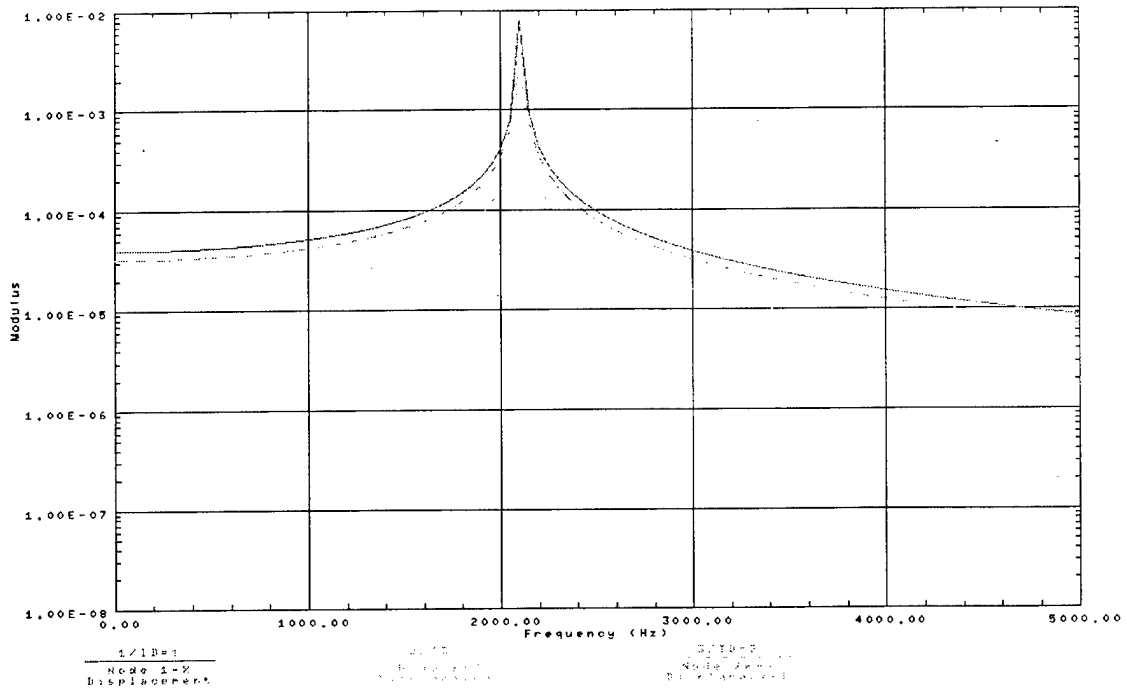


Fig. 31. Frequency response – rebar rock bolt (bottom excitation).

The vertical axis of the graph represents the magnitude of the displacement even though I-DEAS uses the term modulus as a general term for all vertical axis values. Below the horizontal -axis is a list of the rock-bolt nodes at which each displacement was calculated. When the bolt was struck in the lab, the sound that was recorded is a result of all of the nodes. In I-DEAS, the contribution from all the nodes is estimated by choosing a small number of nodes along the length of the bolt. The first axial mode in Figure 31 is shown as a peak at 2150 Hz. Experimental results correlate with the computer analysis for a rebar bolt excited on the bottom. We used the same excitation function on the bolt top. The results were shifted slightly from 2150 Hz to 2200 Hz from the bottom excitation results (Figure 32). This is expected because the length of the bolt does not change, nor do the boundary conditions on the bolt. The only thing that changes is the length from each end to the grips, but that change is small (3/4").

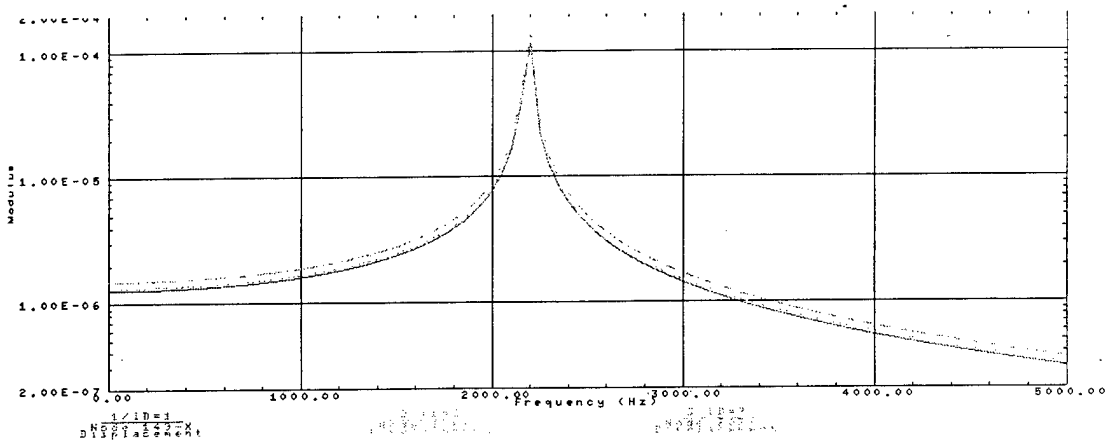


Fig. 32. Frequency response – rebar rock bolt (top excitation).

*Results*

The results from the comparison of experiment results and computer modeling are encouraging. Computer modeling is shown to be reliable when analyzing the effects of excitations and forces on rock bolts. The same initial axial modes that are appearing in the experimental recordings appear in the computer produced frequency response. Because the computer modeling compares well to experimental and closed-form solutions, it will next be applied to the rebar bolts found in the Stillwater Mine.

**Stillwater Mine Experiments**

To simulate the rock-bolt conditions in the Stillwater Mine, a finite element mesh was constructed that was eight foot long. Two varying sets of boundary conditions were used with constant excitations for comparison with experimental results.

The eight-foot rebar was meshed the same way that the smaller rebar bolt was meshed in the prior simulation using the ridges along the bolt. In a previous report by the U.S. Bureau of Mines, a finite element mesh was used to model a rock bolt, however, those results did not agree with experimental results (Serbousek, 1987). One of the reasons given for the disparity was that the finite element model did not truly match the behavior of the rock bolt because the ridges of the bolt were not modeled. In order to avoid this problem, ridges were included in our modeling. Boundary conditions were used at each node, except for the last four inches, to represent a completely bonded bolt. In the Stillwater Mine, part of the rebar protrudes from the wall, which is why four inches of the bolt are not restrained.

Meshing the bar and applying the boundary conditions provides a bolt that is completely bonded, even in between the ridges. In the modeled rebar mesh, the boundary conditions were along the ridges. This is different from the mine conditions in that the Stillwater Mine bolts are grouted, so that the grout bonds to all of the rock-bolt surface, not only to the ridges. The results from an impulse excitation are shown in Figure 33.

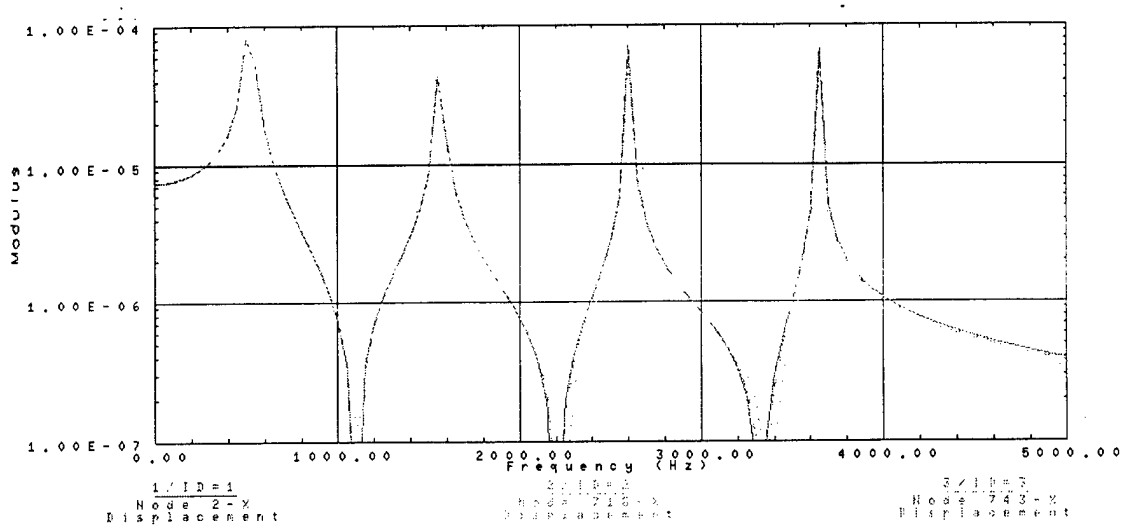


Fig. 33. Modeled Stillwater Mine rebar rock-bolt frequency response - completely bonded.

Frequency transformed sound recordings from the Stillwater Mine rebar rock bolts exhibit a similar series of peaks; however, the amplitude of the peaks decreases with frequency and the location of the peaks is shifted. The variations in the mine-recorded frequencies from the modeled frequencies could result from gaps in bonding, excitation of lateral as well as axial modes, or non-impulse type excitation.

A second set of boundary conditions was used for a rebar rock bolt that was half-bonded. The completely bonded end of the bolt represents the portion of a rock-bold inside a rock mass and the unbonded end represents the portion of the rock-bold external to the rock. The results from the frequency modeling analysis for the half-bonded bolt are shown in Figure 34.

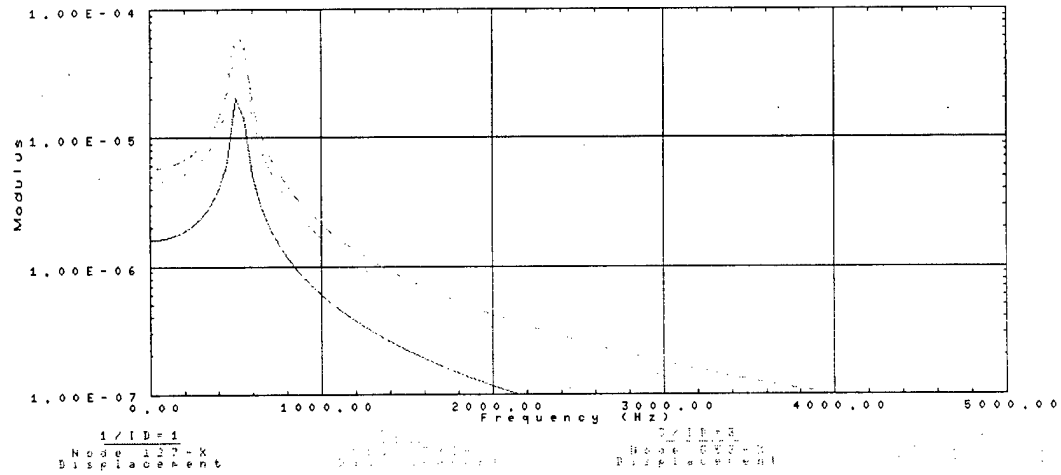


Fig. 34. Modeled Stillwater Mine rebar rock-bolt frequency response – half-bonded.

The most noticeable difference between the completely bonded bolt results and the half-bonded bolt results is the difference in the number of peaks. This seems to indicate that the degree of bonding is related to the number of peaks in the frequency response of the bolts. As can be seen, the first peak of the completely bonded bolt is at the same frequency as the peak of the half-bonded bolt. Further experiments and research can identify bonding conditions of rock bolts in more detail. One possibility is using a pulse-echo system to measure the travel times of sonic pulses in bolts (Tadolini, 1990) rather than a microphone.

## Conclusions

The purpose of this project was to determine the feasibility of modeling rock bolts and their associated frequency responses with finite element modeling as found in the computer software I-DEAS. When compared to closed-form solutions, I-DEAS modeled axial bolt vibrations and lateral bolt vibrations accurately (within 4% for all cases).

Laboratory experimental results were also compared to computer modeled frequency responses. Again, the results of laboratory experiments and the computer models were similar. This modeling was also applied to the rebar bolts used in the Stillwater Mine. Two situations were modeled: 1) completely bonded bolts, and 2) half-bonded bolts. The results of both computer-simulated situations were compared to actual recordings obtained from the Stillwater Mine. It can be inferred that the sample bolts in the Stillwater Mine were well bonded.

In conclusion, the modeling of rock bolts using the finite element methods as in the computer software I-DEAS is a useful technique. Further research will lead to a more detailed understanding of rock-bolt bonding and its role in mining safety.

# FREQUENCY RESPONSE OF ROCK-BOLT SOUNDINGS FROM HAMMER STRIKES

## Introduction

This research consisted of analysis of acoustic rock-bolt signatures to determine frequency content. Rock bolts relieve loading stress and add support along mine walls. Under high stress loading, rock bolts can loosen and fail. This can trigger cave-ins during blasting, earthquakes, and rockbursts (Otuonye, 1998). If viable, this research would contribute to an inexpensive, quick solution to locate areas of increased loading and possible hazard.

The idea for the experiment stems from miner's folklore. Underground miners maintain that they can predict mine wall loading by the sound of a rock hammer hitting a rock bolt. To investigate the merit of this belief, recordings of rock hammers striking rock bolts were made on a pillar under investigation in the Stillwater Mine. To provide a better understanding of the variables involved, rock bolts were also analyzed in a laboratory environment under controlled amounts of loading.

## Experimental Procedure

A two-channel Sony ECM-929L microphone was used for the acoustic data collection for this project. The properties of this microphone include a dynamic range of more than 94 dB and signal-to-noise ratio greater than 48 dB.

### Laboratory experiment

To detect changes in frequency content, experiments were performed on the Montana Tech campus March 13, 1998. These experiments were performed on a DYWIDAG rebar rock bolt, donated by the Stillwater Mine, and a Simmons eye bolt, donated by J.P. Simmons Iron Works Inc. (Figure 35).

The DYWIDAG rebar rock bolt is composed of ¾ inch #6 grade 70 steel with 13/16-inch ridges. This rock bolt is identical to those used in the Stillwater Mine. The Simmons eye bolt is constructed of 5/8 inch cold-rolled steel. The eight-foot DYWIDAG bolt was cut to a length of 27 inches, approximately the same length as the Simmons eye bolt. Each of these Rock-bolts was then inserted into the Tinius-Ohlsen tension/compression tester. The Simmons eye bolt was secured by clamps directly above the eye and directly above the bolt threads. The DYWIDAG rock bolt was secured approximately 3 inches from either end (Figure 36).

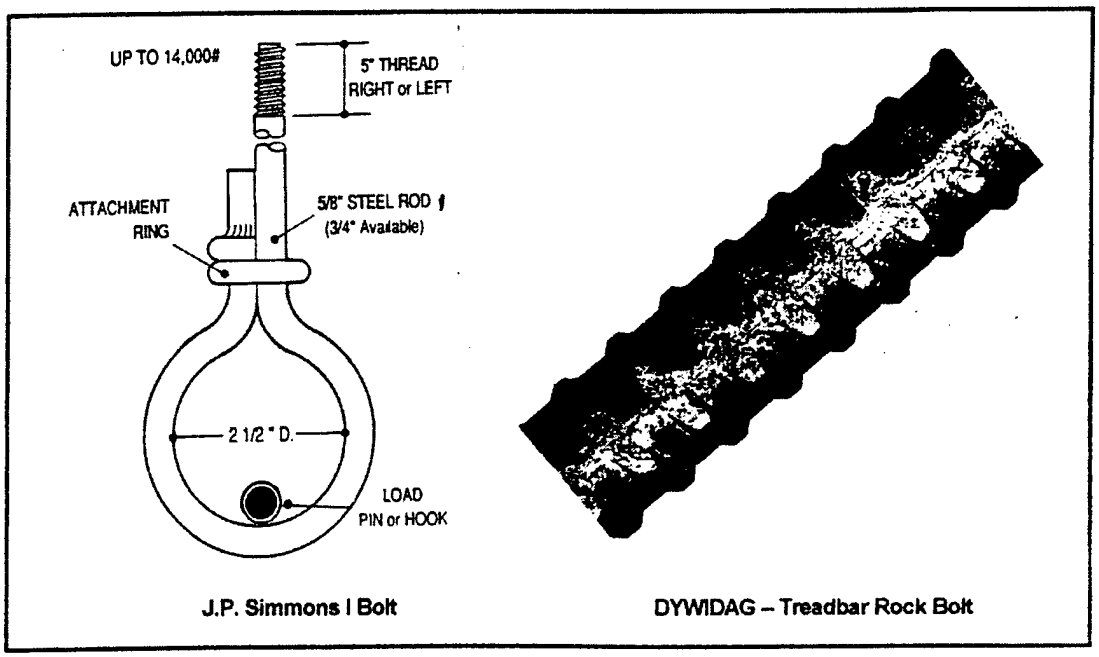


Fig. 35. The Simmons eye bolt and the DYWIDAG rebar rock bolt used for the laboratory tests.

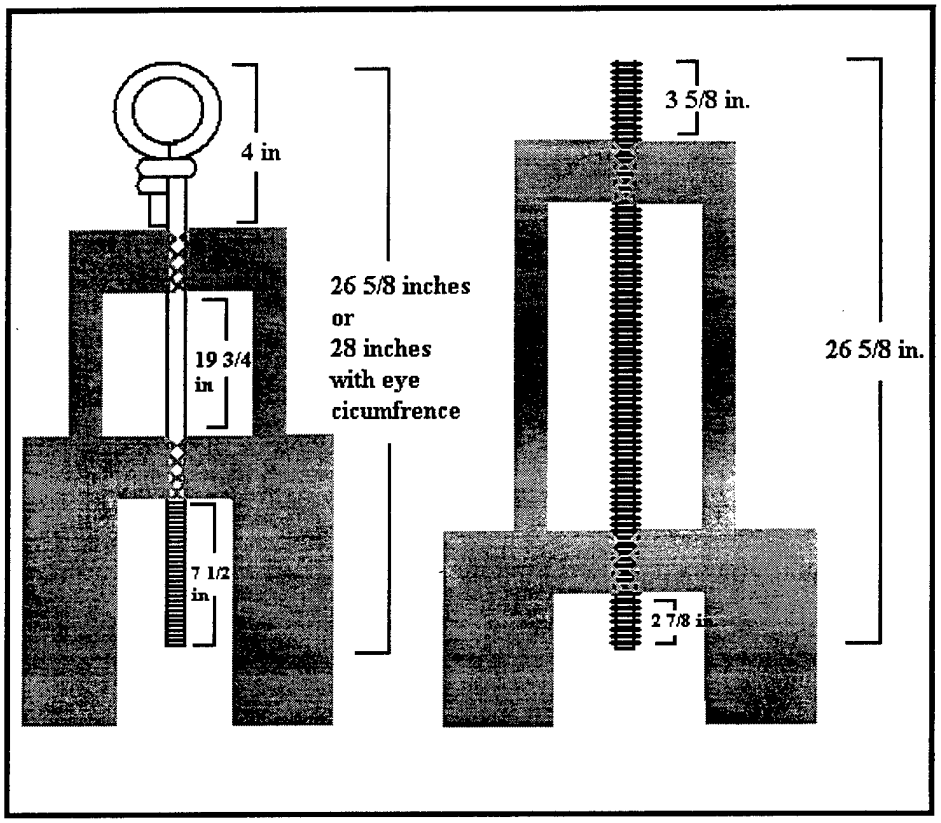


Fig. 36. Rock-bolt and machine setup.

The tensional breaking point of each rock bolt was then calculated. This helped to determine the range of tensions under which each rock bolt would be placed. The results of calculations are as follows:

Simmons eye bolt (Oberg et al., 1996):

$$tensional\ strength = 60{,}000\ \frac{lb}{in^2} \times \pi \times \left(\frac{5}{16}\right)^2$$
$$= 18{,}408\ lb$$

DYWIDAG rock bolt (Oberg et al., 1996):

$$tensional\ strength = 20{,}000\ \frac{lb}{in^2} \times \pi \times \left(\frac{6}{16}\right)^2$$
$$= 8{,}836\ lb$$

Using the tensional strength as the maximum tension the rock bolt can withstand, measurements were taken for the DYWIDAG rock bolt at 1000, 2000, 3000, 4000, and 5000 lb. Measurements for the Simmons eye bolt were taken at tensions of 1000, 2000, 3000, 4000, 5000, 10000, 15000 lb. The tension ranges lie within the approximately 2000 to 11000 lb. tensions found in a typical mine site (Means, 1976).

**Stillwater Mine data acquisition**

The data for this project were acquired at the Stillwater Mine. Acoustic data were recorded at the Bin #2 Pillar at the 3200-foot level. The station locations coincide with those used for the ground penetrating radar tomographic study. The station locations and pillar geometry are shown in Figure 1. Each station contains an upper and lower rock bolt. Each of these individual rock bolts was struck on the end and side two times. The sound produced by each rock bolt was recorded and subsequently analyzed in the frequency domain.

## Expected Outcome

Some uncertainty concerning the true Young's modulus of rebar arose from a paper by Tadolini (1990). His research presented some useful information for calculating Young's modulus for rebar. Tadolini found that a 5/8-inch diameter, 4-foot long rebar rock bolt stretches 0.0064 inches per 100 lb. Using this information, Young's modulus was recalculated to present a range that might more accurately represent rebar. For ease of calculations, English units were converted here to metric units.

$$tensile\ strain = \frac{\Delta L}{L} = 1.333 \times 10^{-5}$$

$$tensile\ stress = \frac{F}{A} = 2.24 \times 10^{6}\ \frac{N}{m^2}$$

$$Young's\ modulus = \frac{tensile\ stress}{tensile\ strain} = 1.68 \times 10^{11}\ Pa$$
$$= 2.43 \times 10^{6}\ \frac{lb}{in^2}$$

To verify the Young's modulus recalculations for rebar, an experiment was conducted to experimentally determine Young's modulus for #6 grade 70 steel (rebar). A rod of ½ inch diameter rebar was placed under increasing tension in the Tinius-Ohlsen testing machine. The change in length was measured with an extensiometer. The results are presented in Table 5.

Table 5. Young's Modulus Laboratory Measurements for Rebar

| Load (lb) | $\Delta$L (x 0.001 in) | Force/Area | $\Delta$L/L | Slope (lb/in^2) |
|---|---|---|---|---|
| 0 | 0.00 | 0 | 0 | 0.0000E+00 |
| 1000 | 1.50 | 5093 | 0.0015 | 3.3953E+06 |
| 2000 | 3.50 | 10186 | 0.0035 | 2.9103E+06 |
| 3000 | 5.50 | 15279 | 0.0055 | 2.7780E+06 |
| 4000 | 7.20 | 20372 | 0.0072 | 2.8294E+06 |
| 5000 | 9.50 | 25465 | 0.0095 | 2.6805E+06 |
| 6000 | 11.10 | 30558 | 0.0111 | 2.7530E+06 |
| 7000 | 13.00 | 35651 | 0.013 | 2.7424E+06 |
| 8000 | 15.00 | 40744 | 0.015 | 2.7162E+06 |
| 9000 | 17.00 | 45837 | 0.017 | 2.6963E+06 |
| 10000 | 19.00 | 50930 | 0.019 | 2.6805E+06 |
| Breaking strength = | 15880 lbs | | Young's modulus = | **2.5620E+06** |

Using linear regression, a best-fit slope was calculated from the experimental data to determine Young's modulus. This value was approximately $2.56 \times 10^6$ lb in$^{-2}$. For comparison, Young's modulus for cold rolled steel is $2.9 \times 10^6$ lb in$^{-2}$ (Sears et al., 1987). This calculated value of Young's modulus for #6 Grade 70 steel was used in all following calculations pertaining to the DYWIDAG (rebar) frequencies.

By striking a rock bolt on both the side and end, two types of fundamental frequencies are produced. Striking the end activates axial (longitudinal) modes, while striking the side activates bending (transverse) frequencies (Morse, 1948). Tannant et al. (1995) report on experiments similar to this investigation on rock bolts. In his experiments, strain gauges were placed on either side of the bolt. When struck, one side of the bolt was in compression while the other was in tension. Based on this concept, Tannant et al. viewed the rock bolt as an anchored beam. Had the rock bold exhibited uniform deformation, the rock bolt would more closely approximate an anchored string (Morse 1948). The calculations for the approximate fundamental frequencies are as follows:

Axial fundamental frequencies (Morse, 1948):

$$f_n = n\frac{V_p}{2L}$$

where

$V_p$ = compressional velocity = $\sqrt{\frac{Y}{\rho}}$,
Y = Young's modulus for steel,
$\rho$ = density of steel = 7.8 $\frac{g}{cm^3}$,
n = frequency mode number, and
L = length of the rebar.

| | | |
|---|---|---|
| DYWIDAG fundamental frequency | = | 2745 Hz |
| Simmons eye-bolt fundamental frequency | = | 3940 Hz |
| Stillwater Mine rock-bolt (rebar) fundamental frequency | = | 1261 Hz |

Bending fundamental frequencies (Morse, 1948):

$$f_n = A_n\frac{1}{2\pi L}\sqrt{\frac{YI}{A\rho}}$$

where

I = moment of inertia = $\frac{\pi d^4}{64}$,
Y = Young's modulus for steel,
$\rho$ = density of steel = 7.8 $\frac{g}{cm^3}$,
A = cross sectional area,
L = length of the rebar,
$A_n$ = 3.52 for one fixed end and one free end,
15.4 for one fixed end and one hinged end,
22.0 for both ends fixed, and
d = diameter of the rebar.

| | | |
|---|---|---|
| DYWIDAG fundamental frequency | = | 10 to 84 Hz |
| Simmons eye-bolt fundamental frequency | = | 15 to 94 Hz |
| Stillwater Mine rock-bolt (rebar) fundamental frequency | = | 4 to 28 Hz |

## Mine Recording Data Analysis

All of the microphone recordings were converted to digital form. A high sampling rate of 44100 Hz sampling rate was used to prevent aliasing and preserve high frequencies. Using the Sound Editor application on a Silicon Graphics Inc. (SGI) workstation, each individual rock-bolt hit was extracted as a digital data subset from the analog recording. These sound files were then converted from *aiff* files to *au* files.

A Matlab program was developed to analyze the sound files in the frequency domain. The program begins by separating the recordings of the two channels. Next, the user graphically picks noise and signal zones (Figure 37).

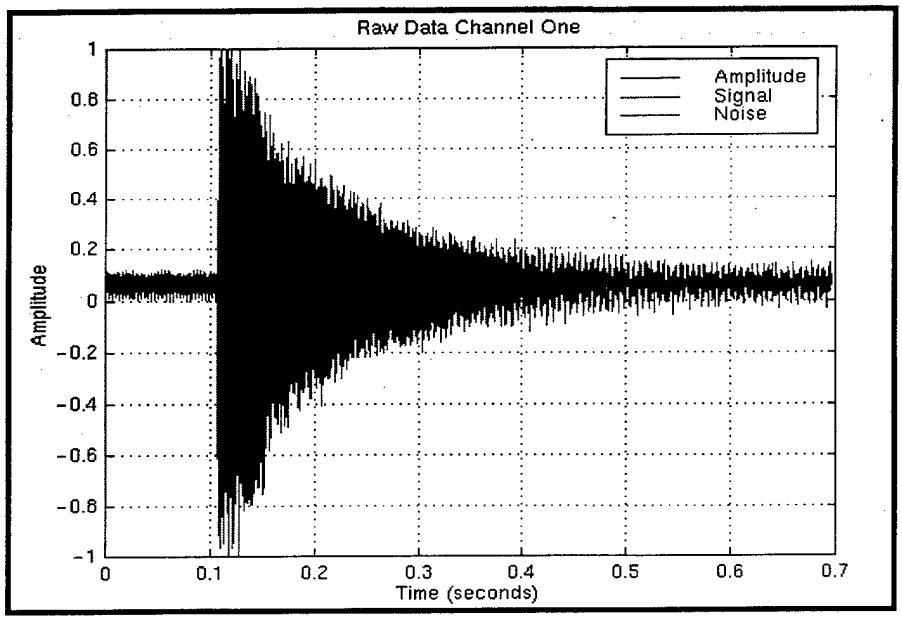


Fig. 37. Example of single hammer hit recording.

Finally, the power spectral content of both the signal and noise intervals were calculated. These values were used to calculate signal-to-noise ratio (S/N). Each hammer-hit recording was analyzed in a similar fashion.

S/N averaged approximately 46 dB for all of the recordings in the higher frequency ranges. S/N was significantly lower in the lower frequency range. This is unfortunately the zone where the bending fundamental frequencies are located (Figure 38). For this reason, research focused upon axial measurements.

**Lab experimental data**

Two frequency peaks at approximately 500 Hz and 750 Hz were prevalent on all of the laboratory recordings. To explain these frequencies, a plot of the Tinius-Ohlsen machine noise was made (Figure 39). This plot clearly demonstrates that the two frequency peaks are the result of machine noise. The Simmons eye-bolt, axial, bottom-hit results are shown in Figure 40.

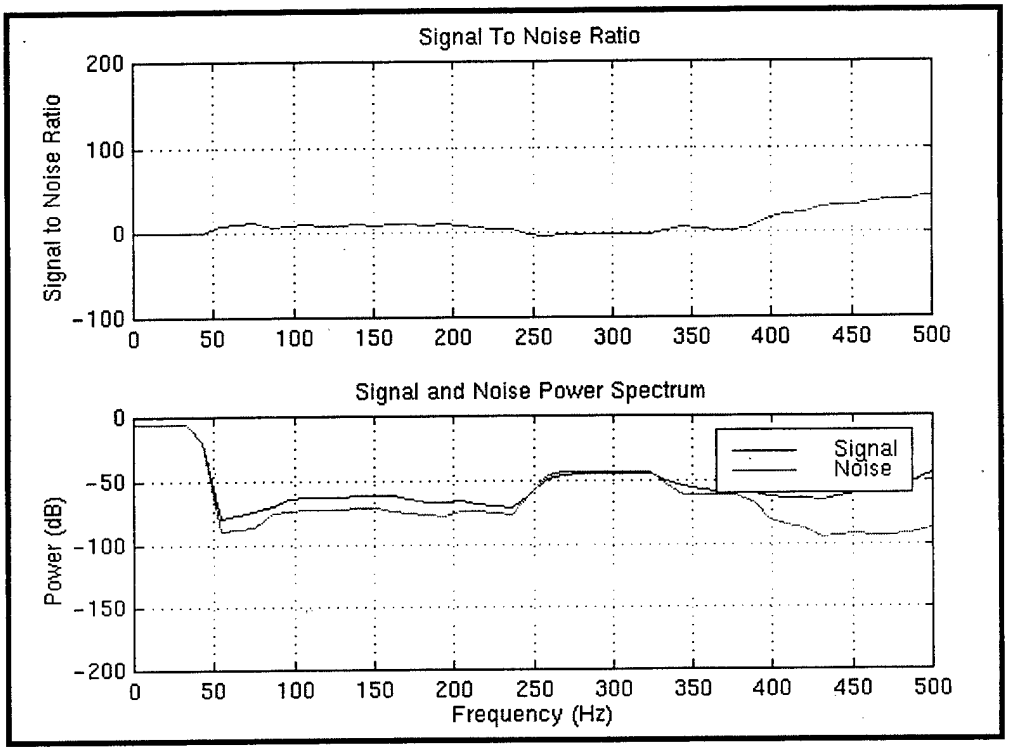


Fig. 38. Typical low signal-to-noise ratio (S/N) of lower frequencies.

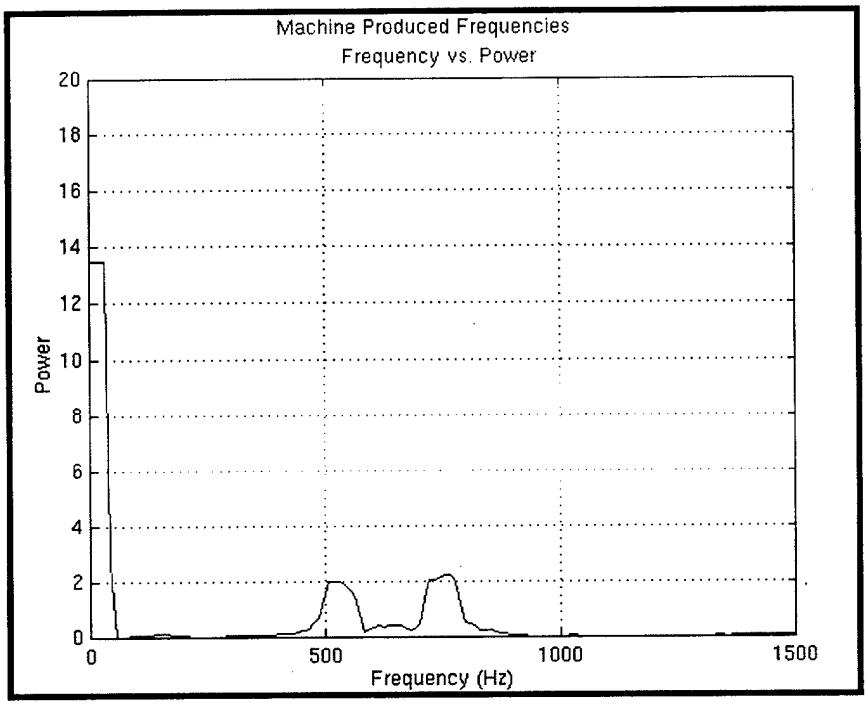


Fig. 39. Tinius-Ohlsen machine noise frequencies.

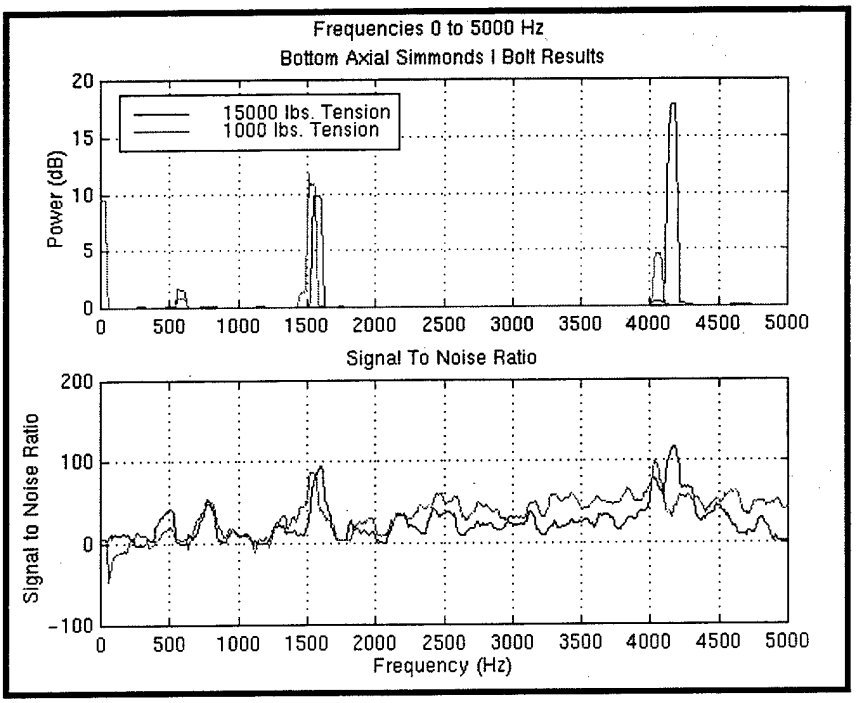


Fig. 40. Axial, bottom-hit Simmons eye-bolt results.

The calculated fundamental frequency of the rock bolt including the eye is 3503 Hz. This value did not correspond with the approximately 4200 Hz peak observed in the laboratory data. However, using this higher frequency value, a calculated rock-bolt length of 22.5 inches is obtained. This length corresponds to the rock bolt without the eye.

The peak located at approximately 1500 Hz is theorized to be a combination of axial and bending frequencies into a torsional frequency (Maxwell, 1941). Both a non-direct end hit and placement of the Tinius-Ohlsen clips could cause this result. The clips contain notched teeth, and were secured approximately three inches from each bolt end. Previously work shown earlier in this report on rock-bolt finite element modeling shows computer models that support this premise. Both axial and bending components were included in the computer simulation, and frequency peaks similar to the 1500 Hz peak appear in the results.

The axial top Simmons eye-bolt recordings display two prominent peaks (Figure 41). The peak at 3450 Hz was close to the calculated value and when the length was calculated using the observed frequency value, a length of 28 inches was obtained. This length corresponds to the length of the rock bolt including the eye. The peak at approximately 2250 Hz is again theorized to be a combination of the axial and bending frequencies. The piece of DYWIDAG rebar rock bolt from the Stillwater Mine was placed under varying amounts of tension and the frequency content was determined. However, none of the results from this analysis exhibited the calculated fundamental frequency.

The frequency analysis results of the axial bottom DYWIDAG results are shown in Figure 42 and the results from the axial top DYWIDAG rebar are shown in Figure 43.

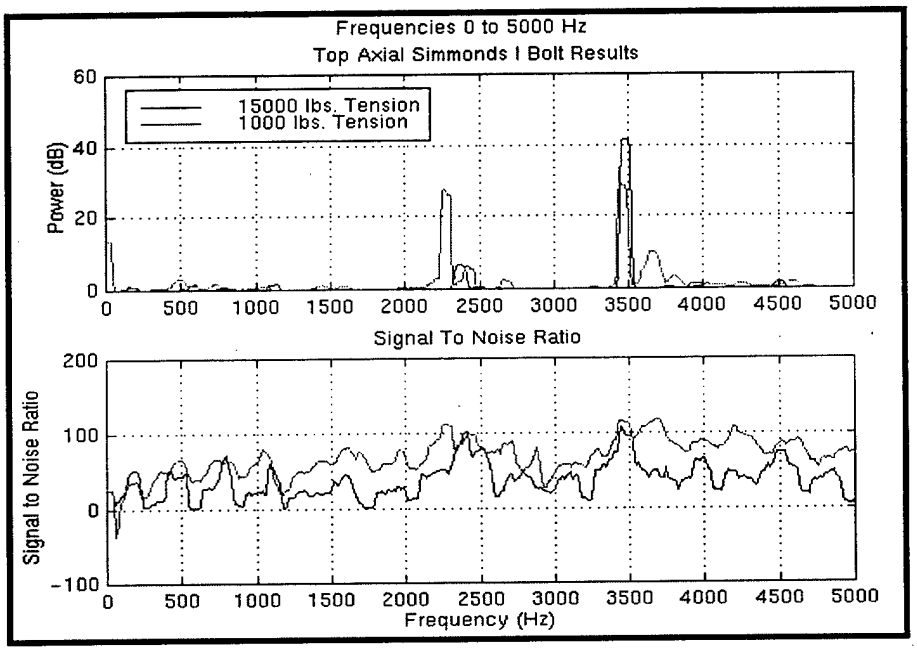


Fig. 41. Axial top Simmons eye-bolt results.

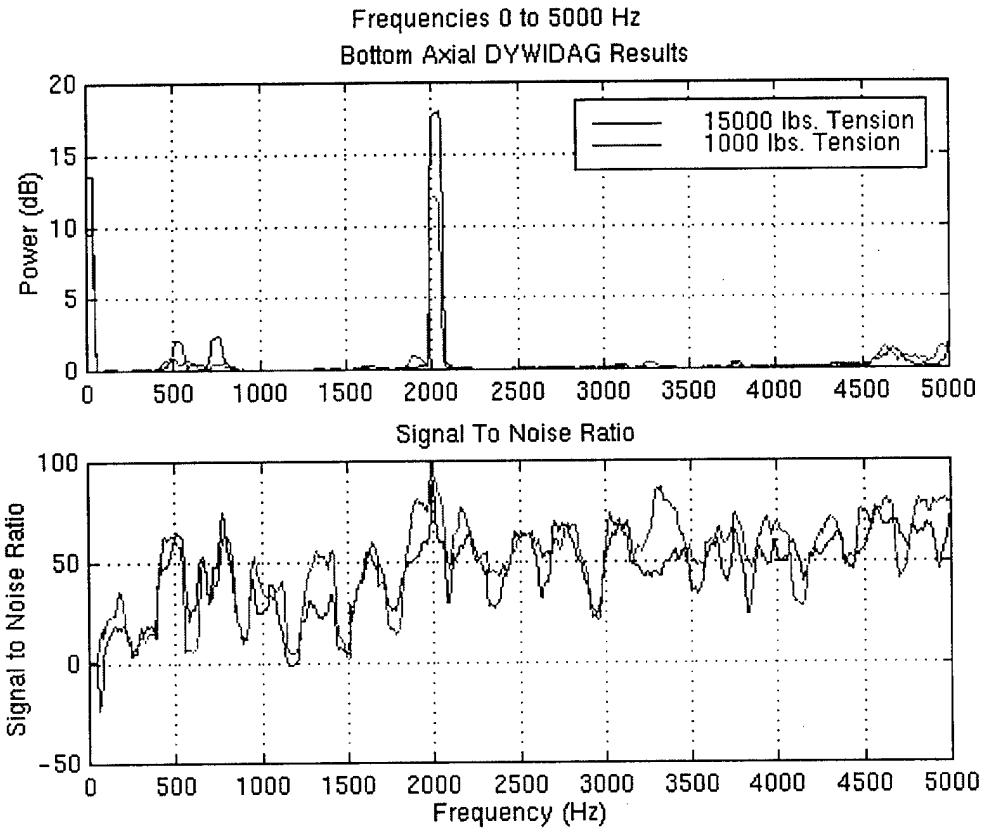


Fig. 42. Axial bottom DYWIDAG rebar rock-bold results.

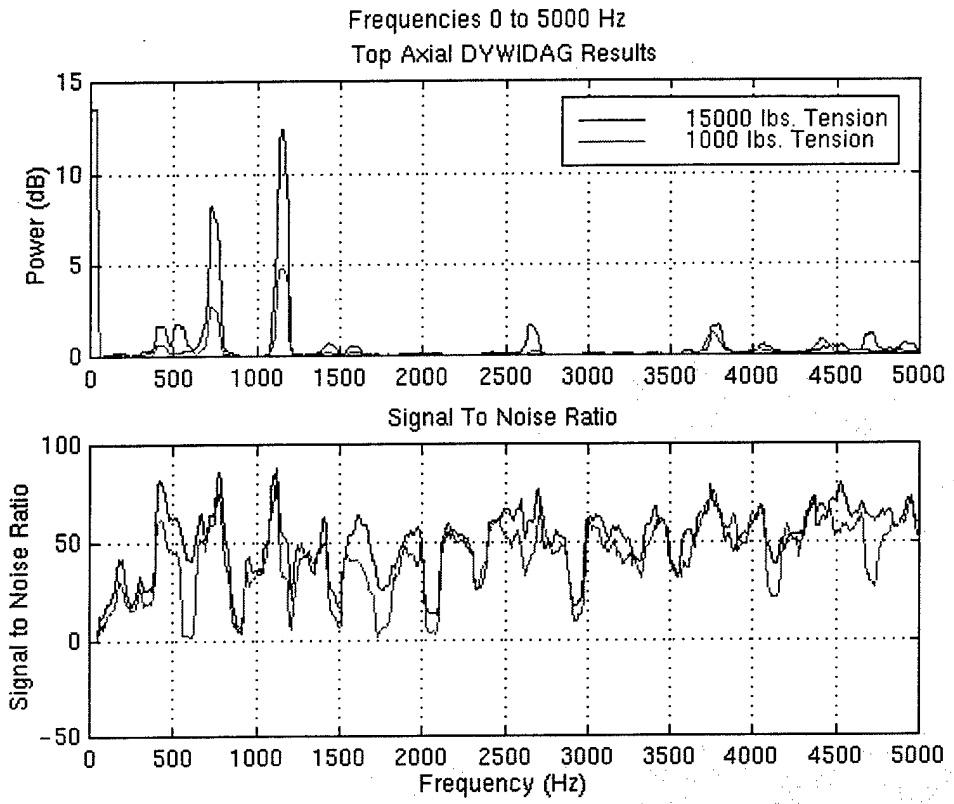


Fig. 43. Axial top DYWIDAG rebar rock-bolt results.

Two dominant frequency peaks occur at approximately 1250 Hz, and 750 Hz. Neither of these frequencies is near the calculated fundamental frequency. To explain these results, a finite element computer model was based upon this data set. Incorporated into the model are the 13/16-inch ridges along the bolt, the position of the clamps, and boundary conditions of the bolt upon these ridges. An axial impulse was simulated on this model. Modeled results give a peak at approximately 2100 Hz. Frequencies of approximately 1250 Hz and 750 Hz are also excited when stuck by an axial hit. The combination of clamping upon the ridges and the ridges themselves has reproduced these lower frequencies in the computer model.

**Stillwater Mine data analysis**

The fundamental frequency expected in the Stillwater Mine rock-bolt data set was calculated to be 1260 Hz. This frequency appeared on almost every axial sound recording from the mine (Figure 44). However, at some of the stations, the dominant frequency was located at approximately 400 Hz. This large variation from the calculated fundamental frequency is difficult to explain. The difference might be due to different length rock bolts, variable coupling of the bolt to the rock, or non-direct hits on the ends of the bolts. In addition, the plates securing the rock bolts to the rock face exhibited a large degree of variation in tightness. Also note that the finite element model of this rock bolt produced frequencies at approximately 2200 Hz and 3300 Hz. These frequencies are also observed in the mine recordings (Figure 44).

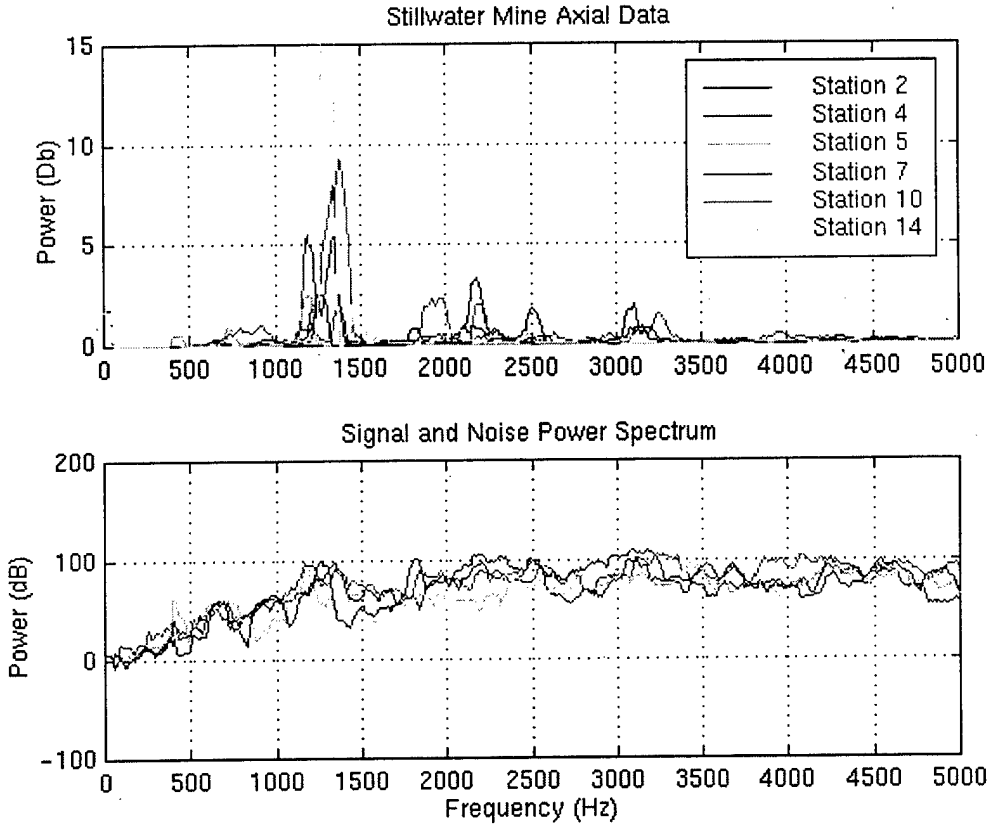


Fig. 44. Stillwater Mine axial sound recordings analysis results.

A set of tables allows easy comparison of frequency peaks contained in the various data sets. Table 6 lists the frequency peaks for the laboratory experiments for the DYWIDAG and Simmons eye rock bolts. Table 7 lists several peak frequencies for typical sound recordings in the Stillwater Mine.

Table 6. Dominant Frequencies for Laboratory Measurements

| | **1000 lb tension** | **5000/15000 lb tension** |
|---|---|---|
| bottom axial Simmons eye | 4157 Hz and 1530 Hz | 4226 Hz and 1578 Hz |
| top axial Simmons eye | 3487 Hz and 2300 Hz | 3491 Hz and 2412 Hz |
| bottom axial DYWIDAG | 2070 Hz | 2078 Hz |
| top axial DYWIDAG | 1187 Hz and 750 Hz | 1188 Hz and 765 Hz |

Table 7. Dominant Frequencies for Stillwater Mine Measurements

| Station | Frequency (Hz) |
|---|---|
| Two | 1362 |
| Four | 1230 |
| Five | 1227 |
| Seven | 1250 |
| Ten | 1412 |
| Fourteen | 1311 |

## Conclusions

The bending or longitudinal frequencies for this data set are very low. As such, they peak in an area with a low signal to noise ratio. Therefore, the focus of the research was on the axial or transverse frequencies. The background noise produced by the Tinius-Ohlsen machine was plotted. Frequencies of approximately 550 Hz and 750 Hz were produced by this machine.

Using the Simmons eye rock bolt, frequencies representing the calculated fundamental frequency were apparent in the data. When striking the bottom of this bolt, it is postulated that the wave travels up the bolt to the point where the attachment ring begins and then returns. The approximate 4200 Hz frequency peak corresponds with this result. Hitting the top of the rock bolt upon the attachment ring, the resulting wave would have to travel a longer distance. This distance of approximately 28 inches corresponds with the 3200 Hz observed frequency. Also, at 2250 Hz, frequency peaks were visualized. Our theory about these peaks concerns the result of both axial and bending frequencies effecting the bolt. These could be due to the placement of the clamps on the Tinius-Ohlsen machine and/or non direct hits on the end of the bolt. Our theory is supported by the computer models.

Two dominant frequencies were evident in the DYWIDAG rebar results at 750 Hz and 1250 Hz. These frequency peaks do not correspond to any calculated fundamental frequencies. However, computer-modeling results suggest possible explanations. The frequency peaks could result from the ridges on the rock bolt, the securing of the rock bolt off the ends of the bolt, and the securing of the rock bolt upon the ridges.

The Stillwater Mine data exhibited the fundamental frequency peak at approximately 1260 Hz over a range of 400 Hz. This somewhat wide range could result from non-direct strikes on the ends of the rock bolts, different rock-bolt lengths, poor coupling of the bolt to the rock, or the ridges on the sides of the DYWIDAG rebar rock bolts.

## REFERENCES


Barkhausen, H., 1919, Two phenomena uncovered with help of the new amplifiers, *Physik. Z.*, 20, 401-403.

Bozorth, 1951, *Ferromagnetism*, D. Van Nostrand, Inc., New York.

Borradaile, G. J., 1996, Experimental stress remagnetization of magnetite, *Tectonophysics*, 261, 229-248.

Clapham, L., Jagadish, C., and Atherton, D. L., 1991, The influence of pearlite on Barkhausen noise generation in plain carbon steels, *Acta Metall. Mater.*, 39, 1555-1562.

Dhar, A., and Atherton, D. L., Correlation between magnetic flux leakage and magnetic Barkhausen noise in steel pipelines, *Brit. J. Nondestr. Test.*, 35, 307-309.

Hoek, E., Kaiser, P. K., and Bawden, W. F., 1995, *Support of Underground Excavations in Hard Rock*, A. A. Balkema Publishers, Rotterdam.

Hudson, M. R., Reynolds, R. L., and Fishman, N. S., 1989, Synfolding magnetization in the Jurassic Preuss Sandstone, Wyoming-Idaho-Utah thrust belt, *J. Geophys. Res.*, 94B, 13681-13705.

Ingersoll-Rand, 1996, *Split-set Friction Rock Stabilizers Information Pamphlet.*

Inman, D. J., 1996, *Engineering Vibrations*, Prentice Hall, Englewood Cliffs.

Jackson, M. J., and Tweeton, D. r., 1996, 3DTOM: Three-dimensional geophysical tomography, *Bureau of Mines Report of Investigations, RI 9617.*

Jagadish, C., Clapham, L., Atherton, D. L., 1990, Influence of uniaxial elastic stress on power spectrum and pulse height distribution of surface Barkhausen noise in pipeline steel, *IEEE Trans. Magn.*, 26, 1160-1163.

Jumikis, A. R., 1983, *Rock Mechanics*, Gulf Publishing Company, Houston.

Krause, T. W., Clapham, L., Pattantyus, A., and Atherton, D. L., 1995, Investigation of the stress-dependent magnetic easy axis in steel using magnetic Barkhausen noise, *J. Appl. Phys.*, 79, 4242-4252.

Mandal, K., Dufour, D., Sabet-Sharghi, R., Sijgers, B., Micke, D., Krause, T. W., Clapham, L., and Atherton, D. L., 1996, Detection of stress concentrations around a defect by magnetic Barkhausen noise measurements, *J. Appl. Phys.*, 80, 6391-6395.

Maxwell, G., 1941, *Strength Of Metals Under Combines Stresses.* American Society for Metals, Cleveland.

Means, W.D., 1976, *Stress and Strain: Basic Concepts of Continuum Mechanics for Geologist*, Springer-Verlag, Inc., New York.

MESA, 1989, *Roof and Rib Control, National Mine Health and Safety Academy Handbook.*

Morse P.M., 1948, *Vibration and Sound*, McGraw-Hill Book Company Inc.

Oberg, Jones, Horton, Fyffel, Green, and McCaulety, 1996, *Machinery's Handbook 25.* Industrial Press.

Otuonye, O., 1998, Response of grouted roof bolts to blast loading, *Int. J. Rock Mech. Min. Sci. & Geomech. Abstr.*, Vol. 25, No. 5,. 345-349.

Peterson, J. E., Paulson, B. N. P., and McEvilly, T. V., 1985, Application of algebraic reconstruction techniques to crosshole seismic data, *Geophysics*, 50, 1566-1580.

Ranjan, R., Jiles, D. C., and Rastogi, P. K., 1987, Magnetic properties of decarburized steels: an investigation of the effects of grain size and carbon content, *IEEE Trans. Magn.*, 23, 1869-1876.

Sears, F.W., Zemansky, M.W., and Young, H. D., 1987, *University Physics: Seventh Edition* Addison-Wesley Publishing Company, Reading, Massachusetts.

Serbousek, M. O. and Signer, S. P., 1987, Linear load-transfer mechanics of fully grouted roof bolts, *Bureau of Mines Report of Investigations, RI 9235.*

SDRC I-DEAS Master Series Software, 1997.

Sundstrum, O., and Torronen, K., 1979, The use of Barkhausen noise analysis in nondestructive testing, *Mater. Eval.*, 37, 51-56.

Tadolini, S.C., 1990, *Evaluation of Ultrasonic Measurement Systems for Bolt Load Determinations*, Bureau of Mines Report of Investigation: 9332, Department of the Interior.

Tannant, D.D., Brummer, R.K., and Yi, X., 1995, Rockbolt behaviour under dynamic loading: field tests and modelling, *Int. J. Rock Mech. Min. Sci. & Geomech. Abstr.*, Vol. 32. No. 6, 537-550.

Tiitto, S., 1977, On the influence of microstructure on magnetization transitions in steel, *Acta Polytech. Scand., Applied Phys. Ser.* 119, 3-80.

Tiitto, S., 1991, Magnetoelastic testing of biaxial stresses, *Experimental Techniques*, 15, 17-22.

Weaver, Jr., W. and Gere, J. M., 1980, *Matrix Analysis of Framed Structures*, D. Van Nostrand Company, New York.

Yates, M.T., 1968, *Elastic Anisotropy In Rocks From the Stillwater Igneous Complex, Montana and the Tinaquillo Peridotite, Venezuela*, Princeton University, Ph.D. Dissertation.

# Appendix A

## Rockburst Events

95011301 .00 47-26.10 115-49.09 -22.61 .30 .0
275 50 -80 .00 6 8.05 .69 .00 20 3 200

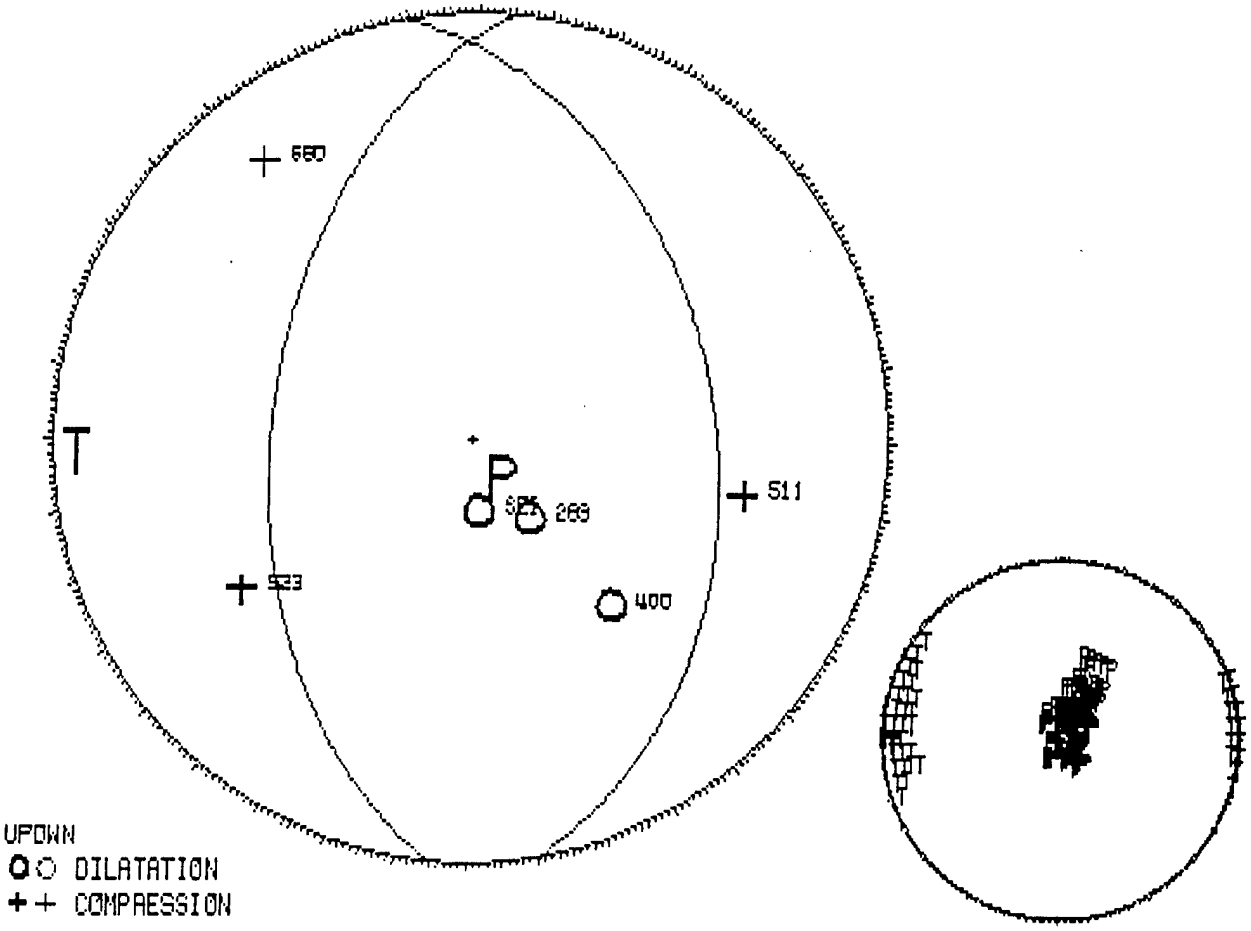

95052700 .00 47-26.10 115-43.09 -23.10 .30 .0
175 60-110 .00 11 8.05 .63 .00 3 5 20

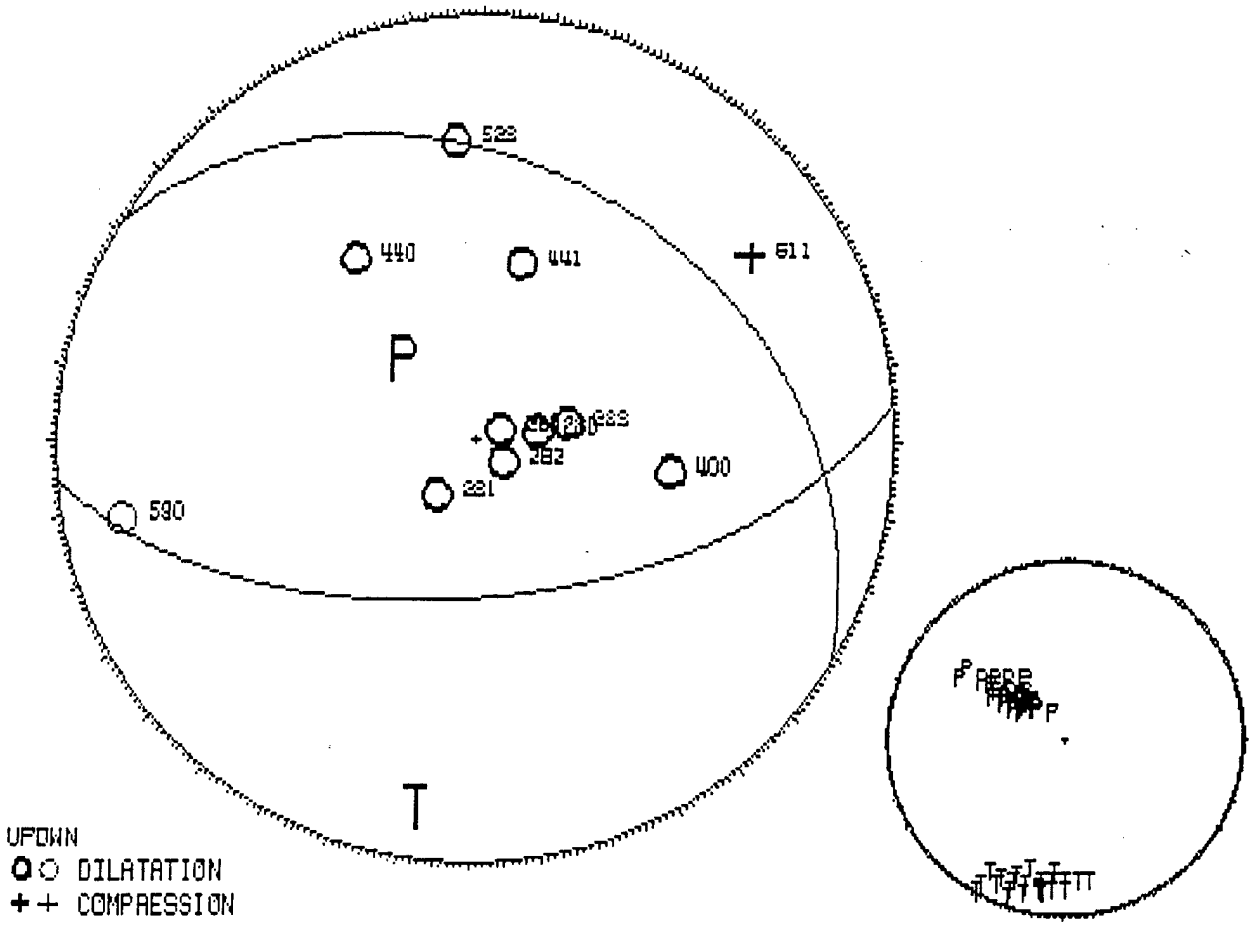

95062206 .00 47-26.10 115-49.09 -22.99 .30 .0
185 45 -90 .00 12 8.05 .72 .00 13 8 25

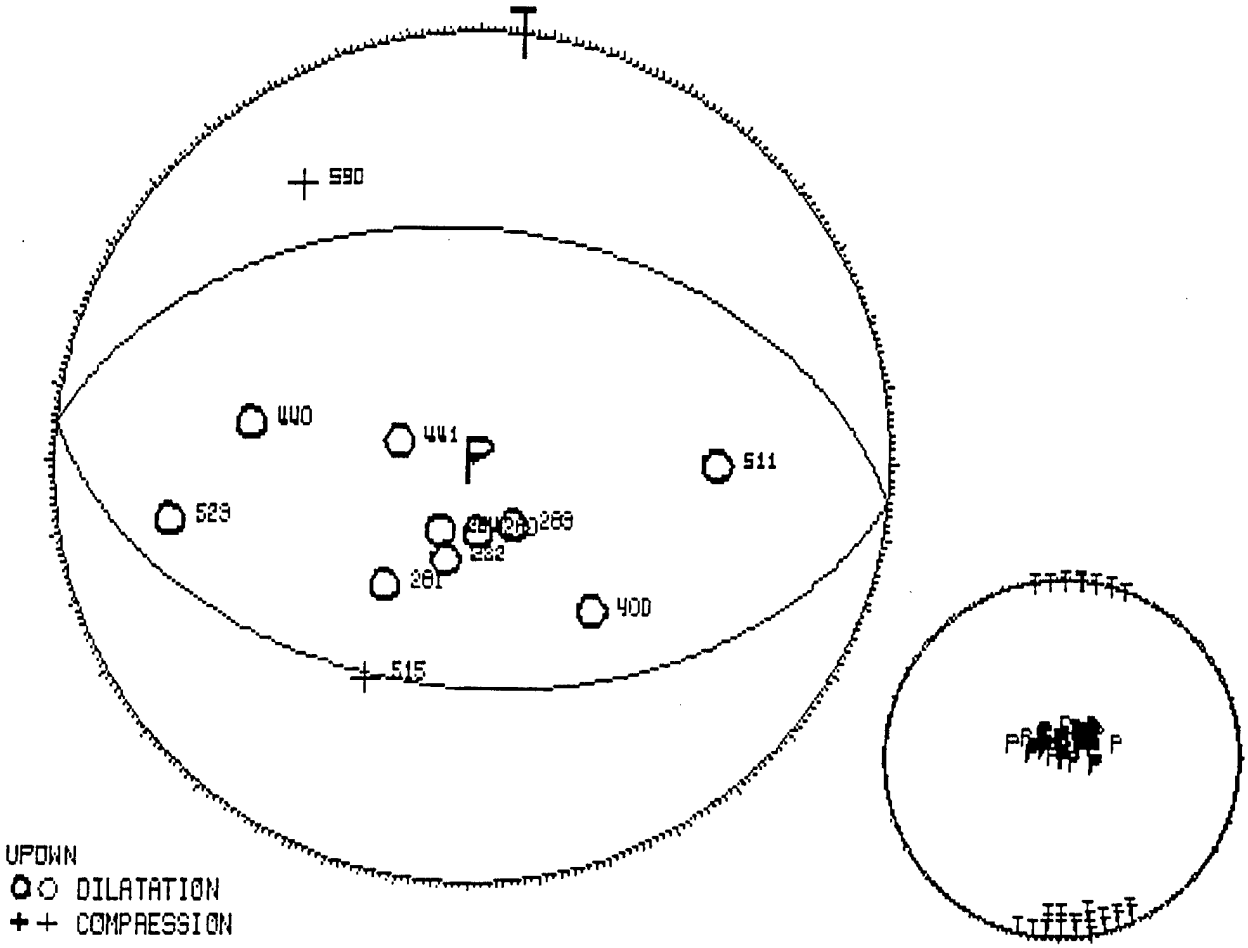

95091905 .00 47-28.10 115-43.09 -20.10 .30 .0
215 70 140 .08 12 8.05 .60 .00 13 5 10

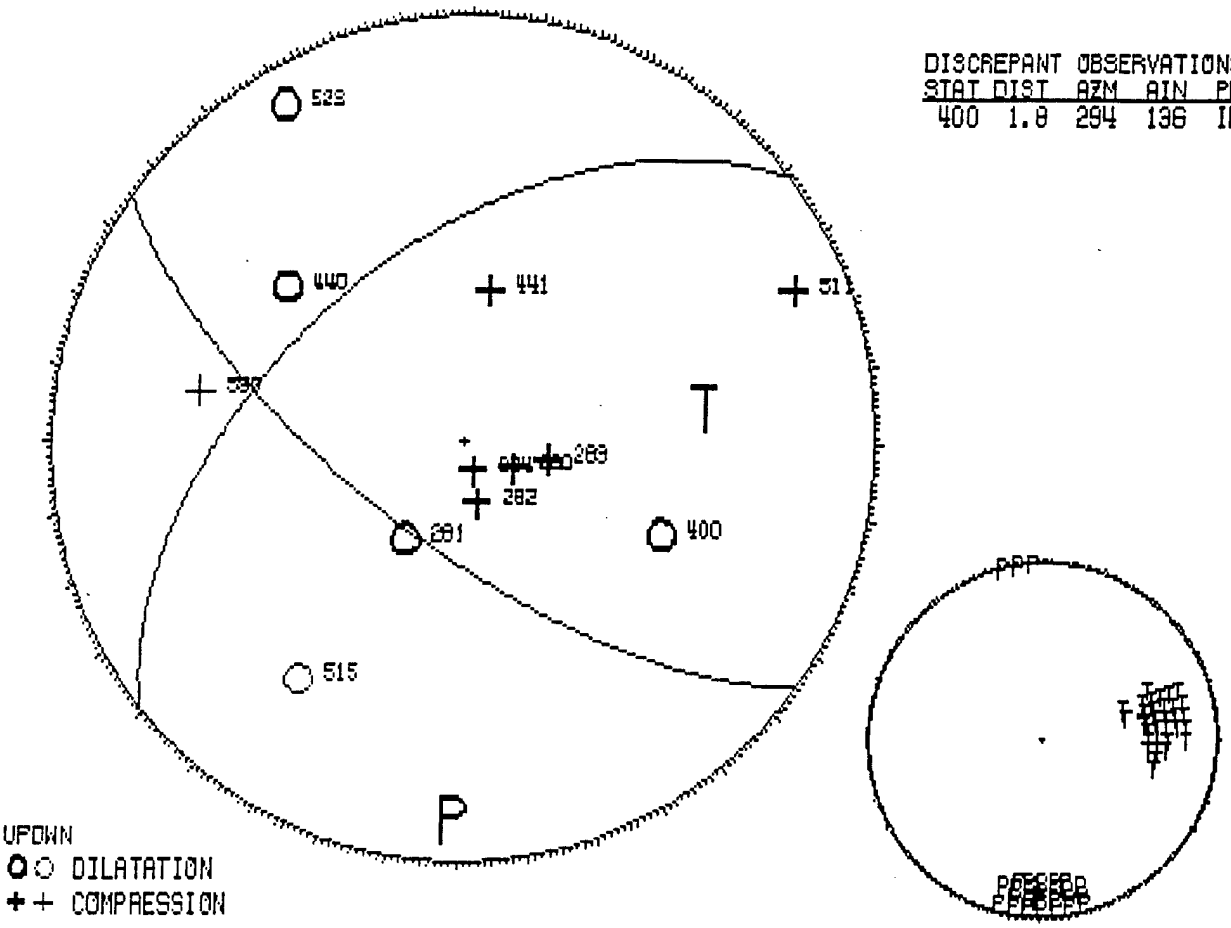


DISCREPANT OBSERVATIONS

| STAT | DIST | AZM | AIN | PRMK |
|---|---|---|---|---|
| 400 | 1.8 | 294 | 136 | IPD |

95091909 .00 47-26.10 115-49.09 -20.10 .30 .0
150 50 -80 .00 10 8.05 .63 .00 3 0 0

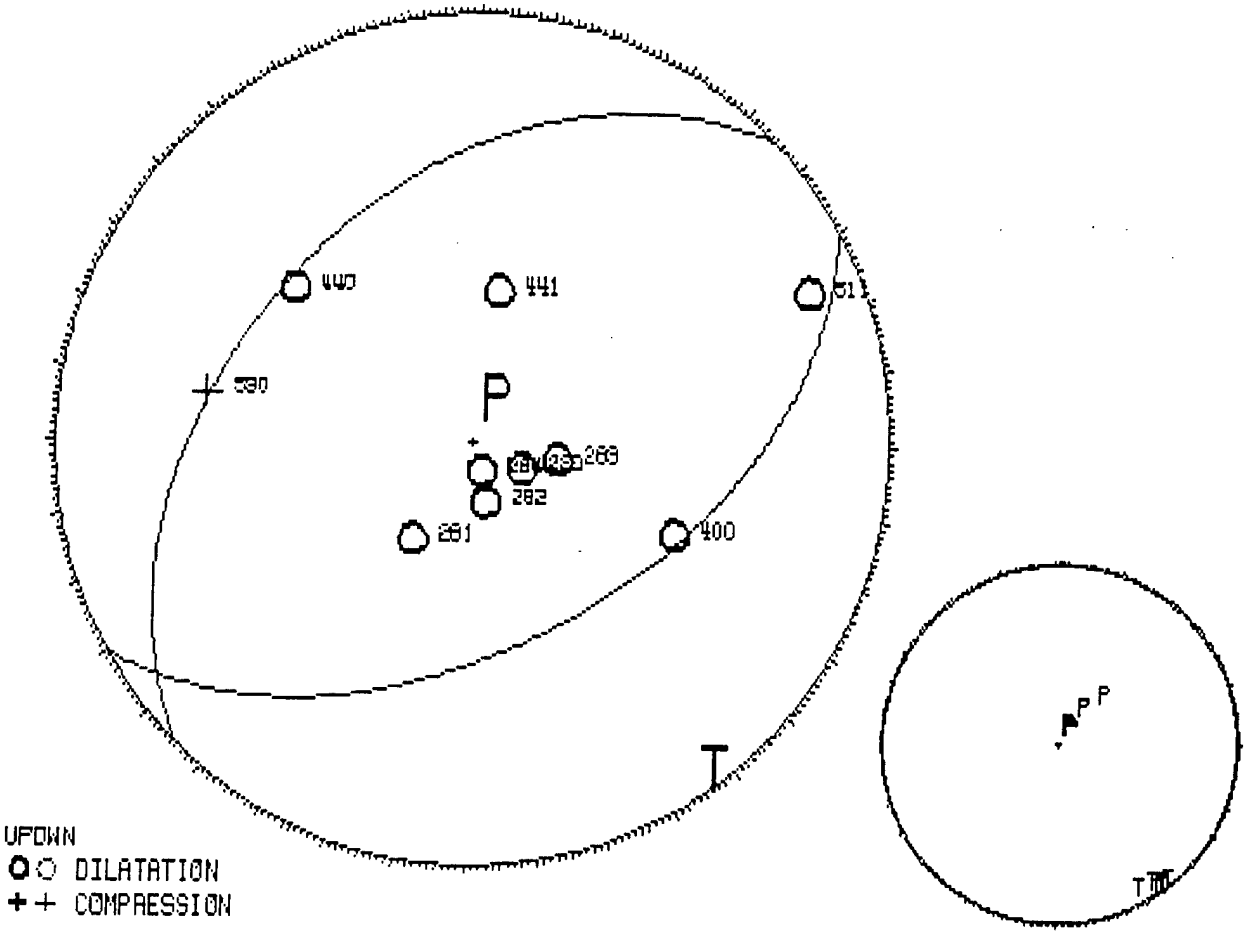


UPDOWN
O○ DILATATION
+ + COMPRESSION

96020600 .00 47-26.10 115-45.09 -22.22 .30 .0
280 60-140 .09 11 8.05 .66 .00 20 5 10C*

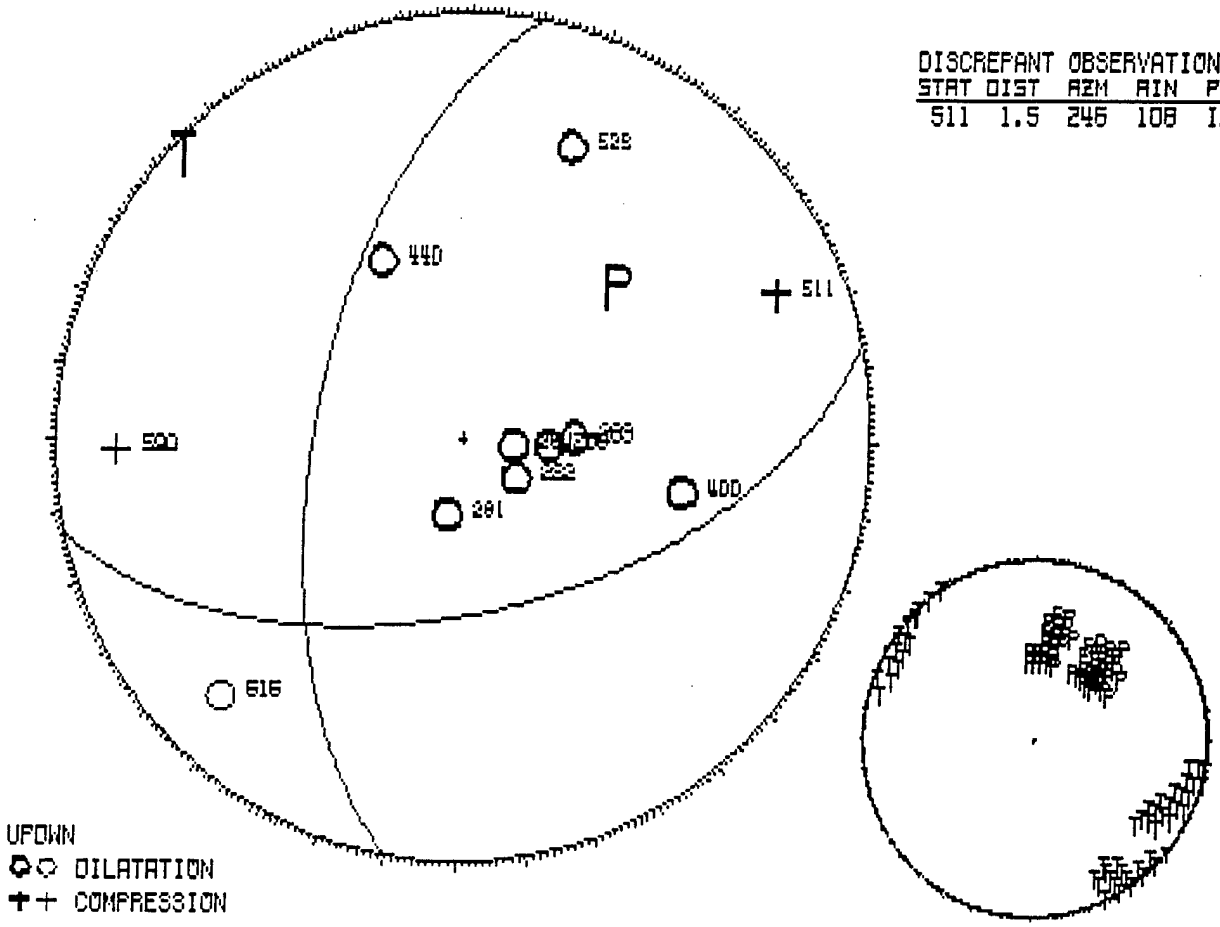


DISCREPANT OBSERVATIONS

| STAT | DIST | AZM | AIN | PAMK |
|---|---|---|---|---|
| 511 | 1.5 | 246 | 108 | IPC |

```
98020800      .00 47-26.10 115-49.09 -22.22    .30          .0
110 40-100    .00  11  8.05  .67  .00  15  5 30
```

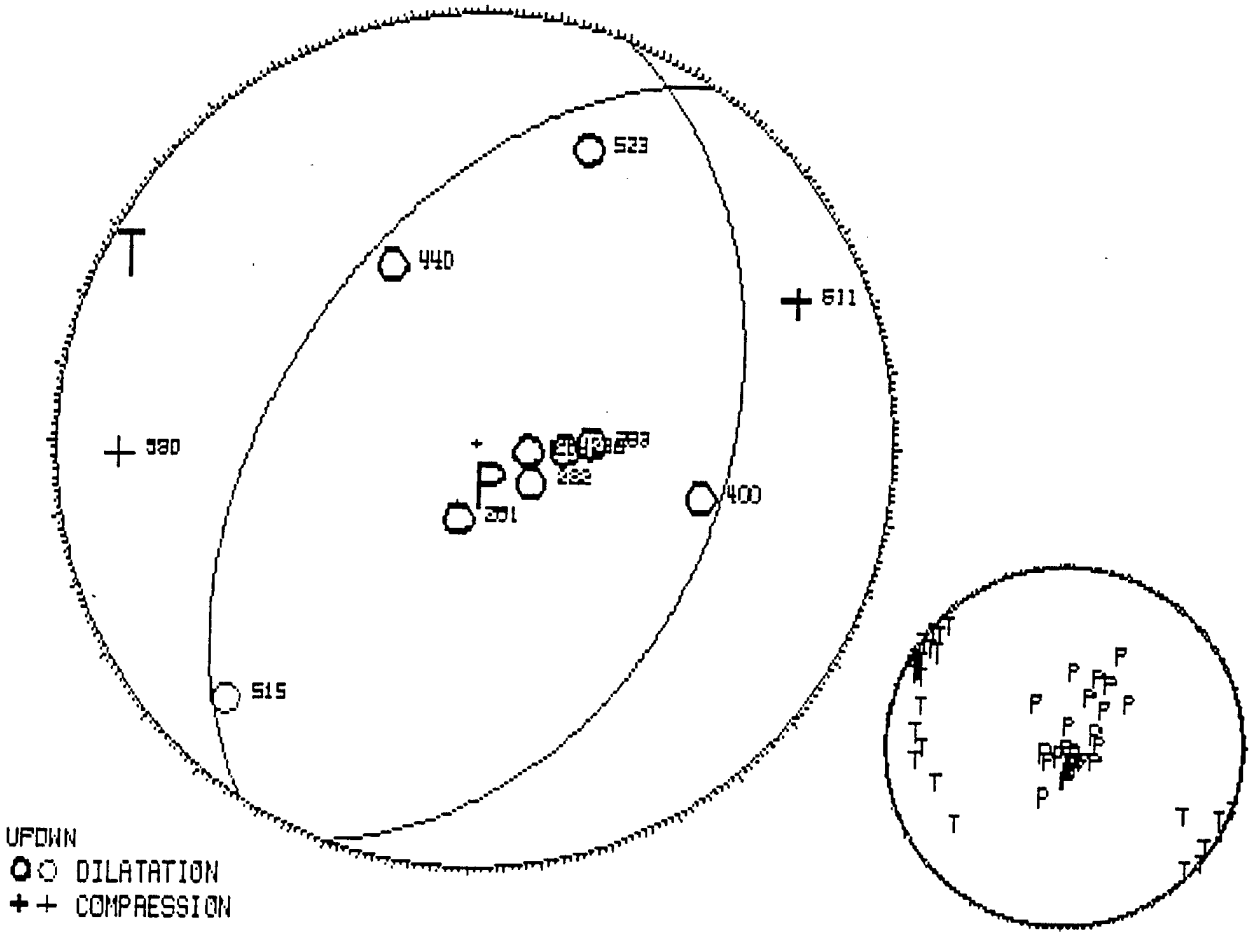

96030200 .00 47-26.10 115-43.09 -22.39 .30 .0
75 50-130 .00 9 8.05 .81 .00 20 10 25

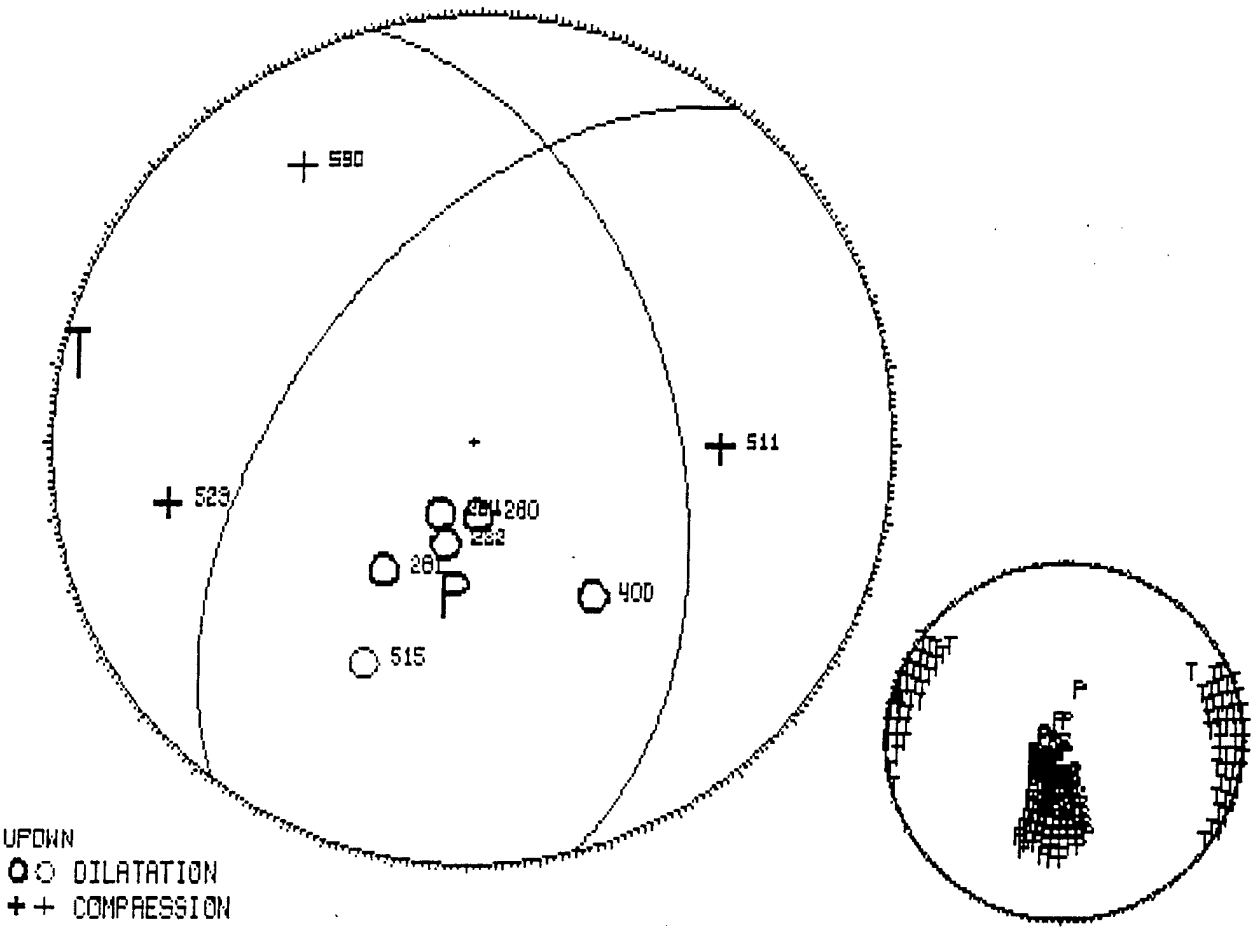


UPDOWN
○ DILATATION
+ COMPRESSION

9604020A .00 47-26.10 115-43.09 -23.10 .30 .0
160 65-170 .00 11 8.05 .44 .00 5 3 5

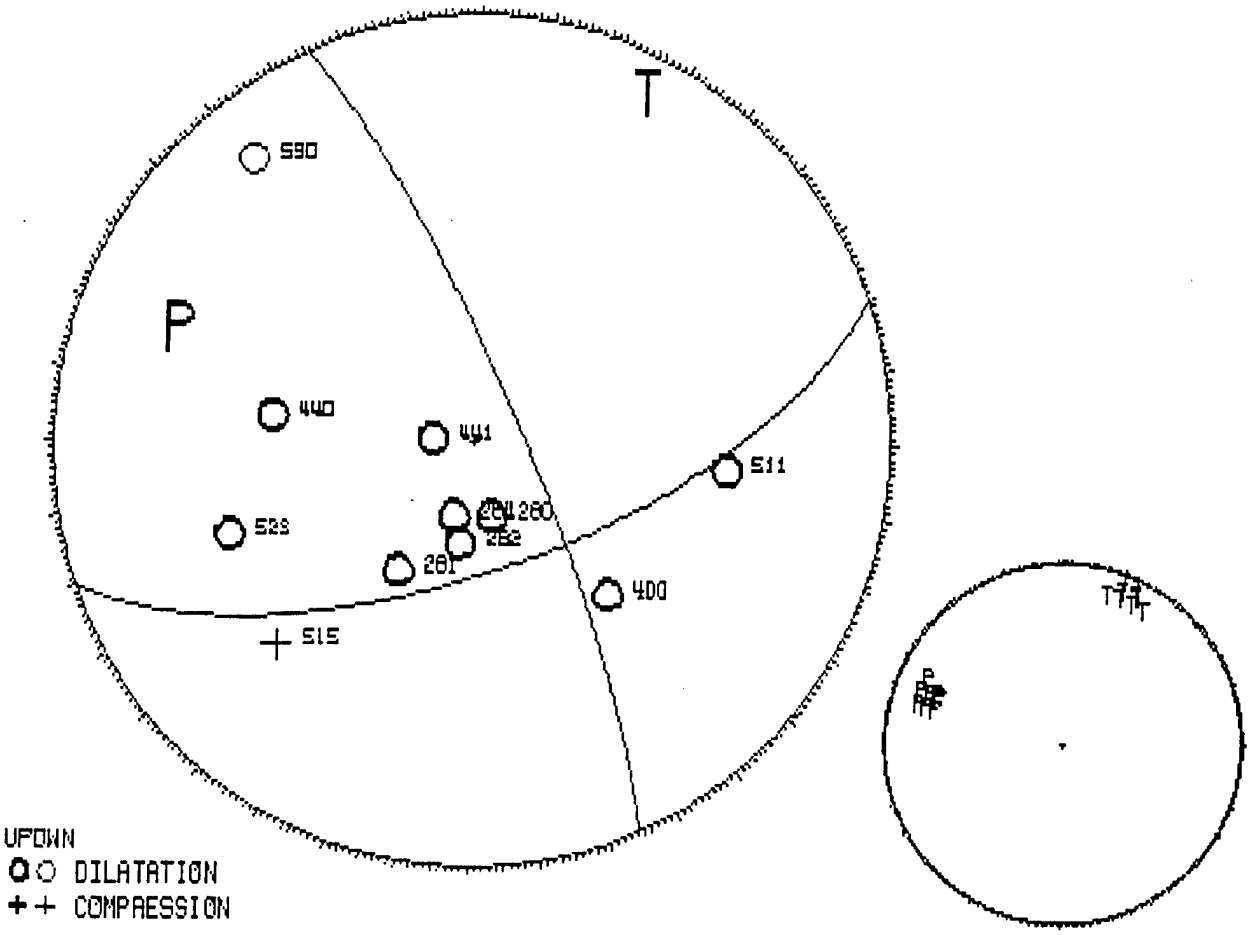

96059001 .00 47-26.10 115-43.09 -17.77 .30 .0
125 90 -80 .09 11 8.05 .60 .00 3 0 25

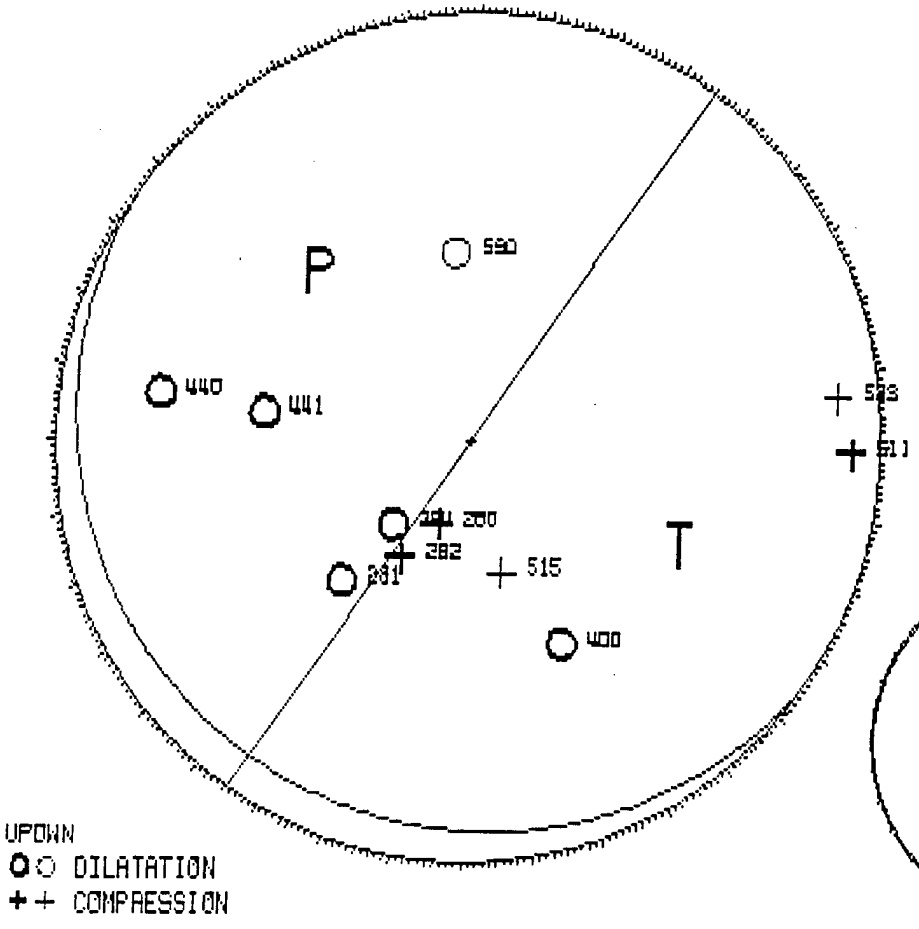


DISCREPANT OBSERVATIONS

| STAT | DIST | AZM | AIN | PRMK |
|---|---|---|---|---|
| 400 | 1.5 | 334 | 136 | IPD |

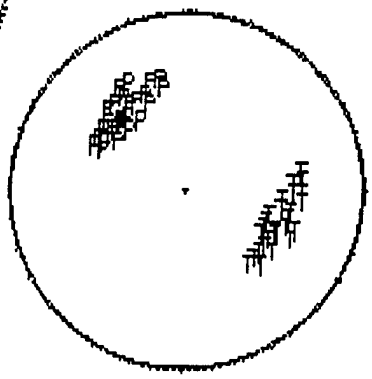

UPDWN
O○ DILATATION
++ COMPRESSION

96092604 .00 47-26.10 115-49.09 -23.16 .30 .0
280 80 130 .10 10 8.05 .63 .00 33 15 30

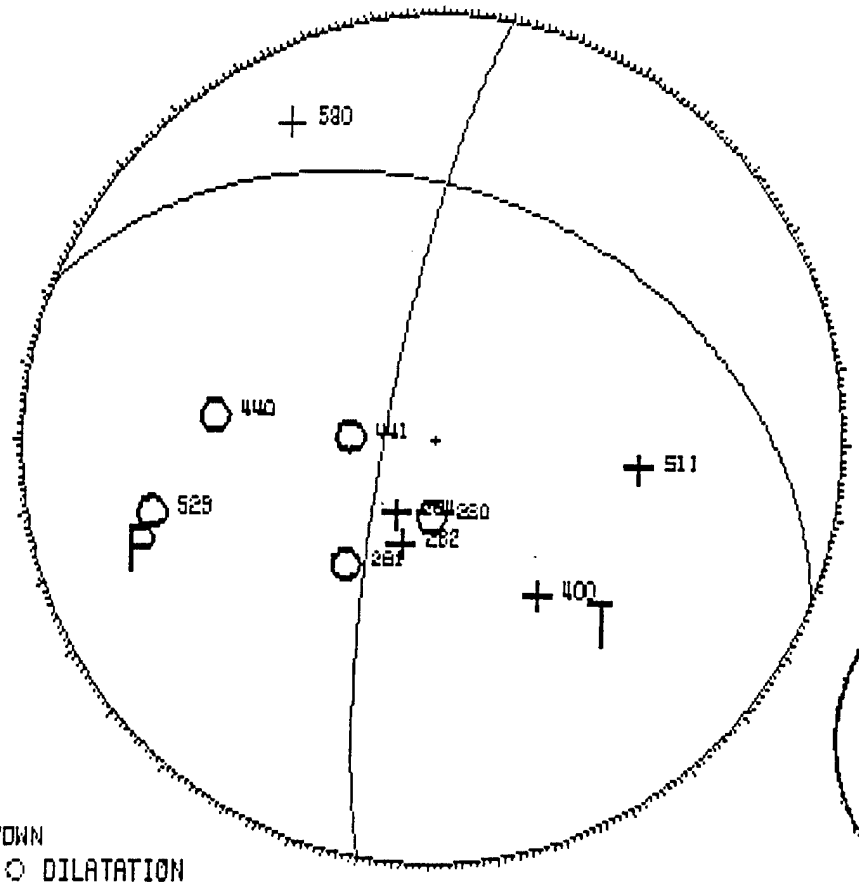


DISCREPANT OBSERVATIONS

| STAT | DIST | AZM | AIN | PRMK |
|---|---|---|---|---|
| 280 | 2.9 | 2 | 165 | IPD |

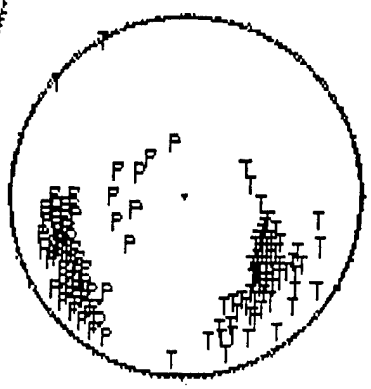

UPDWN
O O DILATATION
+ + COMPRESSION

```
98092604      .00 47-28.10 115-43.09 -23.16    .30          .0
 55 15  80   .10  10  8.05  .52  .00  18  3  0 *
```

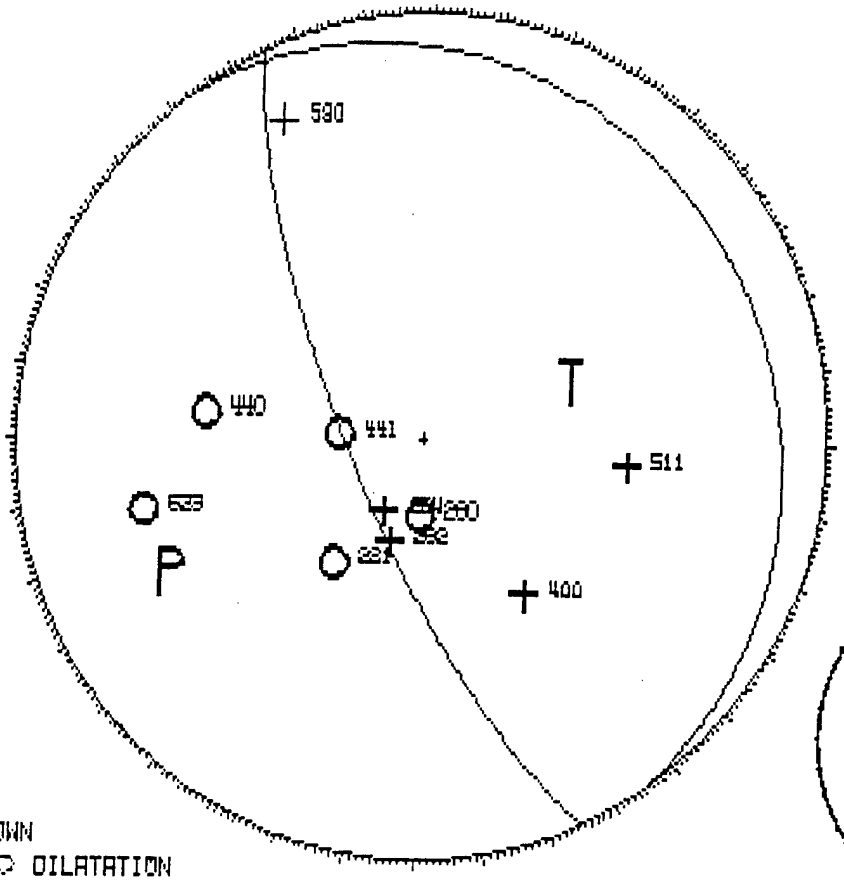


DISCREPANT OBSERVATIONS

| STAT | DIST | AZM | AIN | PAMK |
|---|---|---|---|---|
| 260 | 2.9 | 2 | 165 | IPD |

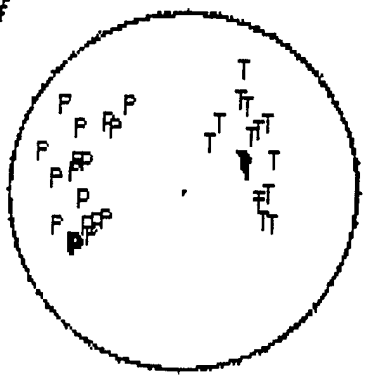

96110101 .00 47-26.10 115-43.09 -26.00 .30 .0
195 65 170 .00 6 8.05 .42 .00 8 5180

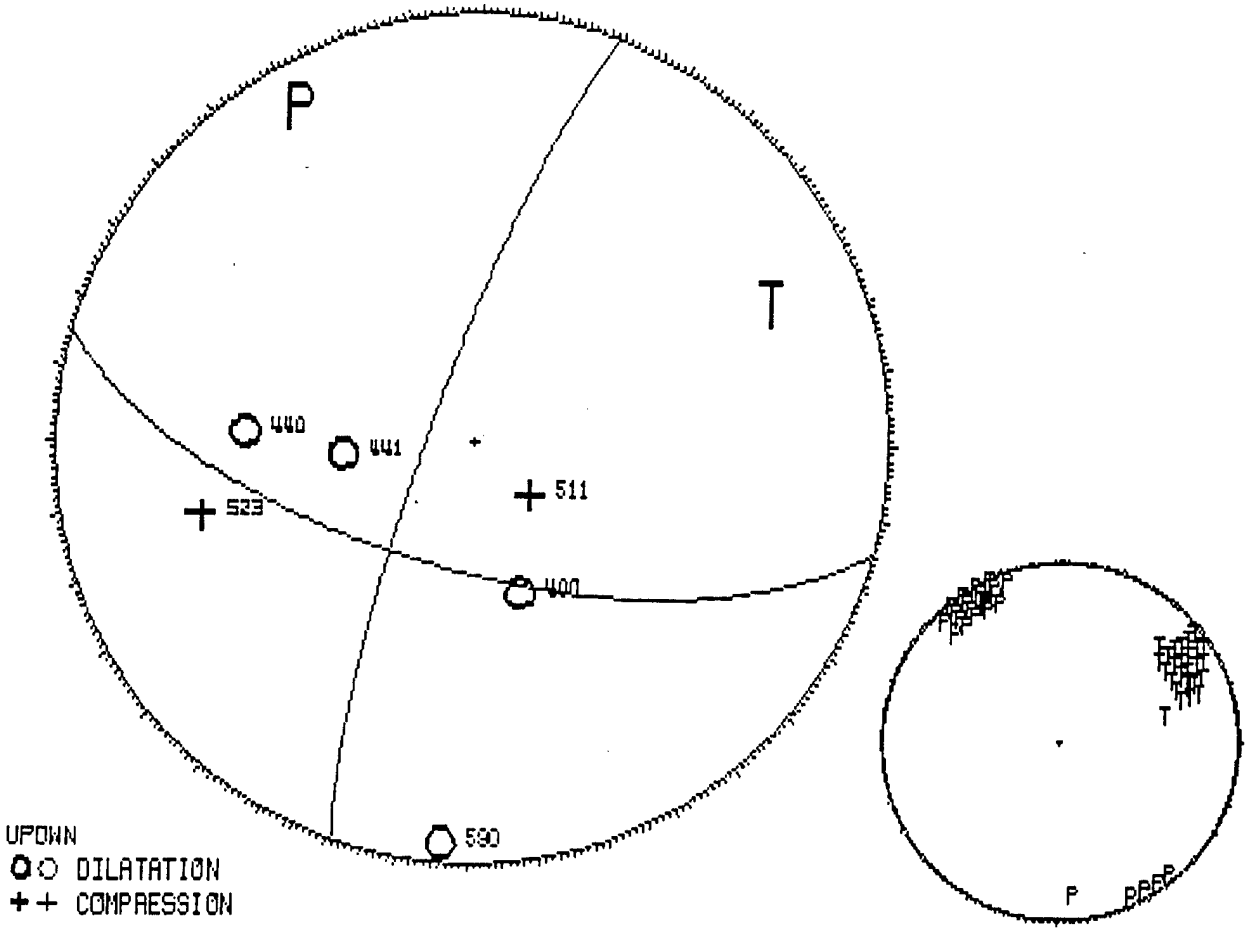

```
96110102      .00 47-28.10 115-43.09 -28.00    .30          .0
 70 45-130   .00  10  8.05  .78  .00  23 10 25
```

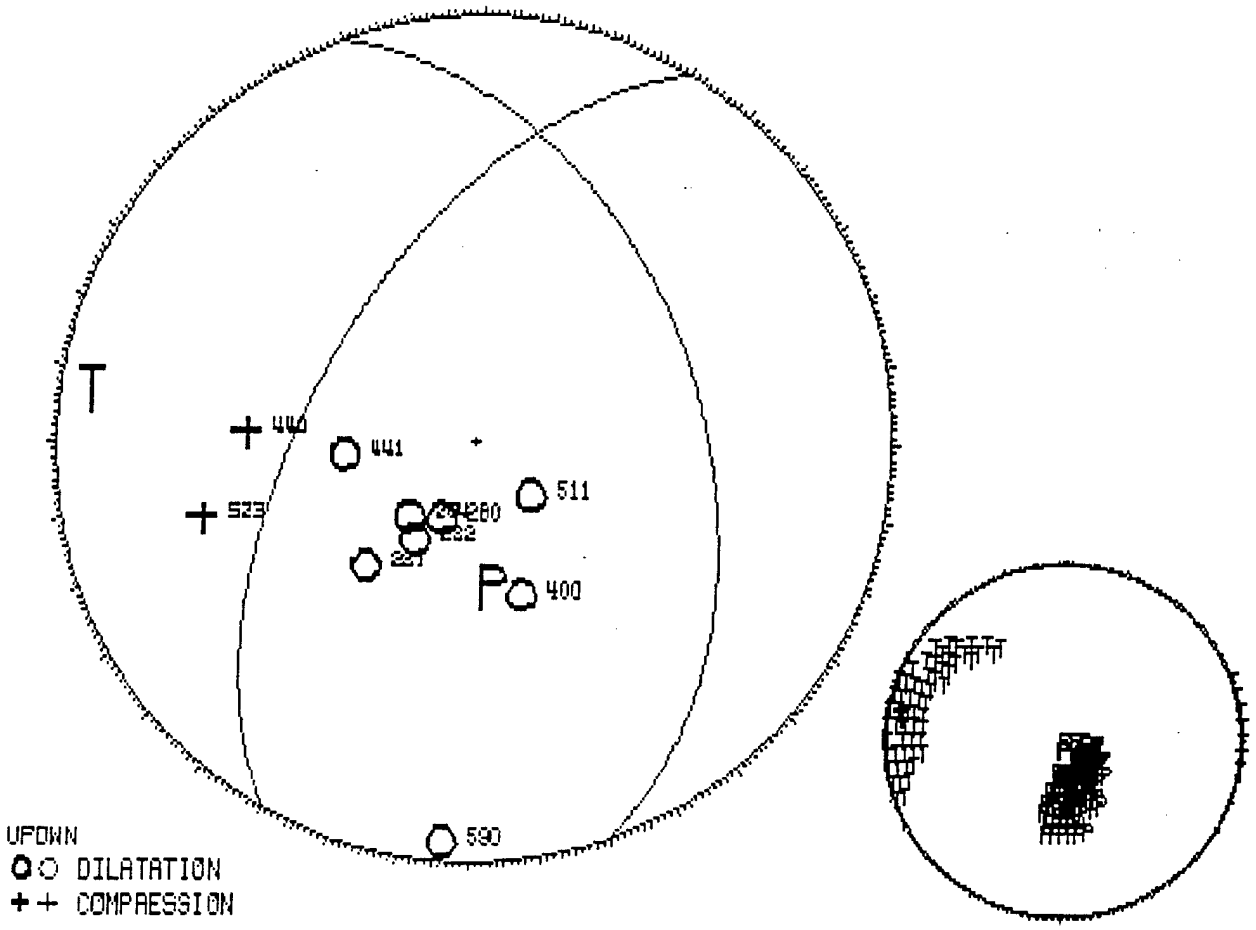

```
98110102      .00 47-28.10 115-45.09 -28.00    .50          .0
100 40 -80   .00  10  8.05  .88  .00  15  5 10C*
```

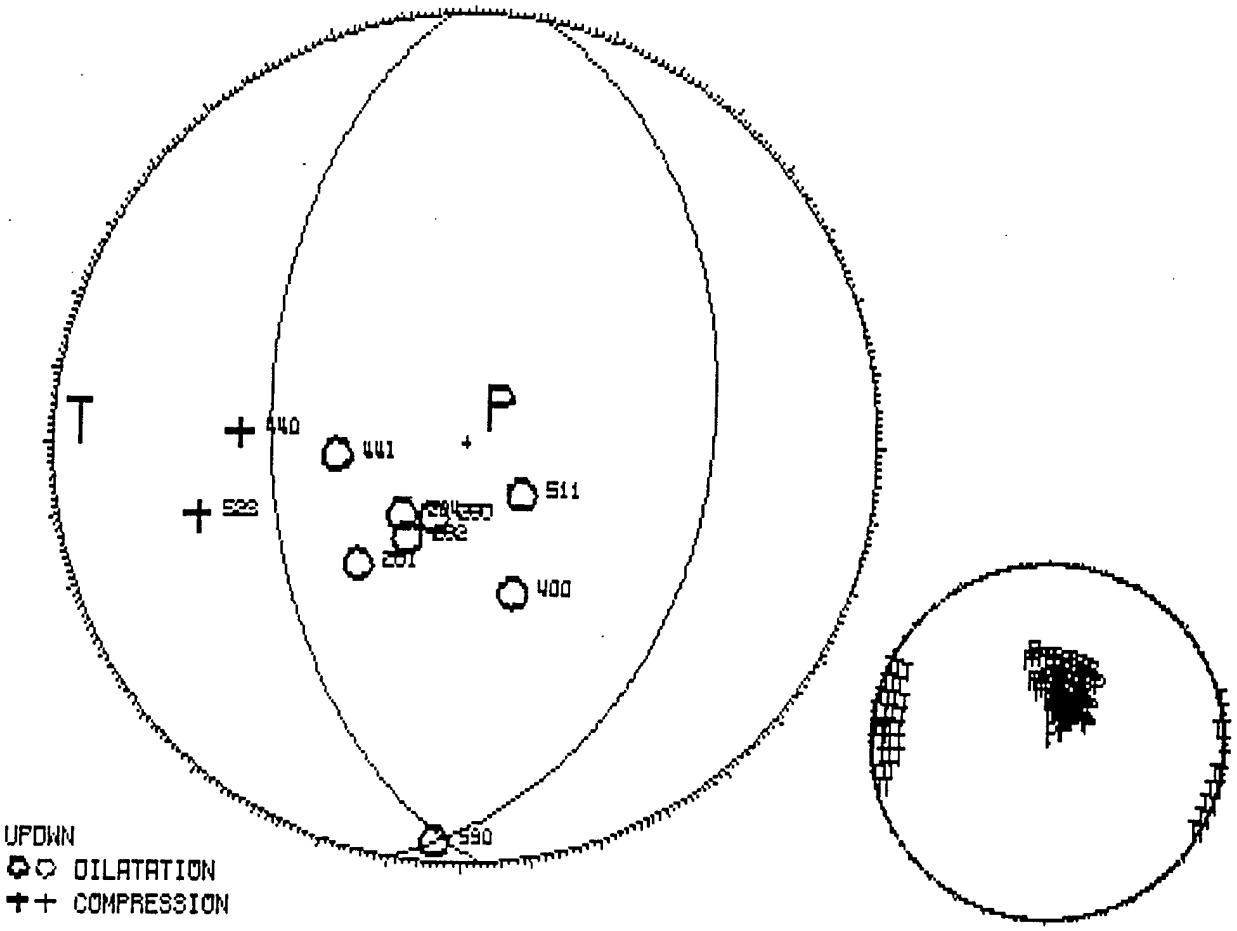

96122001 .00 47-26.10 115-49.09 -23.00 .30 .0
175 30 -90 .00 9 8.05 .87 .00 30 23 25

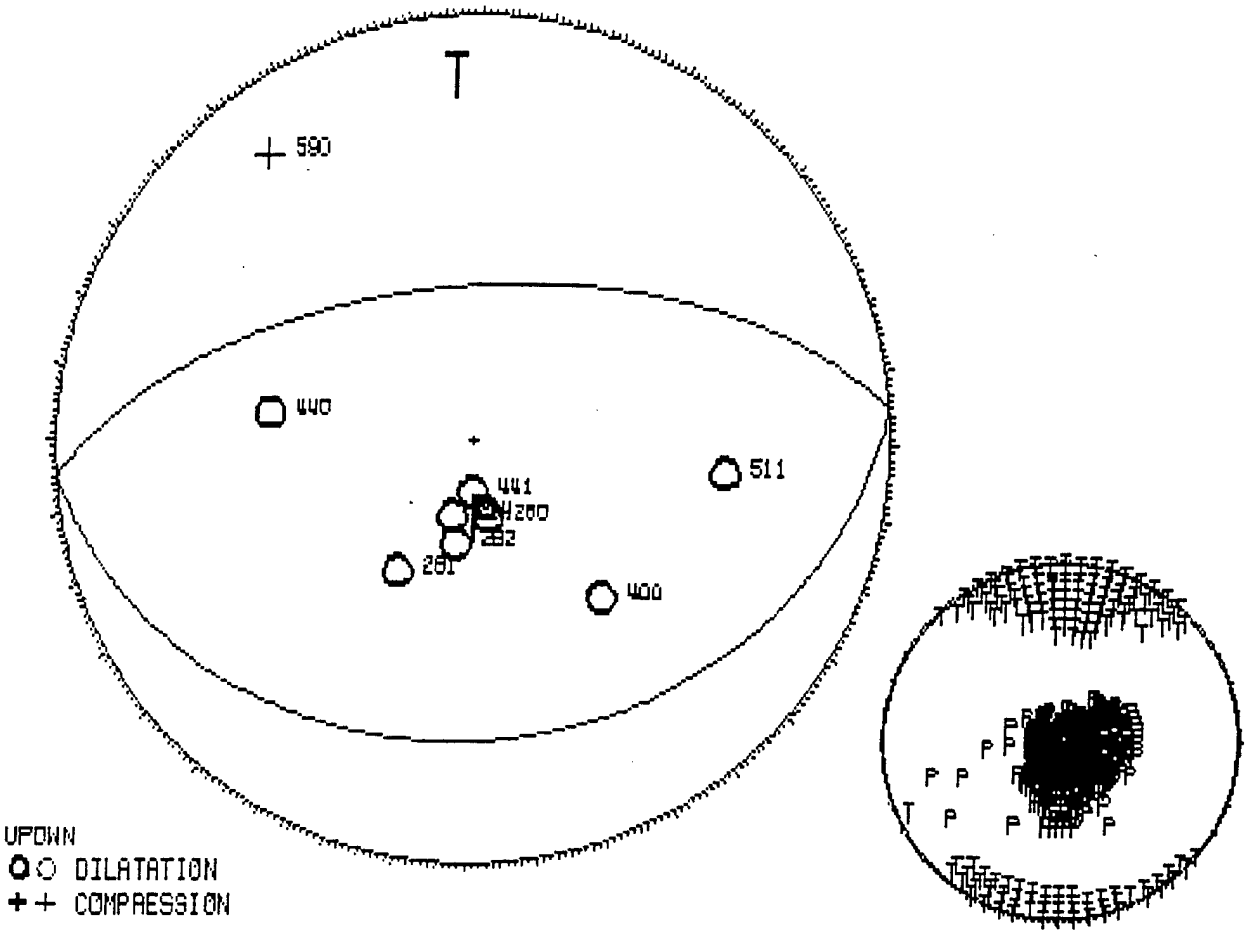

96122001 .00 47-26.10 115-45.09 -23.00 .50 .0
0 65 -60 .00 9 8.05 .79 .00 20 18 10C*

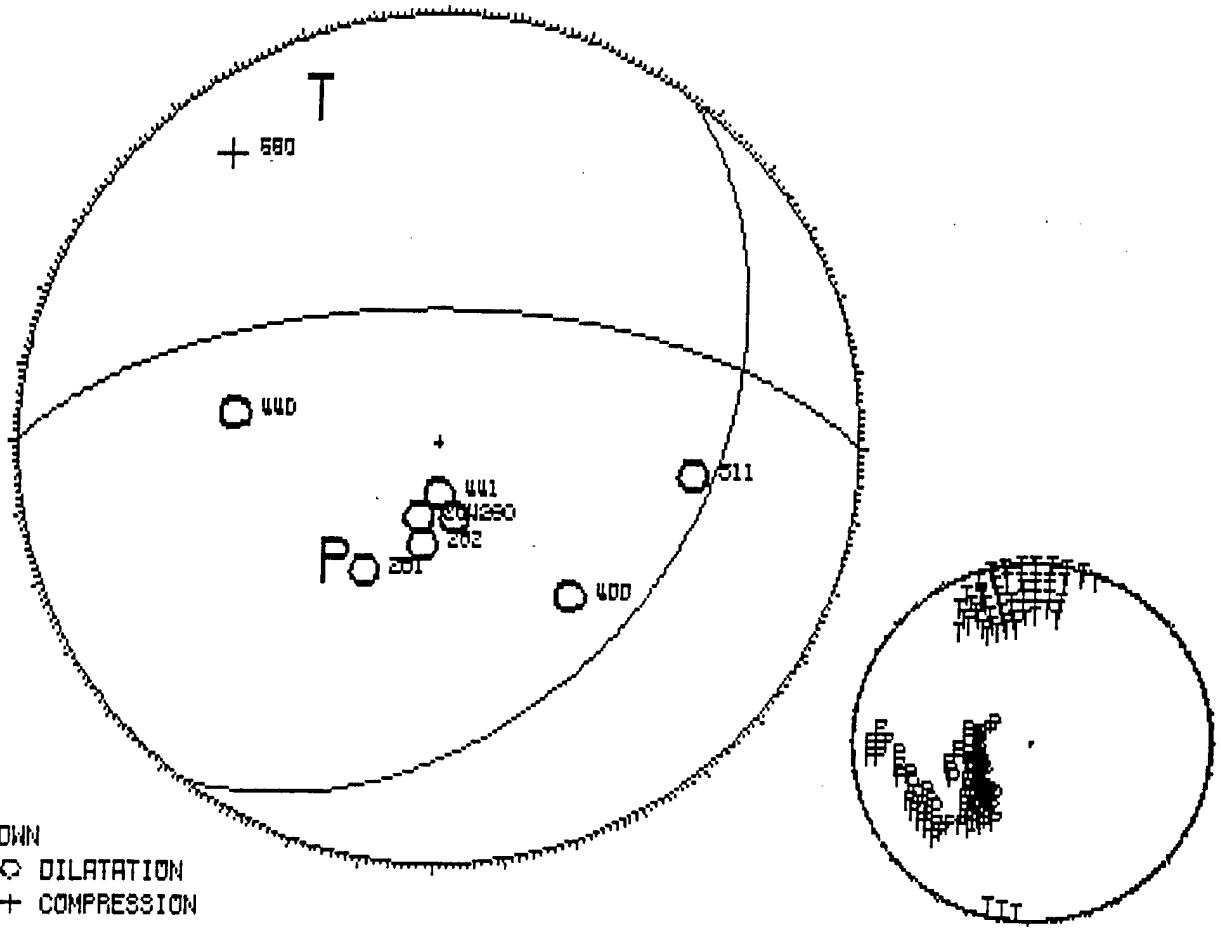

97021400 .00 47-26.10 115-43.09 -24.03 .30 .0
230 40 -60 .00 10 8.05 .75 .00 5 13 15

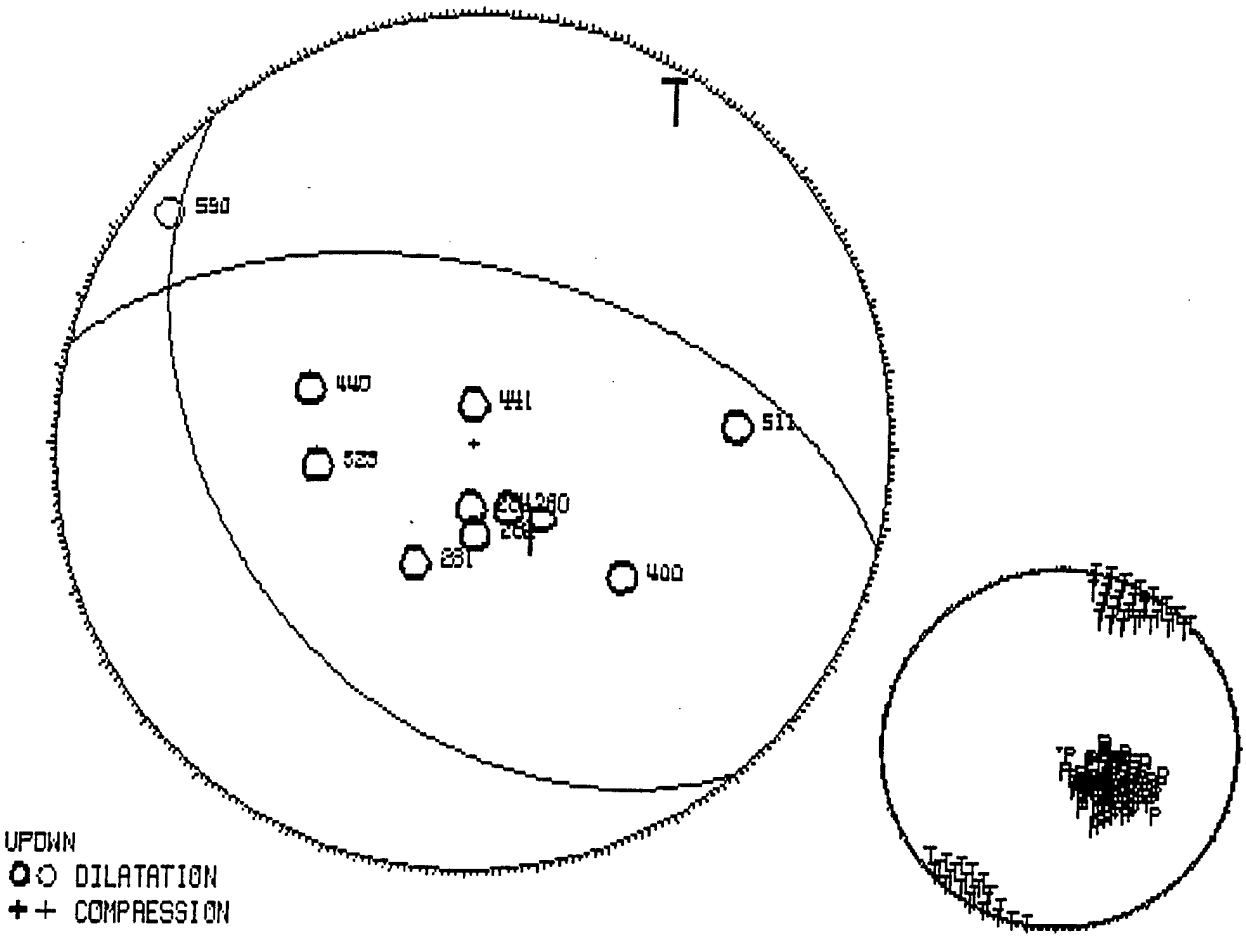

97021400 .00 47-28.10 115-43.09 -24.03 .80 .0
185 45-110 .00 10 8.05 .74 .00 10 13 5 *

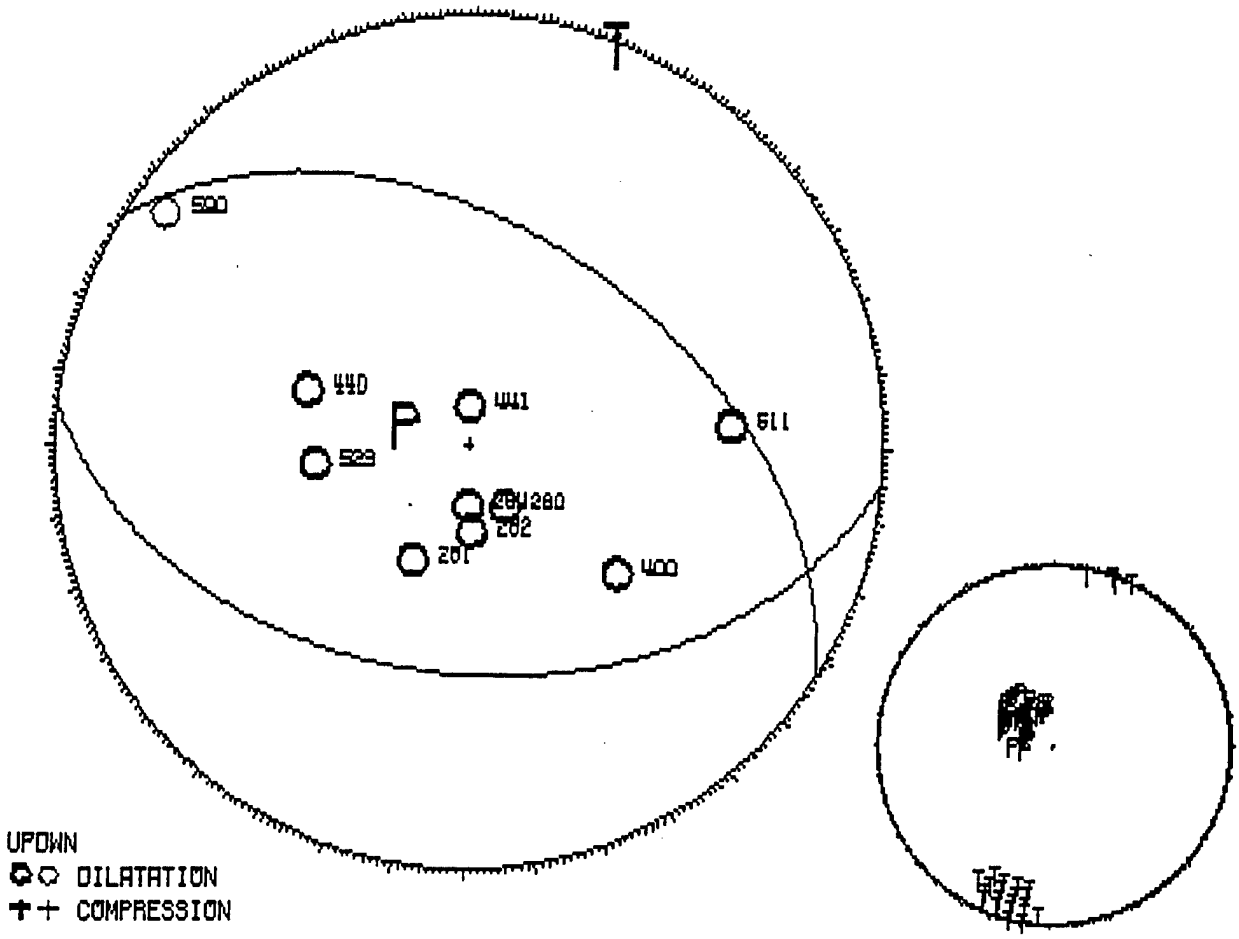

97031400 .00 47-26.10 115-43.09 -26.00 .30 .0
235 50-100 .00 10 8.05 .85 .00 38 10 30

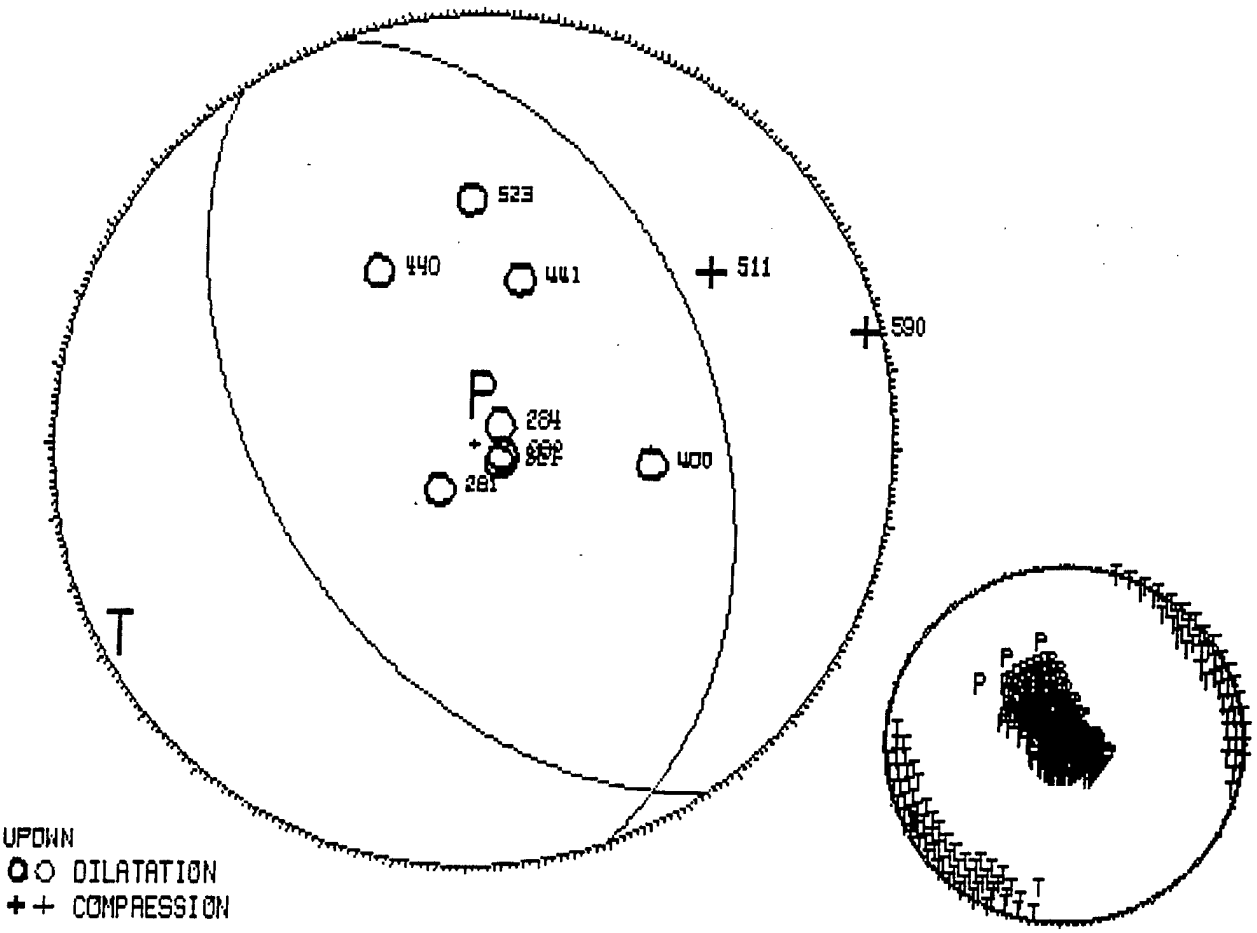

97052500 .00 47-26.10 115-49.09 -24.99 .30 .0
240 40 120 .20 10 8.05 .75 .00 10 10 20C

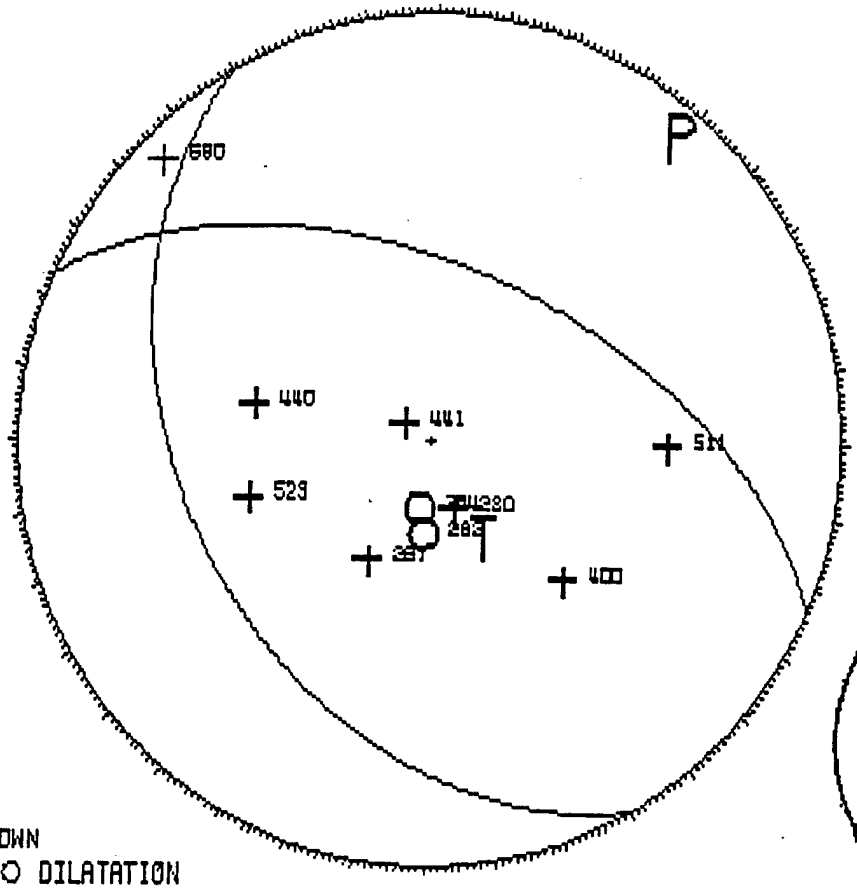


DISCREPANT OBSERVATIONS

| STAT | DIST | AZM | AIN | PRMK |
|---|---|---|---|---|
| 282 | 3.1 | 4 | 162 | IPD |
| 284 | 3.0 | 9 | 167 | IPD |

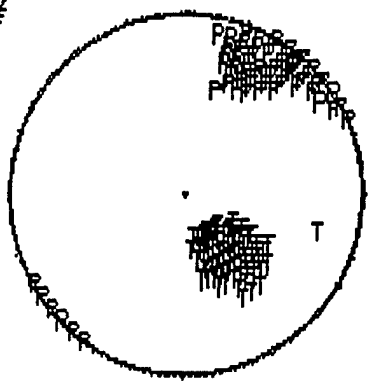


UPDWN
O O DILATATION
+ + COMPRESSION

97052500 .00 47-26.10 115-43.09 -24.39 .30 .0
70 90-180 .10 10 8.05 .38 .00 10 0 5 *

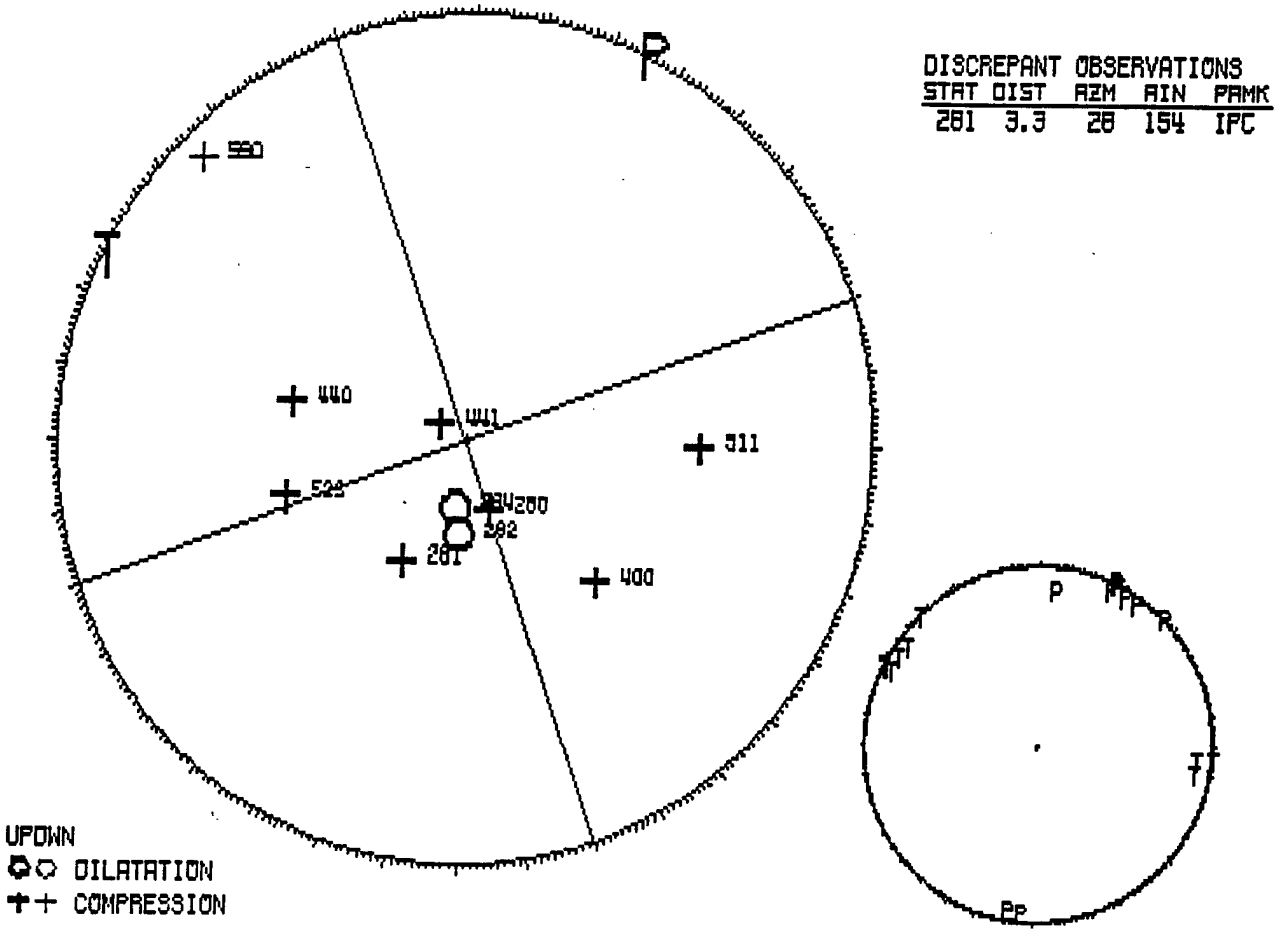


DISCREPANT OBSERVATIONS

| STAT | DIST | AZM | AIN | PAMK |
|---|---|---|---|---|
| 281 | 3.3 | 28 | 154 | IPC |

97052500 .00 47-26.10 115-43.09 -24.39 .30 .0
230 80-170 .10 10 8.05 .31 .00 0 5 15C*

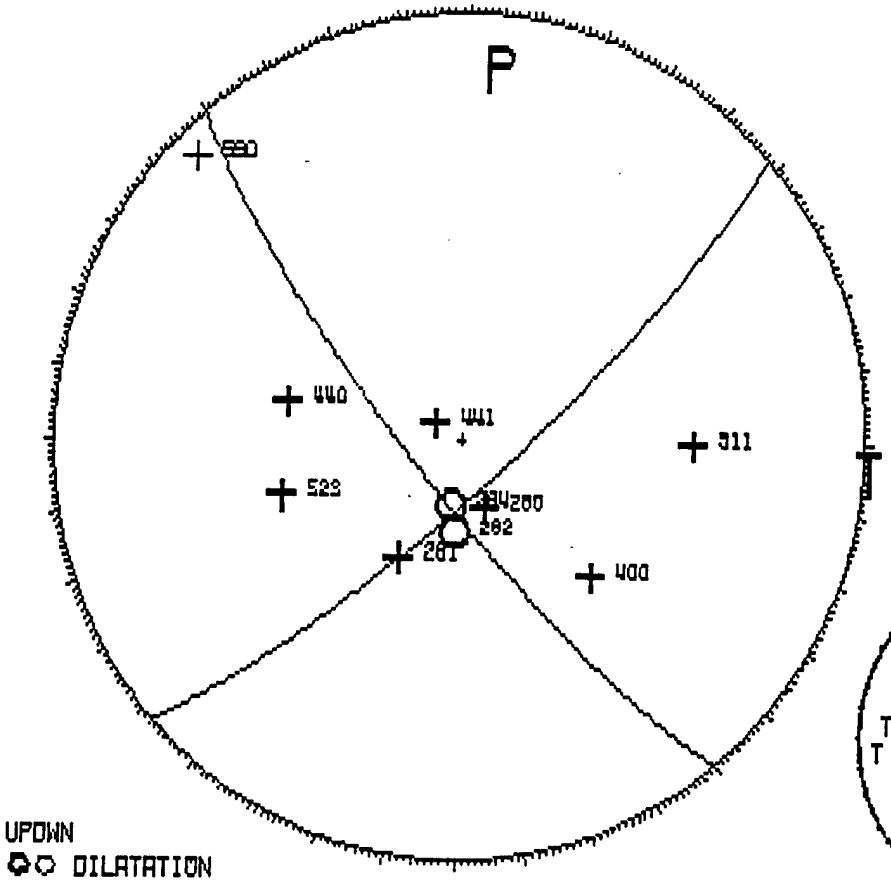


DISCREPANT OBSERVATIONS

| STAT | DIST | AZM | AIN | PAMK |
|---|---|---|---|---|
| 441 | 1.3 | 121 | 174 | IPC |

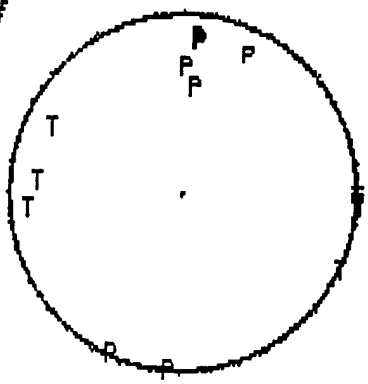


UPDWN
DILATATION
COMPRESSION

97052500 .00 47-26.10 115-43.09 -24.39 .30 .0
220 40 90 .20 10 8.05 .75 .00 10 8 5 *

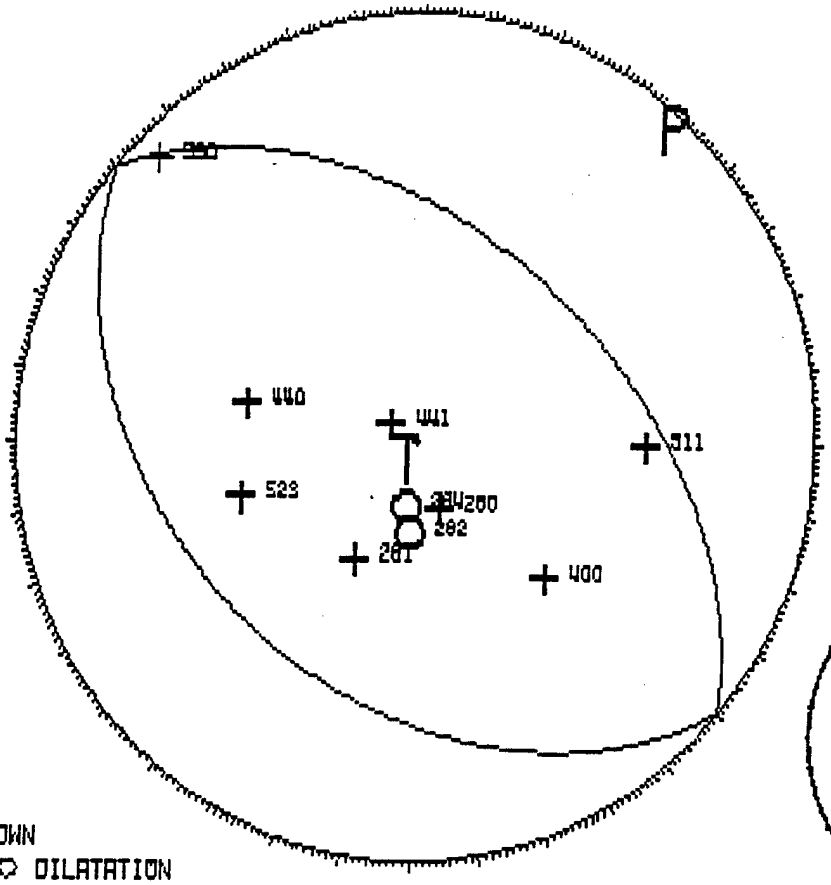


DISCREPANT OBSERVATIONS

| STAT | DIST | AZM | AIN | PAMK |
|---|---|---|---|---|
| 282 | 3.1 | 4 | 162 | IPD |
| 284 | 9.0 | 9 | 187 | IPD |

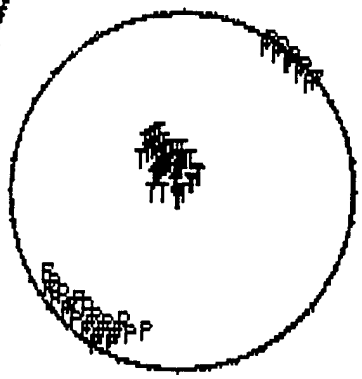

97062700 .00 47-26.10 115-49.09 -21.00 .30 .0
170 50 50 .00 10 8.05 .60 .00 10 0 40

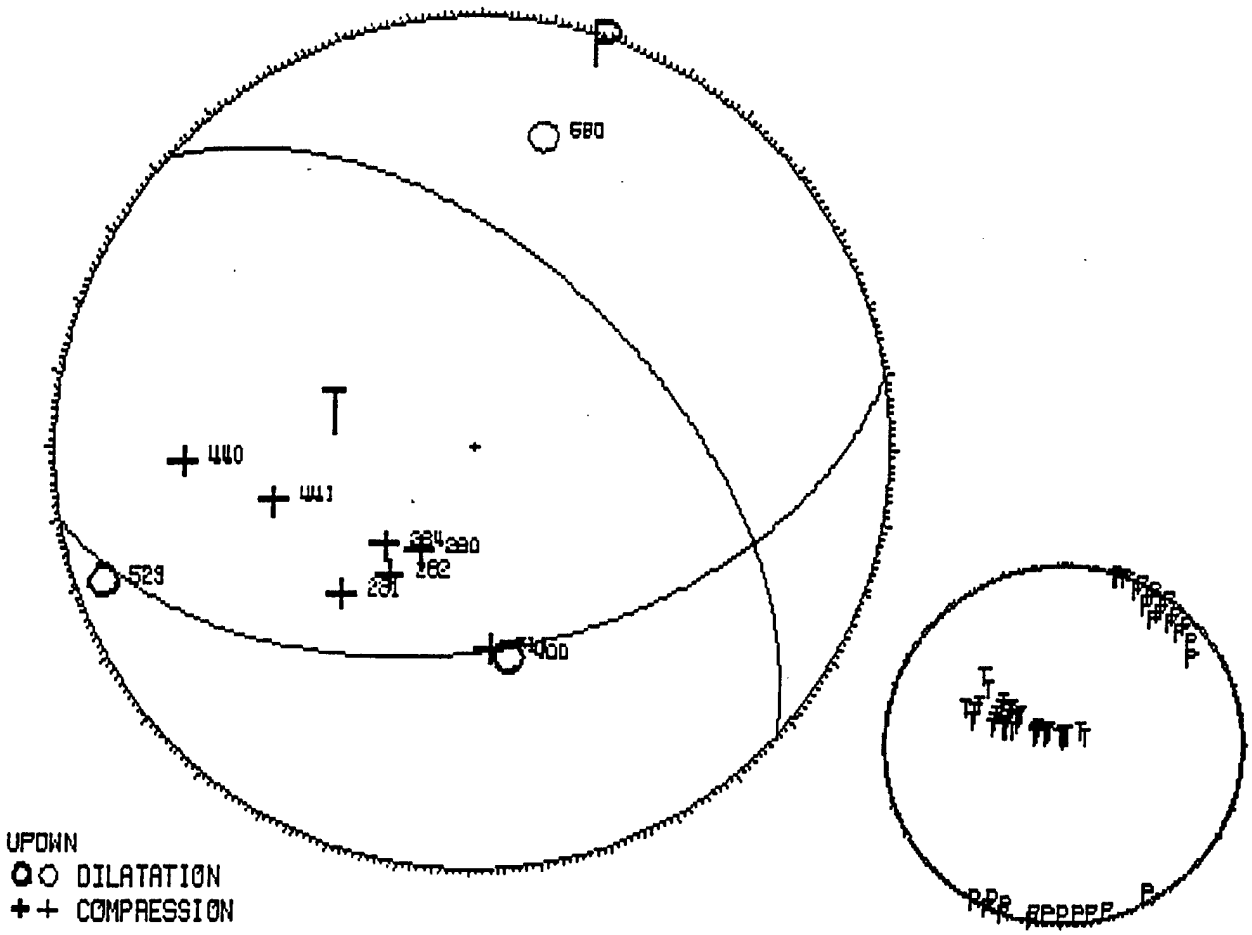

## Appendix B

Fig. B-1. First vibrational mode for split-set rock bolt, $f_1 = 13$ *Hz*.

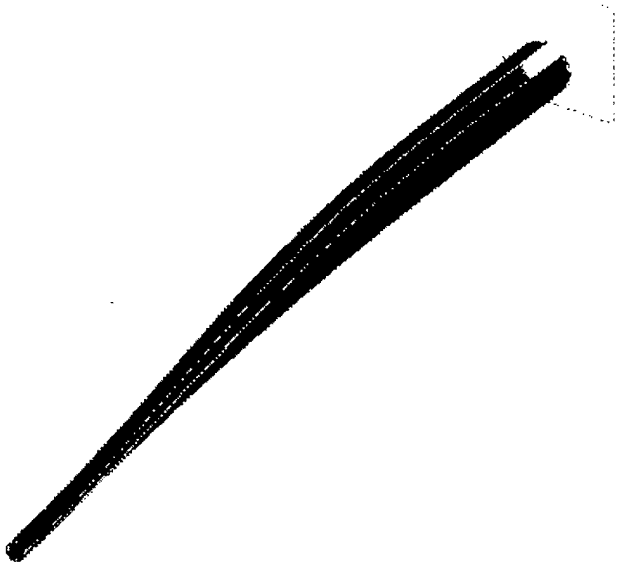

Fig. B-2. Third vibrational mode for split-set rock bolt, $f_3 = 51$ *Hz*.

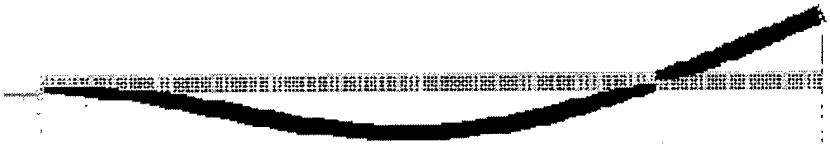

Fig. B-3. Fifth vibrational mode for split-set rock bolt, $f_5 = 83.6$ *Hz*.

Fig. B-4. Sixth vibrational mode for split-set rock bolt, $f_6 = 146.5$ *Hz*.

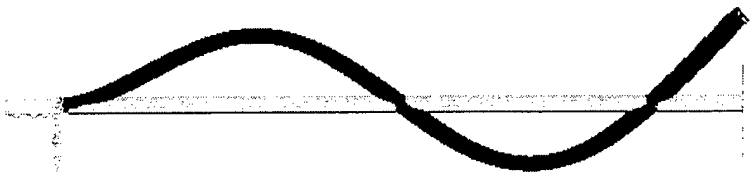

Fig. B-5. Seventh vibrational mode for split-set rock bolt, $f_7 = 232\ Hz$.

# Appendix C

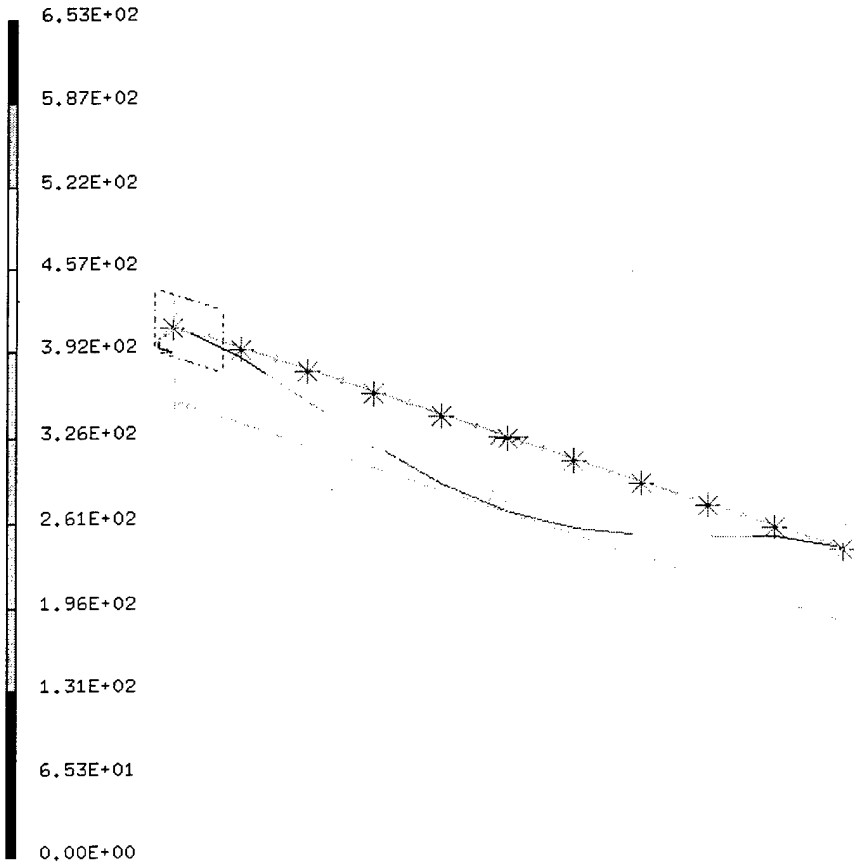


Fig. C-1. 10 kN tension, $f_1 = 28.6$ *Hz*.

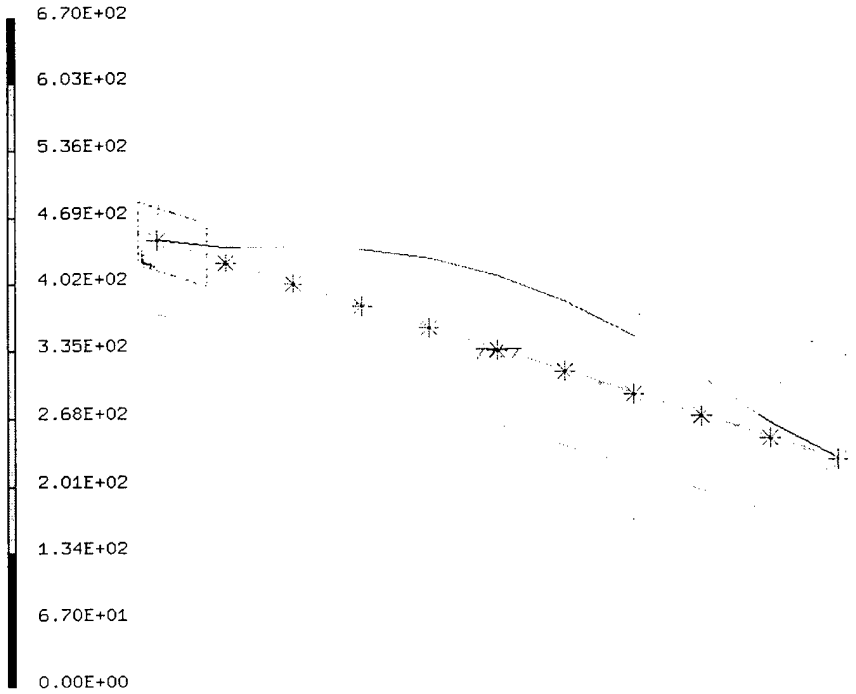


Fig. C-2. 50 kN tension, $f_1 = 51.2$ *Hz*.